AD-A133 808 ON THE RELATIONSHIP BETWEEN TRANSITIONAL AND FULLY TURBULENT SHEAR FLOW.. (U) TEL-AVIV UNIV (ISRAEL) DEPT OF FLUID MECHANICS AND HEAT TRANS.. I WYGNANSKI ET AL. 1/2

UNCLASSIFIED MAY 82 AFOSR-TR-83-0806 AFOSR-77-3275 F/G 20/4 NL

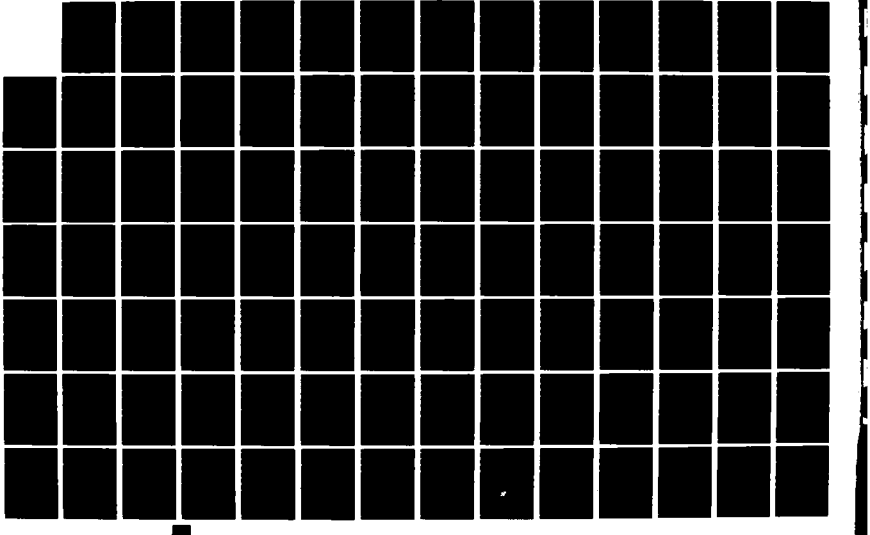

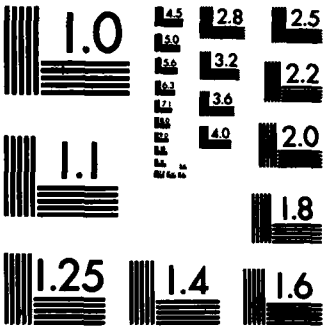

(4)

ON THE RELATIONSHIP BETWEEN TRANSITIONAL AND FULLY TURBULENT SHEAR FLOW

FIVE YEAR SUMMARY REPORT SUBMITTED BY:

PROF. I. WYGNANSKI
DR. S. EINAV

CONTRACT NO. AFOSR - 77-3275

APRIL 1977 - MARCH 1981

MAY. 30, 1982

UNCLASSIFIED
SECURITY CLASSIFICATION OF THIS PAGE (When Data Entered)

REPORT DOCUMENTATION PAGE		READ INSTRUCTIONS BEFORE COMPLETING FORM
1. REPORT NUMBER AFOSR-TR- 83-0806	2. GOVT ACCESSION NO.	3. RECIPIENT'S CATALOG NUMBER
4. TITLE (and Subtitle) ON THE RELATIONSHIP BETWEEN TRANSITIONAL AND FULLY TURBULENT SHEAR FLOW		5. TYPE OF REPORT & PERIOD COVERED FINAL 1 Mar 77 - 31 Mar 82 6. PERFORMING ORG. REPORT NUMBER
7. AUTHOR(s) I WYGNANSKI S EINAV		8. CONTRACT OR GRANT NUMBER(s) AFOSR-77-3275
9. PERFORMING ORGANIZATION NAME AND ADDRESS TEL-AVIV UNIVERSITY DEPT OF FLUID MECHANICS RAMAT-AVIV, 69978, ISRAEL		10. PROGRAM ELEMENT, PROJECT, TASK AREA & WORK UNIT NUMBERS 61102F 2307/A2
11. CONTROLLING OFFICE NAME AND ADDRESS AIR FORCE OFFICE OF SCIENTIFIC RESEARCH/NA BOLLING AFB, DC 20332		12. REPORT DATE May 1982 13. NUMBER OF PAGES 154 15. SECURITY CLASS. (of this report) Unclassified 15a. DECLASSIFICATION/DOWNGRADING SCHEDULE

16. DISTRIBUTION STATEMENT (of this Report)

Approved for Public Release; Distribution Unlimited.

17. DISTRIBUTION STATEMENT (of the abstract entered in Block 20, if different from Report)

18. SUPPLEMENTARY NOTES

19. KEY WORDS (Continue on reverse side if necessary and identify by block number)

FLUID MECHANICS
TRANSITION TO TURBULENCE
TURBULENCE
COHERENT STRUCTURES (IN TURBULENCE)
BOUNDARY LAYER
TURBULENT SPOT
TRANSITIONAL PIPE FLOW

20. ABSTRACT (Continue on reverse side if necessary and identify by block number)

The possible relationship between the transitional spot and the large coherent structures in a fully-developed boundary layer ~~has been~~ established. The final steps of transition and the generation of a turbulent boundary layer was simulated by generating a succession of spots and allowing them to interact in a controlled laboratory environment. Spots were also generated simultaneously at two points separated in the spanwise direction and their mode of interaction was observed. Measurements were made on a flat plate at a representative Reynolds number of 7×10^5 and using two types of

DD FORM 1 JAN 73 1473 EDITION OF 1 NOV 65 IS OBSOLETE

700,000

UNCLASSIFIED
SECURITY CLASSIFICATION OF THIS PAGE (When Data Entered)

rakes of hot wires. The data were processed digitally and the information gathered was used to assess the statistical methods commonly employed in gathering data in a boundary layer undergoing transition. It is established that ensemble averaged velocities do not represent the details of the flow adequately and ensemble averaged turbulent intensities may be physically deceiving. The interaction of spots generated in succession from a single point-source provides a reasonable simulation of the turbulent boundary layer. This mode of interaction inhibits the growth of individual spots in the streamwise and in the spanwise direction. As a result of this interaction the largest excursions of the uv product, representing the instantaneous shear stress occur near the leading interface of each spot. The entrainment of non turbulent flow in the X-Y plane can only account for 20% of the total entrainment necessary to sustain the growth of the turbulent boundary layer which leads one to suppose that the entrainment in the Y-Z plane resulting from vortices oriented in the streamwise direction is dominant. Zone averaged turbulent intensities, Reynolds stress and time-mean velocity profiles measured in a succession of inteacting spots and in a fully developed turbulent boundary layer are in good agreement with one another. Progress on transitional pipe flow studies is also described.

A BRIEF SUMMARY OF THE RESEARCH ACHIEVEMENTS DURING

CY 1977-1981

At the beginning of 1977, the possible relationship between the transitional spot and the large coherent structure in a fully developed, turbulent boundary-layer was recognized. A portion of the spot seemed to retain its identity without observable deterioration for at least 100 boundary-layer thicknesses (Zilberman, Wygnanski, Kaplan, 1977). The experiment was repeated at USC for the purpose of verification and a possible sharper definition of the scales in the spanwise direction. The second experiment incorporated two detector probes used for selection of eddies which were symmetrically aligned with an array of hot wires. The latter recorded the entire velocity profile at any instant rather than the velocity at a single point, which was recorded by Zilberman, et. al. 1977. The finds were quite similar (Haritonidis, Kaplan, Wygnanski, 1978) to the ones established earlier. One could evaluate, however, the effects of signal conditioning on the flow field educed, because instantaneous velocity data spanning the entire boundary layer was available.

The difference between the scale of the transitional spot embedded in a laminar boundary layer and the scale of the structure educed in a fully turbulent environment led to many pressing questions, some of which are listed below:

(1) Is the spot a single large coherent eddy on which small scale turbulence is superimposed or is it an assembly of eddies, both large and small?

(2) How does the spot depend on the character of the surrounding boundary layer?

(3) How does the spot grow? Does it entrain external fluid or does it destabilize the surrounding boundary layer - or both?

(4) Is there any way by which the rate of growth of the spot can be controlled?

(5) How do spots behave when they interact with one another, either longitudinally or laterally?

(6) What are the effects of Reynolds number and pressure gradient on the rate of growth of the spot?

Some of the recent investigations were aimed at answering these questions.

An oblique packet was found to trail a transitional spot (Wygnanski, Haritonidis, Kaplan 1979) at its wingtips. The maximum spreading angle of the packet is 11°, which is identical to the lateral spread of the spot, suggesting a possible relationship between the two. The packet was related to the Tollmien-Schlichting wave instability and the waves detected underwent the strongest amplification, according to the linear stability of the Blasius velocity profile. At higher Reynolds number (Re), these waves broke-down and generated new spots, which trailed the original spot near its wing-tips.

The presence of the wave packet and its breakdown suggests that the spot is not a single coherent eddy, but rather an orderly formation of large eddies. Furthermore, the lateral spread of the spot may have been caused by

the destabilization of the laminar boundary layer. These finds provided the first link between stability theory and the actual spreading of turbulence. We expected the Reynolds number to play an important role in the spreading of turbulence in laminar boundary layer, because the instability of the Blasius boundary layer depends on viscosity. There was, however, no data available which showed any dependence of the spot on Re. A systematic study (Wygnanski, Haritonitis, Zilberman 1980) showed that the rate of elongation of the spot in the streamwise direction is dependent on the Reynolds number existing at the origin of the spot. The differences in the rate of elongation of the spot are limited to the celerity of the trailing turbulent-non-turbulent interface of the spot which decelerates with increasing Re. It appears, therefore, that the trailing edge of the spot is probably most active in destabilizing the boundary layer. The spreading rate of the spot in the spanwise direction is independent of Re while the height of the spot increases with downstream distance in the same manner as the turbulent boundary layer does, and is, thus, only weakly dependent on Re. The different functional dependence of the growth of the spot in the three principal directions on Re implies that the spot does not obey a universal conical similarity proposed by Cantwell, Coles and Dimotakis (1978); it also follows that there is no single mechanism responsible for the spreading rate of the spot. Thus, while the aft of the spot is associated with the breakdown of Tollmien Schlichting waves, the center and the front of the spot may simply engulf and entrain non-turbulent fluid. Detailed calculations of entrainment into an ensemble averaged boundary of the spot on its plane of symmetry were made by Zilberman (1982), who used a rake of x-wire anemometers in his calculations.

This investigation revealed that entrainment calculations based on ensemble averaged data in the x-y plane are inadequate because significant entrainment must occur in the x-z plane. Velocity contours reconstructed from individual realizations also suggested that the spot contains numerous eddies which engulf non-turbulent fluid.

Favorable pressure gradient decreased significantly the rate of elongation of the spot which dropped from $\frac{dL}{dx}$ = 0.45 to 0.29 (L being the length of the spot) at a comparable Reynolds number. The spanwise spreading angle of the spot was reduced from 11° to 5°. These significant differences in the contamination of the laminar boundary layer by turbulence occurred in spite of the fact that the effect of favorable pressure gradient on the laminar boundary layer profile was rather small. (The measured profile corresponded to a Falkner-Skain profile with a parameter = 0.12). However, very slight favorable pressure gradient is required in order to appreciably improve the stability of the boundary layer. The slower destabilization of the laminar boundary layer enabled us to detect the existence spanwise inhomogeneties, which appeared even in a simple ensemble averaged data. A preselection of the events before averaging revealed clearly the existence of longitudinal eddies in the spot. It was the first proof that the spot consists of an array of large hairpin eddies moving downstream in a formation. Measurements at various downstream distances revealed that the number of the hairpin eddies across the span of the spot increased with (Wygnanski 1980) in the number of eddies which is probably caused by continuous breakdown of wave-crests.

Measurements aimed at identifying the large coherent structures inside the spot, in the absence of pressure gradient, were undertaken. The Reynolds number in this investigation was low in order to detect the large eddies more readily and develop a rational scheme for the analysis of the data educing a most probably ensemble averaged flow field, which would be favorably compared with an actual single realization (Wygnanski 1981). This scheme revealed that the number of eddies in a spot increases linearly with increasing downstream distance in both streamwise and spanwise directions. The spot, thus, contains a large number of coherent structures resembling a turbulent boundary layer. What distinguishes the spot from a fully developed turbulent boundary layer is the preferred location of the large eddies with respect to the spot boundaries. Thus, if we are interested in clarifying the dynamics of these large eddies the transitional spot offers a unique possibility.

The study of transition in a pipe, which is related to an investigation of large coherent eddies existing in internal flows, proceeded intermittently over these years. It was established that the "slug" which is a very large turbulent structure whose interior is statistically identical to a fully developed turbulent pipe flow, is generated by an array of "puffs" merging with one another. The latter are orderly structures of clearly identifiable length scale and character. The puff consists of a small number of predominantly toroidal eddies which represent a characteristic transitional mode in the pipe. Periodic oscillations were introduced into the flow in order to assess the relaxation times of turbulence and possible effect of viscosity (i.e., on Re) on the large turbulent structures.

If I had to summarize our research achievements in one sentence, I would state that a link has been established between transition, on one hand, and the large coherent structures governing turbulent shear flows at large Re on the other.

References

1. Cantwell, B., Coles, D. and Dimotakis, P. (1978). JFM, Vol. 87, p. 641.

2. Haritonidies, J.H., Kaplan, R.E. and Wygnanski, I. (1977), "Lecture Notes in Physics, Structures and Mechanisms of Turbulence - I", Proceedings, Berlin, p. 234.

3. Wygnanski, I. (1980). Lecture Notes in Physics, 136, Springer Verlag, Berlin (Proceedings, Madrid).

4. Wygnanski, I. (1981). "On Turbulent Spots - Turbulence in Liquids", Proceedings, Rolla.

5. Wygnanski, I., Haritonidis, J.H. and Kaplan, R.E. (1979). J.F.M., Vol. 92, p. 505.

6. Wygnanski, I., Haritonidis, J.H. and Zilberman, M. To be published.

7. Zilberman, M. (1982). "On the Interaction of Transional Spots and Generation of a Synthetic Turbulent Boundary Layer". Ph. D. Thesis, Tel Aviv University.

8. Zilberman, M., Wygnanski, I. and Kaplan, R.E., (1977). Phys. of Fluids, Vol. 20, 10, part II S 258.

TABLE OF CONTENTS

ABSTRACT

The final steps of transition and the generation of a turbulent boundary layer was simulated by generating a succession of spots and allowing them to interact under controlled environment. Spots were also generated simultaneously at two points separated in the spanwise direction and their mode of interaction was observed. Measurements were made on a flat plate at a representative Reynolds number of 7×10^5 and using two types of rakes of hot wires: (i) wires normal to the flow direction and parallel to the surface, measuring instantaneously the streamwise component of velocity across the entire boundary layer. (ii) A rake of wires which are inclined to the surface and to the mean flow, measuring instantaneously the streamwise and the normal components of velocity across the flow. The data was processed digitally and the information gathered was used to assess the statistical methods commonly employed in gathering data in a boundary layer undergoing transition. It is established that ensemble averaged velocities do not represent the details of the flow adequately and ensemble averaged turbulent intensities may be physically deceiving.

The interaction of spots generated in succession from a single point-source provides a reasonable simulation of the turbulent boundary layer. This mode of interaction inhibits the growth of individual spots in

the streamwise and in the spanwise direction. As a result of this interaction the largest excursions of the uv product, representing the instantaneous shear stress, occur near the leading interface of each spot. The entrainment of non turbulent flow in the X-Y plane can only account for 20% of the total entrainment necessary to sustain the growth of the turbulent boundary layer which leads one to suppose that the entrainment in the Y-Z plane resulting from vortices oriented in the streamwise direction is dominant. Zone averaged turbulent intensities, Reynolds stress and time-mean velocity profiles measured in a succession of interacting spots and in a fully developed turbulent boundary layer are in good agreement with one another.

ACKNOWLEDGEMENTS

Acknowledgements writing has been a way for me to look outward again to appreciate how much I have drawn from others. Thoughtful people have supplied not only ideas, but also criticism and suggestions in each part of my research. All they are receiving in return is a brief mention here, and the promise that I will try to be equally generous and helpful when I have the opportunity.

Seven years ago, Professor Israel Wygnanski opened up a new world for me. Through his insight, the findings of the transitional spot and its relation to the transition process in boundary layers flow were drawn together into an organized theory that may clarify the structure of the fully turbulent boundary layer and its development from earlier stages of the transitional stage. I am grateful for Wygi's teaching, for his guidance and help, and for his example of what it means to be a responsible scientist in this troubled world.

Professor R.E. Kaplan was always generous with his knowledge and time, and the 'footprints' of his computer library are recognizable everywhere in my work.

Dr. J. Haritonidis contributed significantly in developing the calibration schemes as well as in constructing the multi-probes.

Many of the ideas were clarified to me after the interesting talks with Professors J. Laufer and R.F. Blackwelder.

Dr. J. Amini who has been working in our laboratory for some time, taught me a great deal and I am thankful to him.

I would like to convey my deep appreciation to the financial support of the AFOSR 77-3275 grant.

I am grateful to miss Rivka Kurzman and miss Mira Lande who were always willing to help; they represent the goodwill and kindness that allways surrounded me during my studies and work in the Fluid Mechanics Department.

Special thanks to my mother in law Mrs. Dina Jacobs, who took on herself the cumbersome work of proofreading.

I thank my family and especially my wife for many years of support and encouragement.

CHAPTER A

INTRODUCTION

There is an abundance of evidence that the fluid motion within the turbulent boundary layer is not as random as it was once believed, but contains large coherent eddies which may govern some important features of this flow. Although some characteristic behaviour of these eddies was observed and charted, the information available to date is still mostly descriptive in nature. There are considerable difficulties in defining a "detector" which is capable of identifying large eddy structures unambiguously and impartially. Some difficulties are attributed to the fact that we are concerned with repeatable events occurring quite randomly in space and time. Furthermore, these structures are embedded in an environment containing a wide spectrum of finer scales. Thus we cannot define a signature of a large eddy without a priori knowledge of its shape and location relative to the observer and we can not map such an eddy without having a proper criterion for pattern recognition.

Another difficulty in charting the large eddy stems from the fact that at any instant of time it occupies a volume of fluid, while most quantitative measuring devices provide information at a point. For these reasons major contributions towards the recognition of coherent structure were made by visual methods. Blackwelder and Kaplan (1972) are credited to be the first ones to use an array of sensors spanning the boundary layer and providing instantaneous velocity information across the flow, but even this

information is insufficient to describe a three-dimensional structure quantitatively.

A possible solution of the dilemma could be provided by perturbing laminar flow from a point-source in a way which evokes the generation of turbulent spots. In this way one obtains both a time reference and a mean trajectory along which the spot travels. Moreover, because the events are repeatable, the smaller scales which are randomly superimposed on them vanish.

The difficulty with this approach in comparison with the conventional "chasing" of the large eddy is transferred from a detection of a typical large coherent structure to its production. The turbulent spot may be a basic module contributing to the creation of a turbulent boundary layer, but its composition is by no means simple, because it contains a hierarchy of eddies arranged in a particular order, rather than a single eddy which scales with the boundary layer thickness. Thus, the precise relationship between the turbulent spot and the large coherent eddy remains to be shown, although it is known that the spot retains some of its features indefinitely in spite of the prolonged interaction with a turbulent boundary layer (Zilberman, Wygnanski and Kaplan 1977; Haritonidis, Kaplan and Wygnanski 1977; hereafter referred to as ZWK and HKW, respectively).

The onset of turbulence in a boundary layer does not occur along a continuous front but rather at isolated spots which spread while being convected downstream, eventually coalescing with one another to form a turbu-

lent boundary layer (Emmons 1951). The spots occur randomly in time and space but they are easily triggered by roughness elements surface imperfections, small jets or other disturbances. In view of their arrowhead shape the spots are the most clearly identifiable features in the transition process. They may be linked to the instability of the laminar boundary layer (Gaster 1968; Wygnanski, Haritonidis and Kaplan 1979) on one hand and to the turbulent boundary layer on the other. The purpose of this investigation is to provide quantitative data describing the relationship between interacting spots and fully turbulent boundary layer.

The spot was discovered by Emmons (1951) who also developed probabilistic calculations for the transition process based on the following observations and assumptions:

(i) The spot originates at a point.

(ii) There is a sharp distinction between the turbulent region within the spot and in laminar surroundings.

(iii) The spot grows uniformly while being convected downstream.

(iv) There is no interaction among spots.

On this basis an expression was obtained by Emmons, predicting the intermittency at any point in the flow and enabling calculation of skin friction in the transition region.

Some features of the turbulent spot were first documented by Schubauer and Klebanoff (1956). The spot was initiated by means of an electric discharge in a laminar boundary layer and was detected by a hot wire located in the boundary layer downstream of the spark. The general shape of the spot, the celerity of its boundaries and the angles at which it spreads, can all be found in their report. They also observed that a fixed three dimensional roughness element located on the surface produces a turbulent wedge in its wake which spreads laterally at the same angle as the spot, suggesting that the turbulent wedge may have been generated by a succession of spots telescoping into one another.

Elder (1960), who used the same technique to initiate the spots as Scubauer and Klebanoff, provided an experimental evidence for the fourth assumption of Emmons. He simultaneously generated two spots at different spanwise locations and measured the resulting intermittency factor downstream, concluding that the area covered by turbulence was simply the combined area of the spots, assuming that they grew independently of one another. Coles and Barker (1975) made their observations in water using a laser doppler velocimeter. They concluded that the ensemble averaged turbulent spot in a laminar boundary layer can be represented by a single large vortex, which entrains irrotational fluid from the free stream above it and rotational fluid from laminar boundary layer surrounding it. An attempt was made to generate a synthetic turbulent boundary layer by triggering several spots simultaneously and noting the resulting mean velocity profile. Savas (1979) constructed a synthetic turbulent boundary layer in air, by periodically disturbing the flow with protruding arrays of rough-

ness elements, which were placed at various locations along the span. Savas observed that some spots shifted their position laterally as a result of an interaction with their neighbours. The lateral "transposition" of spots might have been associated with a natural regeneration of new structures at the wing tips of the artificially evoked spots (Wygnanski, Haritonidis and Kaplan, 1979; hereafter referred to as WHK).

Wygnanski, Sokolkov and Friedman (1976; hereafter referred to as WSF) mapped the flow field within the spot by measuring all three components of the ensemble averaged velocity inside it. They checked the shape of the spot, its spreading angles and the scales governing its similarity with downstream distance. Furthermore, they proved that the spot attains a universal structure and shape regardless of the type and intensity of the disturbance generating it.

The prevailing views on the: " Coherent Structure of Turbulent Boundary Layers" are expressed in a volume of proceedings from a workshop dedicated to this subject in addition to a number of survey articles which can be found in the open literature (Laufer 1975, Willmarth 1975, Willmarth and Bogar 1977 etc.). The views held most commonly are backed by flow visualization and by measurements using conditional sampling techniques. Laufer (1975) claims that the double-layered nature of the turbulent boundary layer may owe its existence to two types of coherent structures. The outer layer contains large scale three dimensional vorticity lumps, while the inner layer may contain a thin vortex sheet which is occasionally lifted by the outer structures, resulting in the generation of wall streaks (see also

Blackwelder 1978). The relation between the inner and outer structures was investigated by Kim et al.(1971), Blackwelder (1978) and others. The lifting of the wall-streaks occurs periodically and is often referred to as "bursts"; although the bursts occur near the wall the bursting periods scale with the outer flow parameters rather than with parameters governing the wall region (Rao et al. 1971).

Visual studies (Kline 1978, and Gupta et al. 1971) suggested that the spacing between streaks scales with the wall coordinates, in spite of the fact that the outer bulges are an order of magnitude wider than the streaks. Falco (1977, 78) subdivided the eddies in the outer and inner regions of the turbulent boundary layer into two categories. In the outer region he calls them large eddies and "typical eddies", while in the inner region they are referred to as "pockets" and "streaks". The different names refer to different shapes of eddies which presumably also contain different levels of energy. The proliferation of names given to visual observations attempting to describe kinematically a physical process stresses our limited understanding of this subject.

The possibility that the transitional spot and the large coherent eddy in a turbulent boundary layer may have something in common was explored by ZWK (1977). A spot was initiated among spherical roughness elements which tripped the boundary layer and was allowed to interact with this turbulent boundary layer. The evoked structure was then tracked downstream up to 120 typical turbulent boundary layer thicknesses (see also HKW 1977). The structure evoked in this manner agrees in detail with the structure ob-

served in the outer region of the turbulent boundary layer by Kovasznay, Kibens and Blackwelder (1970) and justifies the effort invested in studying turbulent spots. The scale of the artificially evoked structure near the wall is approximately 10δ in the streamwise direction becoming $2\text{-}3\delta$ near the interface. The spanwise extent of the evoked structure is less than 4δ ; and its celerity is $0.9U_\infty$. HKW (1977) repeated the experiment using a rake of hot-wire anemometers and a more powerful data acquisition system. They extended the range of measurements and were capable of assessing the distortion of the evoked structure with downstream distance. The relationship between the educed eddy in a turbulent boundary layer and the artificially evoked spot in a laminar boundary layer is still not well understood in view of the disparity in scales of the two structures. Furthermore, both structures contain finer scales about whose origin and dynamics we know rather little.

Cantwell, Coles and Dimotakis (1978; hereafter referred to as CCD) attribute the additional fragmentation of the spot (or outer bulge) to a centrifugal instability of the Taylor-Gortler type. Klebanoff, Tidstrom and Sargent (1962) attribute the generation of small scale turbulence to the breakdown of Tollmien Schlichting waves. WHK (1979) observed a pair of oblique wave packets located behind the wing-tip of the spot with their wave number vector being inclined at 50° to the streamwise direction. These wave packets were identified as Tollmien-Schlichting waves and their breakdown at a higher Reynolds number caused a generation of new spots. Gad el Hak, Blackwelder and Riley (1980; hereafter referred to as GBR) also suggest that the dominant mechanism contributing to the lateral growth

of a turbulent spot is caused by distabilization of the surrounding laminar boundary layer.

In an attempt to understand the process by which transitional spots merge and generate a turbulent boundary layer, a controlled experiment was undertaken which simulates the interaction of spots. Some of the preliminary conclusions drawn from the interaction of successive spots originating from a simple point source were reported by Wygnanski (1978). The evolution of two spots evoked simultaneously at different spanwise locations was also investigated, in order to supplement the data of Elder (1960). A preliminary study of spots, originating at different spanwise locations and different times, was also made. The broad aim of these experiments was to identify and compare the characteristic features observed in isolated spots with the similar features occurring during the interaction of spots and in a fully turbulent boundary layer. Hopefully this comparison would contribute to the understanding of this complicated flow.

CHAPTER B

EXPERIMENTAL FACILITIES

B.1 Wind Tunnel (fig. B.1.1).

All measurements and calibration procedures were conducted in the low speed, low turbulence, closed circuit wind tunnel which was constructed by Kenney Engineering in Monrovia, California. The test section of the tunnel is 61 cm wide 610 cm long and 91 cm high. The floor and ceiling of the test section are made of plexiglass and are mounted on jacks, thus enabling the height of the section to be changed from 90 cm to 152 cm.

The wind is generated by an axial blower powered by a 25 H.P DC motor and a variable speed controller. The velocity in the test section in absence of any disturbance can vary from 0 to a maximum of 45 m/sec. The maximum non uniformity of speed across the test section is less than 0.5% exclusive of the boundary layer region. The longitudinal turbulence level in an empty test section is approximately 0.04% at 30 m/sec.

B.2 The Plate

An aluminium plate, 360 cm long, 90 cm wide and 0.4 cm thick, was mounted vertically in the test section 28 cm downstream of the inlet and 11 cm from the back tunnel wall (fig. B.2.1a). The plate is pivoted at the leading edge and can be inclined at small angles of attack relative to the

flow. Adjustable screws at the back of the plate hold the plate in position relative to the wall of the test section; these screws can also serve to remove residual waviness from the surface of the plate.

The front side upstream part of the plate was machined to have a circular section of 2 cm diameter where the front surface was tangent to that (fig. B.2.1b). A 60 cm adjustable flap was installed at the trailing edge of the plate in order to control the circulation and assure that the stagnation point is located on the test surface. A slight divergence of the top and bottom walls of the tunnel offered another degree of freedom for fine adjustment of pressure distribution, narrow slots on both sides of the plate (Amini 1978) in addition to the corner fillets were left in order to reduce the influence of the corners. Pressure measurements on the surface of the plate showed a maximum residual gradient of : $(2/\rho U^2)x(dp/dx) = -5x10^{-5}cm^{-1}$ at an ambient velocity of 10 m/s. The velocity profile in the developing boundary layer was measured at five different locations downstream of the leading edge and compared with the theoretical profile of Blasius (fig. B.2.2).

Whenever a comparison with a turbulent boundary layer was required, the boundary layer tripped by the same manner as that of ZWK (1977); by rows of spheres 1.5 mm in diameter which were distributed in a spanwise direction at an x location corresponding to $Re\delta^* = 500$. Turbulent spots were initiated by an electric discharge generated by a commercial car ignition unit and driven by a signal generator which was controlled by the computer. Two electrodes 0.5 cm apart were inserted into a plexiglass plug which was

mounted flush with the surface; the plug served as an insulator (fig. B.2.1b).

B.3 The Traversing Mechanism

The traversing mechanism was designed to translate the probes in 3 directions x,y,z and rotate them in the X-Y plane (fig. B.3.1). The movements in the spanwise (Z) direction and in the streamwise (X) direction along the plate are operated manually with an accuracy of 0.5 mm. The movements in the Y direction (normal to the surface of the plate) and the rotation in the X-Y plane were controlled by the computer via SLO-SYN M061-FD08 stepping motor and STM 1800 DV controller. The repeatability of the motion in the Y direction was approximately 0.04 mm. The angular motion covered a range of 45^{o} with an accuracy and repeatability of $1/2^{o}$. One cannot translate the probe while rotating it. The mode of movements is selected manually by tightening screw number 1 and releasing screw number 3 for translation or by tightening screw number 3 and releasing screw number 1 for rotation.

B.4 Hot-Wire Anemometers

Multi channel constant temperature hot wire anemometers were constructed in the Tel-Aviv University electronic shop from a basic circuit designed by R.E. Kaplan and used at the University of Southern California (fig. B.4.1). Two sets of variable potentiometers provided a choice of over-heat ratios ranging from 0.05 to 1. Present measurements were made at

0.5 over-heat ratio; the frequency response of the set was better than 10 KHz, for 5μ diameter tungsten wires.

B.5 Hot Wire Rakes (probes)

Most of the results presented in this work were obtained using home-made hot wire rakes of two kinds : (i) 10 normal wires, parallel to the surface of the plate and normal to the flow. (ii) 4 X-wires inclined at 45° to the surface and to the flow.

Twenty jewellers broaches were glued in pairs onto a fiberglass board, 5 cm long, 1 cm wide and 0.1 cm thick. Each pair of broaches served as a prong onto which a 5μ tungsten wire was welded. The distances of the wires from the bottom surface were 1.35, 2.39, 3.42, 4.52, 6.28, 8.63, 11.23, 15.48, 20.18 and 24.88 cm (fig. B.5.1).

In the probe of the second kind, sixteen broaches were connected to the board in a configuration yielding a rake of 4 X-wires. The distance between each slanted wire and its neighbour was about 1 mm and between the centers of each X-wire it was about 2 mm (fig. B.5.2).

CHAPTER C

DATA ACQUISITION

The digitizing of the data was done using a minicomputer (VARIAN 72 model) having a 32 K word memory, 16 bit each. Seven and nine track digital tapes were available for storing the data. The data was digitized with 12 bit precision (4096 quantizing steps). Data acquired by normal wires was converted to velocity and recorded on digital tapes immediately. Data acquired with X-wires was digitized and recorded in its raw form, this data was later processed on a PDP 11/60 computer which had a memory of 128 K words, 2 RK07 disks (27 M byte each) and was thus more convenient to use than the VARIAN.

C.1 The Calibration of Normal Wires

The hot wires were calibrated by fitting a third order polynomial to four calibration velocities, in the range 1 m/s to 10 m/s. The latter velocity corresponded to the free stream velocity outside the boundary layer. Thus for a given voltage E_i (where the subscript i denotes the ith wire in the array) the velocity U_j is :

$$(1) \quad U_j = A_i + B_i x (E_i - E_{oi}) + C_i x (E_i - E_{oi})^2 + D_i x (E_i - E_{oi})^3$$

where A_i, B_i, C_i, and D_i are the four calibration coefficients and E_{oi} is the voltage measured in the abscence of any velocity. i is the index of

the hot wire probe (i=1,...,10); j is the index of calibration velocity (j=1,...,4).

At times when the temperature in the laboratory remained constant the hot wires did not drift by more than 2% during an entire day.

C.2 Look-Up Table (high speed conversion of voltages to velocities)

The concept of a look-up table was suggested by Dr. J. Haritonidis (U.S.C) while discussing various possibilities of X-wires calibration. Since the analog to digital converter has only 4096 quantizing steps, it is possible to translate each step to its corresponding velocity, once for every calibration. Hence, the conversion of voltages to velocities becomes a simple readout of tables where the voltages are actually the indices of the vector terms. If for an A/D converter the voltage range is from -V to +V volts, then each quantizing step corresponds to a number between 1 and 4096 with the resolution of 2V/4096 Volts. Having four coefficients A, B, C and D for each wire, the voltages are translated to 4096 velocity values by:

$$(2) \quad U(J) = A+Jx(B+Jx(JxD+C))$$

where J goes from -2048 to 2048

Usually, the number of terms is smaller since not all the range is used. Finally, during 'look-up' conversion the single operation needed is to equate the velocity U of voltage J with U(J) term.

C.3 The Calibration of X-Wires

The calibration of a rake of X-wires has to be efficient in order to save on computing time and memory space. The fastest calibration procedure is attained through the use of look-up tables having two indices for the velocities and the yaw angles of the wires. However, if I and J are the quantizing values for the voltages E_1 and E_2 of both wires, then a two dimensional look-up table would require 1.6×10^7 memory locations per X-wire. This number is prohibitive, bearing in mind that it has to be multiplied by the number of X-wires in the rake; therefore, if a look-up table concept is to be used, it must be accompanied by a space saving scheme. The calibration procedure is based on the fact that within the calibration range the velocity vector Q and its direction α can be obtained by a transformation of the two independent X wire voltages E_1 and E_2 (see Willmarth and Bogar, 1977; Coles, Cantwell and Wadcock, 1978).

It is well known that the voltage E supplied to maintain the hot wire at a constant temperature is increasing monotonically with velocity and depends roughly on the cosine of the angle between the wire and the flow direction. The response of the wire to a change in the flow direction is unique for 90° only.

The relation between the output voltage of each wire and the appropriate velocity and direction can be expressed formally by the following equations:

$$(3) \quad E_1 = E_1(Q,\alpha) \; ; \quad E_2 = E_2(Q,\alpha)$$

where Q is the velocity vector and α is its direction with respect to the probe axis. From the monotonic behaviour of each wire it is clear that for every combination of E_1 and E_2 within the calibration region, one obtains only one combination of Q and α. In fact, the calibration region is defined by the inverse transformation that obeys the relations:

$$(4) \quad Q = Q(E_1,E_2) \; ; \quad \alpha = \alpha(E_1,E_2)$$

In order to predict the calibration range in the E_1-E_2 plane, it is helpful to assume a monotonic behaviour of the wire response for three possible cases of X-wire configurations (illustrated in figures C.3.1a, b and c). In the first case, the two slanted wires are perpendicular to one another. Therefore, a change in direction at a constant velocity Q from α_1 to α_2 would cause a decrease in E_2 and a concomitant increase in E_1 (fig. C.3.2a). The curves for a constant Q on E_1- E_2 plane will have the shapes shown in figures C.3.2b and c (when the angle between the wires is smaller or larger than 90°, respectively). An increase in the velocity will shift the curve diagonally upwards. At the large angles of yaw the response of the wires may not be unique as a result of strong end effects, resulting from the finite length of the wires and the prongs, when the flow becomes parallel to one of the wires. Obviously one cannot rotate the wire relative to the flow by an angle larger than 90°, thus reversing the flow direction relative to the particular wire.

The velocity Q, measured by an X-wire, can be interpolated in a three dimensional space with two independent variables E_1 and E_2 in the same manner as the calibration curve for a single wire is interpolated by the third order polinomial having a single variable E. Assuming that the functional dependence on the angle is not more complicated than on the velocity, the calibration procedure for the X-wire takes the following steps :

1) Storing descrete points measured at selected velocities and angles - plotting equation 3.

2) Calculating surfaces for Q and α while finding equation 4.

3) Data reduction obtaining the velocity Q and the angle α by using equation number 4.

Since the simple minded concept of the 'look-up' table can not be applied directly to a rake of X-wires, the following procedure was used:

a) The E_1-E_2 planes were subdivided into 60x60 grid elements. This number was chosen arbitrarily although the accuracy is improved as the number of elements increases.

b) The velocity and angle at each grid point (figures C.3.3a and C.3.3b) were calculated by using spline interpolation.

c) The velocity range inside each square was of the order of 15 cm/s corresponding to 1.5% from the free stream velocity used in this experiment. Similar angular resolution was not considered satisfactory, because the perturbation in the normal component of velocity during the passage of the spot is much smaller than in the streamwise component, requiring a better angular resolution. Therefore, the values within each element were calculated by interpolation, using a first order two dimensional polynomial.

Those values were stored in the form of a table to be read out during data reduction. If Q is the velocity inside a grid element (i,j) and $(DE_1)_{ij}$ is the voltage increment for one wire, while $(DE_2)_{ij}$ is the voltage increment for the other wire; the polynomial describing the velocity is given by :

$$(5) \quad Q = Q_{ij}+A_{ij}x(DE_1)_{ij}+B_{ij}x(DE_2)_{ij}+C_{ij}x(DE_1)_{ij}x(DE_2)_{ij}$$

similar results hold for the angles.

d) In converting voltages to velocities using the 'look-up' table, the voltage for each wire, divided by the width of the element, is in fact the element number.

The determination of velocity and angle required 7 divisions or multiplications and 4 subtractions or additions. The above procedure is schematically described in the Appendix.

The present X-wire calibration method offers several opportunities for checking the validity of the calibration range. Bearing in mind the limitations concerning the orientation of the slanted wires (fig. C.3.1), it is recommended that before each experiment some typical data records would be displayed on the calibration map. In figure C.3.4 an example of E_1 and E_2 voltages during the passage of a spot in a laminar boundary layer at four locations is given, showing also the borders of the calibration region. Such a plot cannot guarantee that all the other events will behave precisely in the same manner but it can show the trend in each kind of measurement. One may also use the computer to indicate whenever a given

voltage is outside of the calibration window (see the Appendix) so that the latter could be extended whenever the calibration window is exceeded by an arbitrary prescribed percentage of events; however, if the calibration window is exceeded very rarely, the particular event may simply be deleted from the ensemble-averaged data.

C.4 Data Reduction

In all cases considered, data was obtained with a rake of normal wires as well as with X arrays. The normal probe rake, which spanned the entire boundary layer, provided instantaneous readings of streamwise velocity component in a single event throughout the spot, while the multichannel X probe provided a two dimensional flow field over a portion of the spot. With neither probe one was able to study the boundary layer very close to the wall. The closest wire to the wall for the normal rake was 0.07 δ_t and for the X-wire rake 0.12 δ_t. The spatial resolution of the X-wire is limiting its usefulness and accuracy whenever the velocity gradient is strong. Unfortunately this fact is inescapable in a normal study of a boundary layer. At the measuring location closest to the wall the mean velocity gradient did not exceed 1 m/s per 1 mm resulting in a possible error for the mean velocity which could not exceed 3-4%. The streamwise component of velocity measured with an X array was compared to that measured with a rake of normal wires, giving additional confidence to the data. Figure C.4.1 shows the ensemble-average of the streamwise perturbation velocity component during a passage of a transitional spot in a laminar boundary layer. The dotted lines represent the time history of the streamwise component of

velocity obtained from the normal wires, and the solid lines represent the same data obtained from X-wires. It is clearly seen that, within the accuracy mentioned before, the agreement between the two sets of data is good indeed. The distribution of u' measured in the turbulent boundary layer is compared in figure C.4.2, for data obtained by the rake of X-wires and by the rake of normal wires. At y/δ_t=0.12 the measurements with an X array show that the intensity of the streamwise velocity component is 6.5% smaller than the intensity measured with an array of normal wires. The difference decreases further away from the wall and the intensity deduced from X-wire measurements becomes higher in about 5% at y/δ_t.

In order to obtain statistically meaningful results, each measurement was repeated between 100 and 300 times depending on the type of data desired. Each record contained 770 data words per wire, which included two identification words at the end. The sampling rate was 4000 per second per channel corresponding to time resolution of 250 μsec and the skew time between wires was about 10 μsec. Each record thus contained 192 msec of data at frequencies not exceeding 2 KHz. In order to represent the velocity as a function of time, a use of a one dimensional array should be sufficient; however 3 indices can describe the velocity at any time at any one of the 10 wire locations in any particular event. For example the velocity of wire number K at time J in event I may be written as:

(6) U(I,J,K)

Trying to identify a general overall shape of a repeatable phenomenon, one

may ensemble-average the data and express it in the form :

$$(7) \quad \langle U(J,K) \rangle = \sum_{I=1}^{P} U(I,J,K)/P$$

P = number of events.

Temporally averaged data which is only meaningful for steady flow may be evaluated by summing up the ensemble-average for each individual wire. By doing so, one tacitly assumes that the duration is sufficient to give a meaningful time averaged term. The number of arguments in this case reduces to one, i.e the wire number

$$(8) \quad \bar{U}(K) = \sum_{J=1}^{N} \langle U(J,K) \rangle/N$$

N = number of points.

However, when the flow is unsteady like in the case of an isolated spot, only the ensemble-averaged of the perturbation velocity has a physical meaning. Using the above mentioned formulation, the perturbation velocity is defined by

$$(9) \quad U_p(I,J,K) = U(I,J,K) - \bar{U}_1(K)$$

where $\bar{U}_1(K)$ is calculated by using (8) in the laminar boundary layer. The value for the mean perturbation is obtained by combining (7)and (9):

$$(10) \quad \langle U_p(J,K) \rangle = \sum_{I=1}^{P} U_p(I,J,K)/P$$

CHAPTER D

THE ENTRAINMENT OF LAMINAR FLOW BY AN ISOLATED SPOT

D.1. The Ensemble-Averaged Structure

The flow field in isolated transitional spots was remeasured for the sake of comparison with the flow field created by an array of interacting spots and by a fully turbulent boundary layer. Furthermore, new measuring methods using a rake of X- wires offered the opportunity to map the two components of the velocity vector across the entire boundary layer simultaneously. One would like to compare the single spot growing in a laminar boundary layer and the large coherent structure educed in a fully turbulent boundary layer after a prolonged interaction between the turbulence in a transitional spot and the turbulence in the surrounding boundary layer. ZWK (1977) observed that only a small portion of the transitional spot retained its coherence as a result of the above-mentioned interaction. The scales of the educed structure were approximately 10δ in the streamwise direction and about 4δ in the spanwise direction. The length and width of the transitional spot at a comparable location are approximately five times larger.

Figure D.1.1 describes the mean perturbation contours of the streamwise velocity component measured by a rake of hot-wires which are normal to the direction of the mean flow, and located at various y distances from the surface. The ordinate in this figure is stretched in order to exhibit the

flow field. A proper height to length ratio is obtained by multiplying the abscissa by a factor of 65 after converting the time axis to distance by using the free stream velocity; this number would be reduced to 52 if one were to use the convection velocity of the spot for the same purpose.

The flow field described by velocity perturbation relative to the laminar boundary layer in the plane of symmetry of the spot can be divided into two main regions. The rounded triangular region removed from the wall has a velocity deficit in comparison with the unperturbed laminar profile, while the velocity close to the surface is increased relative to the unperturbed Blasius velocity profile. In both regions, the maximum values of the perturbation velocity is about 30%U_∞. A similar description was already reported by ZWK (1977). One may infer from the literature (Coles and Barker 1974, WSF 1976) that the ensemble-averaged data gave rise to the interpretation that the spot can be regarded as a single eddy. Not all the features of the spot can be attributed to such a structure. Furthermore, recent data indicates that the spot contains an orderly array of smaller eddies (Leonard 1979, Wygnanski 1980); nevertheless the ensemble-averaged data is helpful for modeling the flow. Figure D.1.2a is a superposition of the mean two-dimensional velocity perturbation vectors on the streamwise -1% U_∞ and -2% U_∞ perturbation contours [i.e. $(U-U_1)/U_\infty$=-0.01 and -0.02] shown in figure D.1.1. The mean values of the velocity components prevailing in laminar flow in the x and y directions respectively were subtracted from the averaged velocity measurements for each measuring station. Namely, each streamwise component shown is given by $U-U_1$, while each normal component is given by $(V-V_1)xC$; U_1 and V_1 are the mean laminar values of

the two components. In this way the flow field before the arrival of the spot ($T < 10$ milliseconds) is described by dots which represent an unperturbed region. The scale factor C corresponds to the coordinate stretching used in figure D.1.1 and facilitates the observation of the circulatory motion of the flow field in the spot. Along most of the leading edge of the spot ($20 < T < 30$ milliseconds, and $y > 4$ mm) the flow is directed towards the surface, while the perturbation velocity of the streamwise component becomes negative. The perturbation velocity of the normal component decreases and changes its sign near the surface ($y=2.5$ mm) at the leading edge of the spot. The perturbation velocity of the streamwise component attains a minimum in the central region of the spot (corresponding to $T=35$ msec and $y > 2$ mm) while the normal component changes direction. This region may be considered as the core of the large eddy. At a later time ($T > 35$ msec) the gradient of the streamwise velocity component dU/dT becomes positive. The velocity-defect region terminates at the trailing interface, but the positive perturbation in V lingers on. The negative V perturbation component transports momentum to the fluid near the surface causing a positive perturbation in the streamwise component of velocity, while a positive V perturbation occurring at a later time is associated with a deficit in the U component of velocity at the outer region.

At the first measuring level ($y= 2.5$ mm) near the leading interface ($T=10$ msec), one may observe a positive perturbation in both U and V simultaneously. The positive perturbation of the normal velocity component (V) at the lowest measuring level ($y=2.5$ mm) is attributed to a vortex-like motion near the front portion of the spot ($15 < T < 70$ msec), caused by fluid

arriving at the plane of symmetry from other spanwise locations.

The normal velocity component attains a maximum near the trailing edge of the spot and decreases smoothly to its non-disturbed level behind the spot. Very close to the wall, the perturbation in the fluid motion is directed towards the spot's center. This region which was named by Schubauer and Klebanoff (1956) as the recovery trail, has been shown to be stable and devoid of velocity fluctuations. Assuming that the perturbation flow field in the ensemble averaged spot results from the presence of a horseshoe vortex, the direction of flow in the plane of symmetry near the trailing interface could be determined by the outward motion caused by a pair of counter-rotating streamwise vortices which are at the tail of the horseshoe vortex. The outward motion results in an additional region of velocity defect which is represented by the $-1\%\ U_\infty$ contour from figure D.1.1. This region was explored lately by Van Atta, Sokolov, Antonia and Chambers (1981) , while they were measuring the flow disturbance produced in the free stream above the turbulent spot.

The advantages of measurement with a rake of X-wires become apparent by comparing figure D.1.2a with figure D.1.2b. In the second figure the normal velocity component was calculated from the continuity equation assuming that the flow is two-dimensional ($\partial W/\partial z=0$). The scale on both figures is identical. The calculated V shows that the overall direction of flow within the spot is similar to the observed one, but not identical. The angular motion in the ensemble averaged spot in both figures may be modeled by a large vortex but the detailed comparison casts some doubt about

the assumption of two dimensionality. A case in point is the simultaneous positive velocity perturbation of the normal and streamwise components which appears near the solid surface at both interfaces of the spot, and probably results from a non vanishing gradient term $\partial W/\partial z$. Thus, the discussion of the flow field during the passage of the spot will rely on the measured V component of velocity, rather than the two-dimensional, ensemble-averaged continuity equation.

D.2 Entrainment

The spot entrains non-turbulent fluid from the laminar boundary layer and from the potential flow above it. There are a number of factors contributing to the entrainment of non turbulent fluid: firstly, there are a large number of small eddies at the interface which increase the contact area between the turbulent and non turbulent fluid thus increasing the rate of diffusion of turbulence; secondly, the non turbulent fluid is engulfed by the large eddies in a similar manner as in the free shear layer; thirdly, the large turbulent eddies induce velocity perturbations outside the interface which may further destabilize the laminar boundary layer. Figure D.2.1 shows a picture of a dyed spot photographed by GBR (1980) in a water facility. In this picture one sees an elevation view of eddies on the plane of symmetry of the spot. One may also distinguish the large parcels of irrotational fluid which were engulfed into the spot between two adjacent turbulent eddies. Similar observations were made by Falco (1977) on a fully developed turbulent boundary layer visualized by means of smoke in air.

In attempting to understand the mechanism which is responsible for the growth of the spot in both spanwise and streamwise directions, one has first to determine the region which most actively entrains non-turbulent fluid. The most obvious first step is to consider the entrainment into an ensemble-averaged spot on the plane of symmetry. For this purpose, one should know the shape of the interface and the velocity field relative to it. The task is simple in principle but requires tedious and difficult measurements. The first attempt was made by WSF (1976) who measured the streamwise component of the celerity of the leading and trailing interfaces locally and calculated the function $\int_0^H (U-U_{int})dy$ relative to the respective interface. Inferring the entrainment from this procedure implies that the flow relative to the interface is steady and two dimensional [i.e. $(\partial W/\partial z)_{z=o} = 0$]. Furthermore, the growth of the spot in the y direction has been neglected. CCD (1978) argued that in the laboratory coordinates the stream function depends on x, y and t and thus has a total differential: $d\psi = -Vdx + Udy + (\partial\psi/\partial t)dt$; which includes a time dependent term. Consequently the integration of $(U-U_{int})$ with respect to y is insufficient to calculate entrainment. They estimated the rate of entrainment by assuming conical similarity and calculating the particle trajectories relative to the interface.

In the present context an attempt is made to calculate the rate of entrainment directly from measurements, without resorting to the assumption of two dimensionality, the invariance of leading edge celerity with y, or conical similarity. The average velocity field within the spot and its vicinity was measured with a rake of X-wires. The celerity of the interface

was determined from the perturbation velocity contours, by choosing initially four characteristic features on the boundary of the spot and determining the time of their occurrence. These points mark the following locations:

locus 1. The leading edge of the spot near the surface.

locus 2. The most forward-reaching position of the leading interface (the overhang). Both loci 1 and 2 correspond to locus A of CCD.

locus 3. The location of the maximum height of the spot (locus C of CCD).

locus 4. The trailing edge of the spot near the surface (locus F of CCD).

By repeating the measurements at numerous streamwise stations on the plane of symmetry of the spot, the loci labelled 1 through 4 occur at different times depending on the location of the probe. These loci are plotted on x,t coordinates, (fig. D.2.2), in a manner suggested by CCD. Data from 8 measuring stations is shown in figure D.2.2 for streamwise locations varying from 800 to 1500 mm downstream of the spark. The loci marked may be connected by straight lines, whose slopes represent the streamwise component of the celerity of the particular features chosen. The celerity of loci 1 and 2 is $0.9U_\infty$ and that of locus 3 is not appreciably different ($0.82U_\infty$ for the Reynolds number under consideration). The celerity of locus 4 is $0.55U_\infty$. Loci 1, 2 and 3 are situated on the leading interface of the spot. Thus, one may assume that the leading interface on the plane of symmetry moves downstream with approximately constant velocity which is independent of y (y being the distance from the surface). Furthermore, the inclination and shape of the leading interface does not vary with increasing distance from the spark.

The contours $U-U_1/U_\infty=-0.02$ which may represent the boundaries of the spot outside the laminar boundary layer were measured at U.S.C by Wygnanski and Haritonidis and are shown in figure D.2.3. The streamwise separation between adjacent contours is 100 mm. This determination of the spot's boundary was first used by Coles and Barker (1975) and is repeated here for the sake of convenience; a detailed comparison between this criterion and the actual determination of the turbulent-non-turbulent interface is discussed by WSF. Even if the contour $U-U_1/U_\infty=-.02$ does not coincide with the interface of the spot it is an impartially determined characteristic feature of the spot near its outer boundary. One may deduce from figure D.2.3 that the boundaries of adjacent spots are approximately parallel which could lead to the notion that the celerity of the trailing interface in the X direction is <u>locally</u> independent of y. In order to compare the celerity of the trailing interface over long downstream distances, one has to account for the growth of the spot in the Y direction as well. It should be remembered, however, that the coordinates used in figure D.2.3 accentuate the height of the spot which is physically a very flat structure.

The variation of the maximum height of the spot with x can be roughly estimated from figure D.2.3; from it one may calculate the outward propagation velocity of the tip (fig. D.2.4). The forward 'overhang' of the spot (locus 2) does not propagate outwards in the range of the measurements shown; and it is roughly located at y=7 mm from the surface of the plate. It may be assumed that the normal component of the interface-celerity increases linearly with the normal distance from the overhang.

Thus:

$$(11)\quad (V)_{int}/(V)_{tip}=[(Y)_{int}-(Y)_{overhang}]/[H-(Y)_{overhang}]$$

where H is the maximum height of the spot.

Taking advantage of the general similarity of the spot boundaries, one may calculate the streamwise component of the celerity of the trailing interface at similar locations on the boundary, thus accounting for the growth of the spot in Y direction. The data shown in figure D.2.3 leads to the conclusion that U_{te} (trailing edge) accelerates with increasing y. In fact, only the lower portion of the trailing interface is convected at a constant celerity. These results differ from the conclusion of WSF who suggested that the celerity of each interface is constant in the plane of symmetry of the spot. The difference may stem from the fact that the measurements were made locally, mostly at the lower part ($y/H < 0.5$) of the spot (see fig. 10 of WSF).

The celerity of the interface for the elevations at which X-wire measurements are available are tabulated below:

Table 1

LEVEL	y[mm]	U_{le}/U_∞	U_{te}/U_∞	$(V_{int}/U_\infty)x10^3$
1	2.46	.9	.55	0
2	4.34	.9	.55	0
3	6.21	.9	.55	0
4	8.21	.9	.59	1.18
5	9.96	.85	.63	2.90
6	11.84	.84	.66	4.73
7	13.71	.83	.69	6.56
8	15.71	.82	.72	8.51

Figure D.2.5a represents the velocity vectors relative to the leading interface. Each tick mark on the abscissa of this figure represents either a time scale equivalent to 2 msec or a velocity scale of 2 m/sec. Each tickmark on the ordinate represents a vertical distance equivalent to 1 mm or a component of velocity in m/sec equal to $1/(U_{le}x2)$. Thus the inclination of the velocity vector is stretched by the same ratio as the slope of the interface. The vertical distance in figure D.2.5.a is roughly stretched by a factor of 18:1 relative to the horizontal distance. The same procedure was used in figure D.2.5b relative to the trailing interface. One may integrate the relative velocity component normal to the interface and obtain the average entrainment distribution into the spot on its plane of symmetry.

Table 2

	Measured			Calculated		
Boundary	Segment	Segment	Segment	Segment	Segment	Segment
Definition	1-2	2-3	3-4	1-2	2-3	3-4
Interface	21%	19%	60%	15%	5%	80%
2% perturbation	22%	14%	64%	16%	6%	78%
3% perturbation	22%	22%	56%	---	---	---
CCD	---	---	---	16%	5%	79%

The first three rows in Table 2 refer to the present results, while the results of CCD are shown for comparison in the fourth row. The measured data indicates that the leading interface entrains approximately 40% of the total entrainment estimated this way. The amount of fluid entrained under the 'overhang' (segment 1-2) is approximately equal to the amount of fluid entrained in segment 2-3. The ratio of entrainment between the leading and trailing interface corresponds approximately to the ratio of the lengths of these ensemble averaged interfaces, suggesting perhaps that both are equally active in the entrainment process.

The ensemble-averaged perturbation velocity component normal to the surface, which was calculated from the U component (see figure D.1.2b) by assuming that the average flow is two dimensional (i.e., $\partial W/\partial z=0$), was used in order to calculate the velocity vectors relative to the leading and trailing interfaces which are shown in figures D.2.5c and d respectively. The method of stretching the scale in these figures is identical to that used in the measured data (figs. D.2.5a and b) providing a direct comparison

between the measured and calculated data. The relative entrainment by the trailing interface is much stronger if one considers the calculated V rather than the measured one. The calculated results are also tabulated in Table 2. The calculated distribution of entrainment agrees fairly well with the calculated results of CCD. The apparent inactivity of the upper portion of the leading interface stems probably from the fact that the effects of the surrounding laminar boundary layer are neglected in the calculations.

D.3 Results Based on a Single Realization

The results which have been shown so far were analyzed after ensemble averaging the data. A hot wire rake containing nine wires made it possible to examine the time history of the instantaneous streamwise velocity component across the entire plane of symmetry of the spot. The velocities shown in figure D.3.1 are expressed by equation 9. The data is filtered at 250 Hz before the perturbation contours were calculated (fig. D.3.2). A comparison of the contours shown in the present figure with the corresponding ensemble-averaged contours shown in figure D.1.1 is now possible. The broken line in figure D.3.2 represents the $\pm 3\%\ U_\infty$ perturbation contours. Although the overall shape and the instantaneous contours are similar to the ensemble-averaged data, the internal structure appearing in a single realization is blotted by the averaging process for the realization shown in figure D.3.2. One may detect, at least, four regions (marked by 'E's in the figure) at which the perturbation levels attain a local maximum (minimum). The most negative perturbation($U_p=-0.35U_\infty$) appears near the leading

edge of the spot at an elevation corresponding to the local height of the laminar boundary layer . This region is followed in time by three additional defect regions with perturbation velocities ranging from $-0.3U_\infty$ to $-0.1U_\infty$.

Closer to the surface there are regions at which the excess of velocity perturbation attains a local maximum, they usually occur at later times than the corresponding local minima. Each of these pairs of defect and excess velocity regions may represent a large coherent structure. Present observations indicate that the spot contains several large eddies extending from its outer boundaries to the surface. Individual eddies were observed previously in an insipient spot by Amini (1978) who also noted that the number of eddies increases with downstream distance. Four photographs of the streamwise velocity-history taken by Amini (1978) at distances $500 \geqslant x \geqslant 200$ mm from the perturbation are shown on figure D.3.3. The free stream velocity in this experiment was 6 m/s. The number of eddies which may be deduced from these velocity histories appears to increase with x from three at x=200 mm to five at x=500 mm.

D.4 A Comparison Between The Transitional Spot And The Turbulent Boundary Layer (mean velocity)

The velocities measured in conjunction with isolated transitional spots evolving in a laminar boundary layer will now be compared with conventional measurements (time averaged) of velocity in a turbulent boundary layer. A sequence of ensemble-averaged velocity profiles taken on the

plane of symmetry of the spot is shown in figure D.4.1; the mean profiles which were measured at 8 millisecond intervals are represented by solid lines, while the laminar profiles measured at the same x location are marked by dotted lines. The velocity perturbation contours are shown in the lower part of the figure for the sake of comparison. The strongest velocity deficit in the profile occurs in the central part of the spot, while the maximum velocity gradient near the wall and the maximum positive velocity perturbation occur at the trailing edge of the spot. One may plot the velocity profiles in the spot on a logarithmic scale and compare them to the universal profiles taken in a turbulent boundary layer. Such a comparison was made previously by Coles and Barker (1975), WSF (1976) and CCD (1978). Six velocity profiles measured at X_s=103 cm and labelled in figure D.4.1 are shown in figure D.4.2. These profiles span the entire duration of the spot. A straight line drawn through the data points in the wall region and extrapolated to y^+=10 yields the friction velocity U_τ for this case. The same procedure was repeated at two additional measuring stations 84.5 cm and 122 cm downstream of the spark and the values of U_τ/U_∞ are tabulated in Table 3. The time intervals between adjacent profiles was increased with increasing downstream distance in order to preserve the scaling relative to the overall duration of the spot. The dimensionless time intervals are tabulated in the first row of table 3 followed by the values U_τ/U_∞ for the six profiles appearing in figure D.4.2. The right hand column in table 3 gives the friction velocities measured in the tripped turbulent boundary layer at the same three measuring stations. The wake component (Coles 1964) for the profiles measured at X_s=103 cm appear in the fourth row of Table 3, and is compared with the appropriate number in a fully tur-

bulent boundary layer.

Table 3

T/SPOT DURATION @Xs	0.275	0.375	0.475	0.575	0.675	0.775	T.B.L
84	.0385	.0407	.0425	.0445	.0460	.0465	.0435
103	.037	.0385	.0400	.0415	.0435	.045	.0415
122	.037	.0385	.0395	.0410	.0425	.0445	.0410
$\Delta U/U_\tau$ @Xs=103 cm	4.8	4.9	4.3	3.9	3.1	2.7	2.7

The maximum deviation of the local velocity in the outer part of the turbulent boundary layer is referred to by Coles (1964) as the strength of the wake component. This quantity ($\Delta U/U_\tau$) is a function of $Re\theta$(i.e. Reynolds number based on momentum thickness). For $Re\theta > 6000$ the wake component $\Delta U/U_\tau$ equals 2.7 and it decreases at lower Re until it completely disappears in the neighbourhood of $Re\theta=500$. When the turbulent boundary layer was artificially thickened, the strength of the wake, closer to the disturbance, was higher than its asymptotic value far downstream. Coles attributed this effect to the large eddies which originated at the roughness elements. The data on the last row of Table 3 indicates that the strength of the wake component decreases towards the trailing edge of the spot, suggesting perhaps that the scale of the large eddies also reduces as one proceeds towards the trailing edge. This observation is consistant with the dye picture D.2.1 and with the velocity contours shown in figure D.3.2, in which the contours resulting from a single realization are plotted.

The friction velocity, on the other hand, increases towards the trailing edge, reaching a maximum value at the location corresponding to the ensemble-averaged trailing interface near the surface. The friction velocity in the turbulent boundary layer measured at the same x location (X_s=103 cm) equals the friction velocity observed around the center of the projection of the spot on the surface, and lags behind the location at which the spot attains its maximum height. The average height of the spot at the location at which U_τ is maximum is 0.8 H corresponding to 1.0 δ_t. The magnitude of the wake component which is equal to the magnitude prevailing in a turbulent boundary layer occurs even closer to the trailing interface of the spot. Identical observations were made at other measuring stations.

D.5 Velocity Fluctuations

The measurement of velocity fluctuations in a non-stationary flow field requires careful definition. In a stationary turbulent flow the velocity fluctuations are defined by:

$$(12) \quad u(J) = U(J) - \bar{U}$$

where U(J) is the instantaneous velocity at a point J and:

$$(13) \quad \bar{U} = (1/T)\int_0^T U(t)dt \ .$$

In a stationary turbulent flow the average velocity may also be given by:

$$(14) \quad \bar{U} = \sum_{J=1}^{N} U(J)/N$$

where N is the number of points sampled.

In the present case the sampling of the data was initiated prior to the arrival of the spot and the duration of sampling depended on the length of the spot. Thus, the average velocity $\bar{U}$ which depends on the length of the sampling window is no longer an objective quantity and can not be used for reference. It is customary to define u by decomposing U into three components :

$$(15) \quad U = \bar{U}_1 + \langle U_p \rangle + u$$

where u is the fluctuating term; $\bar{U}_1$ is the same as in (9) and $\langle U_p \rangle$ is the value of the ensemble-averaged velocity ($\langle U_p \rangle = 1/N \sum_{1}^{N} (U-U_1)$; N=number of realizations).

One may define a local intensity of the velocity fluctuations on its root ensemble mean square value (r.e.m.s) of the u term (from eq. 15) at each measuring location as done by Van Atta and Helland (1980):

$$(16) \quad \langle u'(J) \rangle = [\sum_{I=1}^{N} (U(I,J)-\bar{U}_1(I,J)-\langle U_p(I,J) \rangle)^2/N]^{1/2}$$

where N is the number of events and $\bar{U}_1$ is calculated in the non-disturbed laminar boundary layer.

The results computed from equation 16 are shown in figure D.5.1. Equation 16 relates turbulent activity to specific regions in the spot, however, the interpretation of the results described by this equation is difficult and prone to errors. The results near the solid surface indicate that the turbulent intensity in the vicinity of the leading or the trailing interface is higher than in the central region of the spot (Van Atta and Helland 1980).

Since the length of the spot is not identical in every realization, nor is the time of arrival of the spot at the measuring station precisely repeatable, the jitter in both quantities may contribute to an apparent turbulent intensity. In order to estimate this "apparent" intensity, an attempt was made to reduce the jitter by aligning all events at one of the interfaces. The bottom trace in figure D.5.2 represents simple ensemble-averaged velocity in the vicinity of the leading interface. The trace above it was generated from the same data; however, the velocity signal in each realization was shifted by the time difference between the arrival of the interface in that realization and the average time at which the leading interface of the spot appeared at the particular location in the flow. As a result of the alignment process, the rate of increase in velocity after the arrival of the leading interface is much stronger than the rate estimated from the simple ensemble-averaged data, while in the interior of the spot the aligned and the non-aligned ensemble averages are identical. The top trace in figure D.5.2 represents the absolute value of the difference between the two methods of averaging. It is obvious that in the vicinity of the leading interface the difference is significant. The

second trace from the top represents the conventional r.e.m.s distribution of the turbulent fluctuations near the leading interface of the spot. The apparent increase in the intensity of the fluctuations relative to the interior of the spot is of the same order of magnitude as the difference between the two ensemble averages. One may thus conclude that: the apparent turbulent activity near the leading interface of the spot is an artifact of the definition of the r.e.m.s fluctuations and the method of averaging. Making the same comparison near the trailing interface of the spot leads to a similar conclusion. These results do not imply that there is no enhanced turbulent activity near the interfaces of the spot, but rather that the conventional data acquisition and the definition of intensity of the fluctuations is inadequate in this region. The time scale of the 'enhanced' turbulent activity near the leading interface of the spot corresponds to the jitter in the time of arrival of the leading interface. This was determined from the histograms of the arrival times shown in figure D.5.3a. Near the surface, for example, the average time of arrival of the leading interface from the initiation of counting was equal to 19 msec. The standard deviation from the mean is 1.5 msec. This number (also plotted in figure D.5.2) indicates that the duration of the apparently enhanced activity corresponds indeed to the standard deviation in the time of arrival of the leading interface of the spot at the chosen location. Although the jitter in this time increases at large distances from the surface, the apparent error in the determination of the r.e.m.s values of the velocity fluctuations may not necessarily increase, because only near the surface the arrival of the spot is marked by a significant increase in velocity.

The duration of the spot can be computed for each realization by knowing the time of arrival of the leading and trailing interface respectively. A histogram showing the duration of the spot is plotted in figure D.5.3b. The mean duration of the spot is shown by a vertical line drawn at each level. The standard deviation (which is marked by triangles on the baseline of each histogram) increases with increasing distance from the surface. This is particularly true if one normalizes the deviation by the local duration of the spot. The values obtained are also shown in figure D.5.3b. Further examination of the histograms indicates that the probability density distribution is not centered arround the mean duration of the spot, but appears to be lumped in groups which are merely represented by the mean duration indicated on the figure. Although the number of samples is too small for a conclusive interpretation of the histograms, the characteristic times (shown on the figure) suggest something about the interior structure of the spot. If the spot contains a finite number of large coherent eddies, then the length of the spot depends on the number of eddies within it. The probability density distribution for $y/\delta_t < 0.3$ suggests that most of the spots at this location and Reynolds number vary from one another by two to four large coherent eddies. The duration of each eddy in this case is approximately 3 msec and corresponds also to the variation in the time of arrival of the spot. During the time elapsed between the arrival of the leading interface and the trailing interface at the measuring station the spot almost doubles in length. The variation in the time of arrival of the trailing interface (fig. D.5.3c) is twice as large as the variation in the time of arrival of the leading interface. Once more the length of the spot seems to depend on the number of large coherent struc-

tures contained in it. Each structure (Kovasznay, Komoda and Vasudeva, 1962), most probably originates at the edge of the laminar boundary layer, or at least within the laminar boundary layer, and slowly grows in all three directions while propagating downstream. Thus the maximum height of the spot is comparable to the thickness of the local turbulent boundary layer. Since some structures originate later than others and they also do not extend as far out as the edge of the corresponding turbulent boundary layer, producing large variations in the maximum height of the spot and its length at the outer edge, the standard deviation in the length of the spot at its outer edge must also increase significantly (figure D.5.3b).

D.6 The Zone Averaged Intensities $\overset{\sim}{u'}$ and $\overset{\sim}{v'}$ and The Zone Average Product $\overset{\sim}{u'v'}$

In order to compare the average turbulent intensity in an individual spot to the turbulent intensity prevailing in interacting spots or in a turbulent boundary layer, one has to average the velocity fluctuations during the time corresponding to the duration of the turbulent regions only. The method used presently is the zone-averaging technique suggested by Kovasznay, Kibens and Blackwelder (1970). A telegraph signal I(t), corresponding to the occurrance of turbulence and having an average value of :

$$(17) \qquad \gamma = \bar{I} = (1/T)\int_0^T I\,dt$$

which is commonly referred to as intermittency, defines a 'turbulent zone average' of any property S by the following:

$$(18) \qquad \bar{\bar{S}}=(1/\gamma T)\int_0^T IxSdt \quad .$$

Thus the turbulent intensities of u and v were calculated during the passage of the spot as:

$$(19) \qquad \bar{\bar{u}}'=[(1/\gamma T)\int_0^T Ix(U-\langle U\rangle)^2 dt]^{1/2} \quad ; \quad \bar{\bar{v}}'=[(1/\gamma T)\int_0^T Ix(V-\langle V\rangle)^2 dt]^{1/2}$$

where, <U> and <V> are the ensemble-averaged values for the two velocity components U and V, respectively.

The intensity of the u component in isolated spots is shown in figure D.6.1, for the three measuring stations at distances of 84.5, 103 and 122 cm from the perturbation, together with the 'turbulent zone average' in a fully turbulent boundary layer. The intensity $\bar{\bar{u}}'$ (ordinate) is normalized by the free stream velocity, while distance from the surface (abscissa) is normalized by the height δ_t of a fully turbulent boundary layer existing at the particular location and Reynolds number. The zone-averaged $\bar{\bar{u}}'$ in the spot is higher by approximately 30% than the corresponding value in a fully developed turbulent boundary layer. The distribution of $\bar{\bar{u}}'$ in both flows is similar for $y/\delta_t<0.6$. It should be remembered that the turbulent bulges in a boundary layer extend beyond δ_t, therefore, if the maximum height of the spot and a turbulent bulge are to be compared, the spot data should be normalized by its maximum height, while the boundary layer data should be normalized by 1.2 δ_t (i.e. the maximum extent of the turbulent bulges). It turns out that this normalization will not improve the agreement between the data taken in isolated spots and in the turbulent boundary

layer, because the maximum height of the spot is also approximately $1.2\delta_t$. The present results in the turbulent boundary layer are compared with the data of Kovasznay et al. (1970). The agreement between the two sets of data (fig. D.6.1) is very good in spite of the different Reynolds numbers ($Re\delta_t$) at which the measurements were made (13,200 and 27,500, respectively). Similar data for the normal component of the fluctuations is shown in figure D.6.2; It indicates that the $\overline{v'}$ intensity in turbulent spots is lower than in the turbulent boundary layer. Thus, while the intensity $\overline{u'}$ within the spot is larger than the intensity prevailing in a turbulent boundary layer, the intensity $\overline{v'}$ within the spot is less than in the turbulent boundary layer. The zone-averaged $-\overline{u'v'}$ within the spot is also less than in the corresponding fully turbulent boundary layer (figure D.6.3.).

D.7 The Distribution of the Reynolds Stresses and Turbulent Intensities Along the Spot.

The zone-averaged data contains no information about the distribution of physical properties along the spot. It would be naive to assume that the distribution of the Reynolds stress and turbulent intensity along the spot is homogeneous, thus instantaneous and ensemble-averaged results are examined. The generation of turbulent energy is given, on the average, by the product $[\overline{u'v'}(\partial\bar{U}/\partial y)]$ where $\overline{u'v'}$ and $\partial\bar{U}/\partial y$ refer to time-mean data. It is not easy to correlate the time averaged production to the local instantaneous occurrence in a turbulent boundary layer. The instantaneous velocity gradient $\partial U/\partial y$ may not necessarily resemble the mean gradient. Furthermore, the instantaneous velocity gradients in other directions may

be significant in spite of the fact that they vanish in the mean; thus, when coupled with the appropriate stress they too may cause a local production of turbulence. Kline (1978) reviews some of the available results on the structure of the turbulent boundary layer obtained during the past decade and suggests that 70% of the turbulent production occurs during the outward ejection of low momentum fluid from the wall region (bursting). The rest of the positive contribution to production of turbulence is related to the inflow of high momentum fluid towards the wall layers (sweep). The scales of both phenomena are related to the large coherent eddies (Laufer and Narayanan, 1970). Since the mean production term is a product of two averages, $\overline{u'v'}$ and $\partial\bar{U}/\partial y$, one may consider one aspect contributing to the production by assuming $\partial\bar{U}/\partial y$ as being constant with time and looking for the intermittency in uv; where uv is defined by:

(20) $uv=(U-\langle U\rangle)x(V-\langle V\rangle)$

$\langle U\rangle$ and $\langle V\rangle$ are the same as in (19).

Typical time histories of the instantaneous uv product at given y locations are shown in figures D.7.1a and b for two different realizations. At $y=0.12\ \delta_t$ most of the contribution to uv occurs intermittently along the spot and the amplitude of the instantaneous uv excursions exceed by a factor of fifteen the long time-average observed in a turbulent boundary layer. At y/δ_t 0.21, 0.31 and 0.41 the instantaneous excursions in uv are often smaller.

A probability density of $uv/\overline{u'v'}_t > 15$, obtained from 90 realizations,

is shown on the lower part of figure D.7.2. ($\overline{u'v'}_t$ is the zone averaged uv product measured in a turbulent boundary layer at the same location and same ambient velocity). The highest concentration of the spikes exceeding the prescribed threshold occurs in the wall region near the leading edge of the spot. One may suspect that the activity near the interface results from the statistical method used in obtaining ensemble averaged <uv>, (see the discussion in section D.5) but the time scale of the enhanced <uv> activity is much too long to be attributed to differences in the time of arrival of the spot. The duration of the standard deviation in the spot arrival times, which is also marked on the figure, is only 1.5 msec while the enhanced<uv> activity near the wall lasts 10 msec.

The second term contributing to the local production of turbulence is the instantaneous gradient, $\partial U/\partial y$, along the spot. Unfortunately the number of instantaneously measured velocities in a profile does not suffice for proper differentiation and therefore the ensemble-averaged data is presented instead (figure D.7.2, top). The dark lines represent a low-pass filtered velocity gradient $\partial\langle U\rangle/\partial y$ which was averaged over 100 events. The dotted lines represent a portion of the velocity profiles shown in figure D.4.1; the boundaries of the spot (i.e the 2% U_∞ perturbation contour) are shown on this figure for ease of comparison. The distribution of the velocity gradient before the arrival of the spot is identical to the gradient prevailing in a laminar boundary layer. Soon after the arrival of the spot there is an abrupt increase of approximately 40% in the maximum value, $\partial\langle U\rangle/\partial y$ occurring near the surface. The distribution of $\partial\langle U\rangle/\partial y$ remains similar during the passage of the spot, but the maximum value of

$\partial\langle U\rangle/\partial y$ at the trailing edge exceeds by a factor of 2 the maximum value in the laminar boundary layer. The data was obtained by a rake of wires fixed in space, thus when $\partial\langle U\rangle/\partial y$ near the wall is large, there are too few data points to determine its value accurately. The distribution of $\partial\langle U\rangle/\partial y$ in the central region of the spot (marked on the figure) is almost identical to the distribution of $\partial\langle U\rangle/\partial y$ in a fully turbulent boundary layer.

One may examine the contribution to the production of turbulence at each section along the spot, by calculating the value of $\langle uv\rangle x\partial\langle U\rangle/\partial y$. The closest location to the surface at which u'v' data is available is: $y=0.12\,\delta_t$, at this location ensemble averaged velocity gradient during the passage of the spot is increased by a factor of 1.6. The ratio between $\langle uv\rangle$ at the leading edge and $\langle uv\rangle$ at the trailing edge of the spot was found to be 2.5, therefore the production at the leading edge exceeds the production at the trailing edge by a factor of 1.56 (which is 2.5/1.6). Closer to the surface, however, the distribution of the ensemble averaged turbulence production along the spot may be different.

CHAPTER E

INTERACTION OF SPOTS GENERATED IN TANDEM

E.1. The Mean Velocity Field

In spite of their complexity, isolated spots may still be regarded as fundamental structures in the transition process. In this experiment they were generated artificially by an electric discharge or a jet emanating momentarily from a small orifice in the plate. An insertion of a roughness element instead of a momentary disturbance results in a generation of a continuous cone of turbulence spreading laterally with increasing distance downstream. The cone of turbulence degenerates into an array of spots whenever the Reynolds number is reduced below a certain threshold level. A further reduction in Re does not trip the boundary layer. In the transitional Reynolds number range, the spots appear randomly in time although they occur directly downstream of the perturbance. In order to simplify the data aquisition process and the concommitant statistical analysis, one may produce spots at regular intervals, from a single source and let them interact downstream. The interaction process generates a quasi steady turbulent boundary layer which is discussed in this chapter. The spots are considered merged whenever the intermittency factor becomes unity for $y/H < 0.3$ (since H corresponds to $1.2\ \delta_t$ in a fully turbulent boundary layer in absence of pressure gradient and the latter is intermittent whenever $y/\delta_t > 0.4$).

The present experiment could be performed most naturally by generating a continuous array of spots at equal time intervals. In such an experiment the data would be acquired continuously, provided one channel was connected to the spot-generator for time reference. However, the spark perturbing the laminar boundary layer is generated by a high voltage source (20 KV) which induces spurious signals on the data acquisition lines. It is thus advantageous to digitize the data while the spark generator is idle. By interrupting the electric discharge during the acquisition of data, one generates a train of spots whose length depends on: the frequency of the disturbance, the distance between the generator and the measuring station and U_∞. Only the first and the last spots in the train are different from the rest because they interact, at one of their interfaces, with the unperturbed laminar boundary layer rather than a neighbouring spot; this is advantageous because it enables one to assess the effects of partial interaction on the overall structure of the spot.

An array of five successive spots originating from a point source at predetermined time intervals was monitored by a rake of hot-wires located on the plane of symmetry at several distances downstream of the disturbance. The degree of interaction between adjacent spots could be altered by either changing the frequency of their generation, or by changing the downstream distance at which the spots were monitored. Two sets of velocity histories are shown in figures E.1.1a and b. Individual spots are clearly recognizable in figure E.1.1a, where the time interval between adjacent spots was 66 milliseconds and the measurement was made 86 cm downstream of the disturbance; however, when the time interval was decreased

to 40 milliseconds at Xs=124 cm, a continuously turbulent velocity signature was observed over a large fraction of the boundary layer thickness. This signal is quite similar to velocity histories measured in a fully turbulent boundary layer although a periodic behaviour is visible at large distances from the surface.

A velocity profile obtained by ensemble-averaging the data over all the events and then averaging over time (excluding the first spot and the calm region behind the last spot in an array) is shown in figure E.1.2 for the various cases considered. Measurements made in the fully turbulent boundary layer at the same location on the plate are marked by diamonds on the figure. The interaction of successive spots produces a mean velocity profile which tends to a conventional profile as the interaction becomes stronger. An array of transitional spots will give rise to a logarithmic profile whenever $T_n=\Delta TU_\infty/Xs < 0.4$, where ΔT is the time interval between adjacent spots (Wygnanski 1978).

When the velocity histories are ensemble averaged conditionally to the first spark, the periodic behaviour introduced by the disturbance becomes apparent. Contours of constant velocity patterns are plotted in figures E.1.3a,b and c. The contours representing excess of velocity relative to the mean are shown as solid lines, while the contours showing defect are marked by dashed lines. The perturbation contours in figures E.1.3 refer to the laminar velocity profile existing at the measuring station in absence of any disturbance. When the dimensionless interval between adjacent spots is $T_n=1.16$, the velocity perturbation contours (fig. E.1.3a) are

very similar to those plotted for the isolated spots (fig. D.1.1). The contours showing positive velocity perturbation which stretch over a long time period behind an isolated spot appear to join together in figure E.1.3b, where T_n=0.465. This time interval is sufficiently short to result in a continuously turbulent signal near the surface. Two velocity profiles are drawn to the same scale in the upper left corner of figure E.1.3c, one shows a velocity distribution in laminar flow, the other the turbulent velocity profile, both existing at Xs=124 cm. The perturbation contours shown in the figure correspond approximately to the difference between the two profiles when the Blasius profile is taken as reference. The sequential interaction of transitionsal spots contains therefore some of the most important elements of the turbulent boundary layer which justifies this somewhat artificial experiment.

E.2 The Ensemble-Averaged Structure and Entrainment

In this section the ensemble averaged structure resulting from the interaction of spots originating from a single source is examined. For this purpose the shortest time interval (27 msec) between successive spots was chosen in order to assure that the dimensionless time (T_n) at the first measuring station (Xs=84.5 cm) was less then 0.4. As mentioned before, (sec. E.1), T_n=0.4 represents a threshold value below which the spots merge to form a continuous region of turbulent flow. Thus, for the chosen time interval, the free stream velocity and distances from the source, the value of T_n varied from 0.31 to 0.22. The mean velocity perturbation contours on the plane of symmetry, 103 cm downstream from the disturbance are

represented in figure E.2.1. The perturbation velocity was calculated relative to the laminar boundary layer profile (using eq. 9), repeating the procedure adopted for the isolated spots (fig. D.1.1). The first spot in the array maintains a maximum height of H/δ_t=1.2, which is equal to the maximum height attained by isolated spots in spite of the fact that its trailing interface was overtaken by the leading interface of the following spot. All spots, with the exception of the last one, lose the 'calm' high velocity region which always follows an isolated spot. As a result of the interaction, the absolute level of the perturbation $(U-U_1)/U_\infty$ is reduced by approximately 20% in comparison with similar perturbations observed in the isolated spots.

The -2% perturbation contour, assumed to represent the average position of the interface, oscillates around a mean location y/δ_t=0.78. The convection velocity of the leading interface is fairly constant ($0.88U_\infty$) and is independent of the degree of interaction between successive spots which is determined by "T_n". This is in agreement with the data of Savas (1979) who observed that the celerity of interacting spots is constant ($0.88U_\infty$), independent of their scale. The celerity of the trailing interface, however, increases from $0.55U_\infty$ at T_n=0.96 to a value of about $0.8U_\infty$ at T_n= 0.26. With the exception of the extreme spots in the train, the perturbation contours of the streamwise component of velocity can be divided into two families. In the outer region of the boundary layer the defect contours are wavy and parallel to one another. Near the surface the excess-velocity contours are almost straight and parallel to the solid surface. The crests of the defect contours correspond to the high points on

the spots while the valleys correspond to the potential fluid engulfed in the region of interaction between adjacent spots. One may draw straight lines (fig. E.2.1) joining the bottom of the valleys or the crests of all contours for a given ensemble averaged case. The inclination of these lines to the surface is 15^{o} for the valleys and 10^{o} for the crests when based on an average convection velocity $0.88U_{\infty}$. It is interesting to compare these results with the data presented by Brown and Thomas (1977) who correlated the shear-stress near the surface with the streamwise velocity at four locations in the turbulent boundary layer over short-time periods. The location of the probes at which the correlation was maximum at T=0 could be nearly connected by a straight line inclined at 18^{o} to the wall. The large coherent eddies in a fully turbulent boundary layer when visualized by smoke are inclined to the surface at approximately the same angle (see Falco 1977). The turbulent non-turbulent interface for the interacting spots was detected in the usual manner (e.g WSF 1975) for the case when T_n=0.465. The average shape of the interface is clearly distinguishable between y/δ_1=1.3 and y/δ_1=2.2 (fig. E.1.3b). The leading interface is inclined to the surface of the plate at 18^{o}. Since the crests of the spots or the valleys interconnecting them are not always at the same elevation above the surface, it is difficult to define the average position of the interface for $y/\delta_1 > 2.2$ and $y/\delta_1 < 3.2$ unambiguously. One may notice in figure E.1.3b that the 2% defect perturbation contour no longer coincides with the location of the interface. When $T_n < 0.4$, in fact, no contour representing constant velocity perturbation is even approximately parallel to the interface.

The flow field within the region of interaction may be examined by plotting the ensemble averaged perturbation velocity vectors in the X-Y plane obtained from a rake of X-wire probes (fig. E.2.2). The perturbations considered are relative to the laminar boundary layer (using eq. 9 and 10 for $\langle U_p \rangle$ and $\langle V_p \rangle$). The -2% U_∞ perturbation contour is also replotted in figure E.2.2 for reference. A negative value of the normal velocity component is observed only once near the leading interface of the first spot, where the flow is free from interactions with other turbulent structures. The normal velocity component during the passage of the other spots in the array is rarely negative, resembling the prevailing direction of the flow inside a transitional spot (fig. D.1.2a). There is however an apparent periodicity in the magnitude of the outflow from the surface, matching the time interval between spots.

The rate of entrainment of irrotational fluid by a turbulent boundary layer is always of interest because it is coupled with the growth of the boundary layer and often serves for calculation purposes (Head 1958). The entrainment of irrotational fluid by an array of successive spots on their plane of symmetry may not only give us some insight into the kinematic description of the entrainment process but also into the relative importance of some three dimensional effects. The following calculations were done in the same manner as for the isolated spot (section D.2):

(i) The entrainment was calculated relative to the -2% U_∞ contour.

(ii) The velocity field in the X-Y plane is provided by the rake of X-wires.

(iii) The streamwise component of the celerity of the interface ($U-U_1=-2\%\ U_\infty$) is obtained from the arrival times of the interfaces at the three x-stations at which measurements were made. The celerities of the leading and trailing interfaces far away from the surface are $0.9U_\infty$ and $0.8U_\infty$ respectively. It is difficult to estimate the celerity of the interface precisely, in particular in the region where two adjacent spots merge. (i.e. at the bottom of the turbulent valleys). Fortunately however, the difference between the celerities of the leading and trailing interface is not as large as in the isolated spot, and the possible error incurred in the calculations of the entrainment is not large.

(iv) The normal component of the celerity of the interface is estimated to be a constant independent of y: $V_{int}/U_\infty=6.5\times10^{-3}$. This estimate is based on the rate of growth of the apex of a typical spot in the array with downstream distance. In isolated spots V_{int} varies with normal distance from the "overhang" and although the same variation may still exist in the present case the total variation in the height of the interface (which is approximately 15% δ_t) does not warrant the added difficulties in calculating the entrainment.

(v) The total amount of fluid entrained by a typical spot

in an array on its plane of symmetry is obtained by integrating the normal velocity component relative to the interface over the length of the interface.

For the specific case chosen, the rate of entrainment is 6.5×10^{-3} m^2/sec; 40% of which occurs through the leading interface.

The flow field relative to the ensemble averaged interface of a typical front in an array, (fig. E.2.3a) may be compared qualitatively with the flow field relative to a bulge in turbulent boundary layer, observed by Blackwelder (1970) and reproduced in figure E.2.3b. The scales of the bulge and the spot are different, because the latter contains a number of eddies (section E.3) which do not retain their precise phase relative to the interface; nevertheless the general flow field relative to the interface is similar in both cases.

One may compare the entrainment calculated, by assuming that the spots in the array are two dimensional, with the entrainment calculated from their overall growth-rate; or, the gross behaviour of the comparable two dimensional turbulent boundary layer. The rate of entrainment of irrotational fluid in a turbulent boundary layer is given by:

(21) $dq/dX = d/dX\{U_\infty(\delta_t - \delta_t^*)\}$ (Head 1958)

and is tabulated below:

Table 4

	$U_\infty(\delta-\delta^*)x10^3[m^2/sec]$		$(1/U_\infty)x(dq/dX)x10^4$		$((1/U_\infty)xq/U_\infty\Delta T)x10^4$
X_s [cm.]	SPOT TRAIN	T.B.L	SPOT TRAIN	T.B.L	2-D CALCULATIONS
84.5	144.7	143.4	139	131	---
103	170.5	167.6	133	132	27
122	195.7	192.8	---	---	---

The rate of growth of spots in a train is similar to the rate of growth of the turbulent boundary layer and is roughly equal to 1.3% of the free stream velocity. The entrainment velocity calculated assuming that the flow is 2-dimensional is 5 times smaller! The discrepancy between the two methods of calculation stresses the relative importance of the entrainment in the X-Z plane (i.e by the V and W components of velocity). Furthermore, calculations based on ensemble averaged data underestimate the entrainment because both the contortions of the interface and the velocity relative to it are smoothed by the averaging process.

E.3 A Single Realization

One often asks how much information is lost by the averaging process and how much distortion may be introduced by a particular eduction scheme. A simple answer may be obtained by comparing an individual realization with the ensemble-averaged data. The velocity history, measured with a rake of normal wires, was low-pass filtered at 250 Hz (fig. E.3.1) and used for plotting the streamwise perturbation contours (fig. E.3.2). A comparison is made with the 3% ensemble averaged perturbation contours which are represented in the figure by the dashed lines.

Four successive spots can be identified by the outward excursion of the -3% contour, which occurs at the same time as the corresponding ensemble averaged results. However, while the ensemble average contours show only 4 eddies corresponding to the four artificially evoked spots, the single realization is composed of at least twice as many eddies. One may identify 2 eddies per spot which are marked by A and B on the figure. With the exception of the leading spot, the length scale of the average structure is approximately 6δ which is, at least, comparable to the length scale of the large coherent eddies educed by correlation techniques (Kovasznay et al. 1970), or to the structure evoked by letting a spot interact with a tripped turbulent boundary layer. The number of structures observed in a single realization of an isolated spot at comparable Re is much larger than two. It is thus suggested that the number of large eddies in a spot is reduced by the interaction process; this is accompanied by a corresponding reduction in the scale of the spot and also a reduction in its capability

to engulf non-turbulent flow.

The flow in a single realization was also examined by plotting the instantaneous velocity vectors, relative to the convection velocities of the interface in the T-Y plane (fig. E.3.3). (i.e $0.88U_\infty$ was subtracted from the measured streamwise component of velocity, and an average normal component of the interface celerity ($0.0065U_\infty$) was subtracted from the normal component of velocity). The approximate length of the eddies, which appear in this figure, is only $2\delta_t$ as was deduced from multiplying their duration time (3-4 msec) by the streamwise convection velocity ($0.88U_\infty$). Thus it appears that the scale of the large eddies in interacting transitional spots is comparable to the large scales in a normal turbulent boundary layer.

E.4 The Distribution of Mean Velocity

The evolution of the mean profile in an array of spots is examined in figures E.4.1 and E.4.2. In figure E.4.1, the ensemble averaged streamwise velocity profiles taken at 8 msec intervals (solid lines) are compared with the laminar velocity profile (dots), existing at the same location (X_s=103 cm). The ensemble-averaged profiles at each section are also compared with the time averaged profiles along three central spots in the array (figure E.4.2). The appropriate perturbation velocity contours are replotted in figures E.4.1 and E.4.2 for ease of comparison. The ensemble-averaged and the time-averaged profiles are almost identical, provided the first spot in the trains is excluded from the comparison. The velocity profile in the

latter may deviate by $0.1U_\infty$ from the time average profile in the interacting spots.

The ensemble averaged profiles plotted on a semilogarithmic scale and taken at three successive locations ranging from 84.5-122 cm downstream from the perturbation are plotted in figure E.4.3 (upper part). The Reynolds number based on the momentum thickness increases, with increasing downstream distance from 1200 to 1700, and the wake component increases from 1.5 to 2.7. When comparing these results with the corresponding logarithmic profiles in the turbulent boundary layer at the same Reynolds numbers (figure E.4.3, lower part), one may observe that:

(i) The velocity distribution in the wall region converges to the same logarithmic law, but the friction velocity in the case of the interacting spots is 4% higher than in the fully developed turbulent boundary layer.

(ii) The wake component of the interacting spots is smaller by 40% at X_s= 84.5 cm and by 10% at X_s=122 cm.

One may attribute the high friction velocity and the low wake component seen in interacting spots to a smaller number of coherent eddies contained in the spot relative to the number of eddies contained in a turbulent boundary layer during the same period of time. Similar behaviour was observed in a turbulent boundary layer with increasing x, i.e, the friction velocity decreases while the momentum thickness increases. Seven of the ensemble averaged profiles (measured at X_s=103 cm) marked by arrows in figure E.4.1 are replotted on semilogarithmic scale (fig. E.4.4) and the con-

stants derived from this plot are compared with the universal constants recorded over the years in a turbulent boundary layer.

The values of the friction velocity and of the wake component for these profiles are tabulated below:

Table 5

Time [msec]	$\Delta U/U_\tau$	U_τ/U_∞
84	2.05	0.0435
88	2.27	0.0435
92	2.73	0.043
96	2.50	0.043
100	2.10	0.043
104	1.40	0.044
108	1.80	0.044
T.B.L	2.70	0.0415

The results indicate that the friction velocity in the central region of the spot is higher than in the turbulent boundary layer while the concomitant wake component is lower. One may conclude that, for $Re_\theta < 1700$, the interaction among successive spots is not complete and that the distribution of the friction velocity and of the wake component along the spots is not homogenuous.

E.5 Turbulent Intensities and Reynolds Stress

The calculation of turbulent intensities and Reynolds stress during the passage of a train of spots raises similar difficulties to the ones encountered in the analysis of isolated spots. The flow is non-stationary, thus the analysis of the data should be conditioned to the leading interface of the second spot and the duration of the sampling window should contain an integral number of events ($\Delta T \times N$ when ΔT is the time interval between successive spots). The fluctuations were calculated by subtracting the ensemble averaged data from the instantaneous values.

The level of the u fluctuations in the interacting train of spots, far from the surface, is lower than the level encountered in the isolated ensemble averaged spot by approximately 20% (fig. E.5.1). The regularity at which these spots are generated, which smoothes the contortions of the outer interface, may also cause smaller variability in the instantaneous velocity and thus reduce the apparent intensity of the turbulent fluctuation. The intensity in the vicinity of the leading interface of the first spot in the train is also higher than the intensity prevailing in other spots and resembles the effect discussed in section D.5 (fig. E.5.1). In order to check whether this effect stems from the jitter in the time of arrival of the leading spot at the measuring station, a histogram of the arrival times was calculated together with the standard deviation from the mean time of arrival (see insert on fig. E.5.2). This data was compared and found to be identical to the standard deviation calculated previously for isolated spots, suggesting that the increase in the intensity $\tilde{u}'$ near

the leading interface is probably an artifact of the statistical procedure. The zone-averaged distributions $\tilde{u}'$ and $\tilde{v}'$ are shown in figure E.5.3 and compared to the zone-averaged data in a fully turbulent boundary layer. The agreement between the two distributions is good. The values of the $\tilde{u}'$ intensity drops below the values observed in the turbulent boundary at $y > \delta_t$ as a result of the decrease in the height of the spots within the array.

The intensity of the normal fluctuations $\tilde{v}'$ is somewhat lower for $y > 0.5\ \delta_t$. The agreement between the distribution of uv in interacting spots and the turbulent boundary layer is poorer than between the intensities of u and v separately. Near the surface ($y < 0.4\ \delta_t$) the value of $-\widetilde{u'v'}$ in the case of the interacting spots is higher than in the turbulent boundary layer, while in the intermittent region ($y > 0.6\ \delta_t$) it drops below the prevailing value measured in a turbulent boundary layer by as much as 30% locally (fig E.5.4). An examination of the uv signal reveals that the largest excursions in uv occur in the wall region near the leading interface of each spot (marked by "LE" in figures E.5.5a and b) suggesting that turbulent production does not occur randomly in the spot.

E.6 Observations Made Far Away From the Plane of Symmetry

Thus far, the flow field resulting from the interaction of successive spots generated in tandem, was examined only on the plane of symmetry, directly downstream of the perturbation. Some effects of the interaction on the spanwise evolution of the spots are discussed in this section. Measurements were made with a rake of normal wires located at $z/X_s = 0.15$,

while a single wire located on the plane of symmetry (i.e at $z/X_s = 0$) monitored the passage of the spots.

A typical velocity history, resulting from a passage of an isolated spot is shown in figure E.6.1. The uppermost trace in this figure was recorded by the monitoring wire at $z/X_s = 0$ while the other 9 traces refer to the rake of wires located at $z/X_s = 0.15$ and $0.07 < y/\delta_t < 0.995$ as marked. The wave packet following the spot is clearly seen at $y/\delta_t < 0.12$ (see WHK, 1979). The duration of the spot at $z/X_s=0.15$ is much shorter than on the plane of symmetry as may be deduced by comparing the duration of the turbulent signatures at $z/X_s=0$ with signatures recorded at $z/X_s=0.15$.

The velocity history during the passage of a train containing 5 spots is shown in figures E.6.2a,b. Although the trace recorded at z=0 shows clearly the passage of 5 successive events at intervals of 33 msec (i.e $T_n = 0.32$), the trace recorded at $z/X_s = 0.15$ shows only either 3 or 4 distinctive turbulent regions (see fig. E.6.2a and fig. E.6.2b respectively). The second and fourth spots are missing in figure E.6.2a while the third spot is missing from figure E.6.2b.

A telegraph signal representing intermittency is plotted in figure E.6.3 and a probability density distribution for a region to be turbulent is plotted in figure E.6.4. The first spot in the train is on the average the widest. The second spot in the train is narrower than the rest because in 50% of the events the turbulent region did not reach $z/X_s = 0.15$. The probability distribution indicates that the remaining 3 spots in the train

are wider than z/X_s =0.15 in approximately 75% of the events. This effect may be linked with the "eddy transposition" phenomenon observed by Savas (1979), however this could not be proven in the experimental setup described. The prolonged interaction of spots in the streamwise direction may simply cause a reduction in their width.

The wave packet trailing every individual spot all but disappears as a result of the interaction process.

CHAPTER F

LATERAL INTERACTION BETWEEN TWO SPOTS

The evolution of two spots, evoked simultaneously, was investigated by Elder (1960). A plan view of the intermittency contours in the region of interaction between the two spots indicated that the spreading rate of each spot was not influenced by the presence of its neighbour. In the first part of this experiment the vertical evolution of two spots was examined by monitoring the velocity field in the plane of symmetry between two spots generated simultaneously from two sources located 15 cm apart in the spanwise direction. The ensemble average contours of the streamwise component of the velocity perturbation on the plane of symmetry between the spots is shown in figure F.1 (by solid lines).

Switching-off one of the spots generators and recording the data at the same location (i.e $z/X_s = 0.06$ for a single spot) provides direct estimate of the importance of such interaction (fig. F.1 by dashed lines). The effects of the interaction seem negligible near the surface although the maximum height of the contours, produced by the interacting structures, may be somewhat increased. Elder's observation related to the superposition of spots is thus valid. The ensemble averaged velocity vectors (figs. F.2a,b), obtained from a rake of X-wires, indicates that two large eddies may be required to represent the velocity field in the laterally interacting spots (i.e the average sense) while only one may suffice to represent the velocity field in isolated spots.

By delaying the generation of one spot relative to the other, one may observe the interaction of two spots in a skewed configuration (fig. F.3). All the preliminary data available confirms the superposition observation of Elder. The relatively small effects produced by the interaction of neighbouring spots are in accord with the supposition that the spot contains a number of large eddies which are continuously interacting among themselves.

As was shown before, the pattern of spots created in tandem is not the best for generating a synthetic turbulent boundary layer (in agreement with the conclusions of Savas 1979). However, since the growth of the spots is non-sensitive to the presence of other spots at different spanwise locations, an optimistic way of generating the turbulent boundary layer, plus marking large structures in it would be: to spread over the surface a small number of spot generators which may be activated randomly.

CHAPTER G

CONCLUDING REMARKS

The simulation of a fully developed turbulent boundary layer by an array of artificially generated transitional spots, which are allowed to interact under controlled conditions, was examined. The turbulent boundary layer is usually described statistically using time averaged quantities of mean velocity, turbulent intensity, Reynolds stress and space-time-correlations. More recently conditional sampling techniques are used in an attempt to understand the mechanism governing the structure of the turbulent boundary layer.

An array of successive transitional spots, generated from a single source at regular time intervals, simulates the mean velocity profile encountered in a turbulent boundary layer fairly well. A comparison of the logarithmic and the wake components of the velocity profile reveals no major differences between the synthetic and the natural turbulent boundary layers. (The term synthetic boundary layer was coined first by Coles and Barker 1975).

Although the periodicity at which the spots were generated could easily be detected by considering phase-locked averaged data, the turbulent intensity and the Reynolds stress (averaged over time) within the turbulent zone of the synthetic and the natural boundary layers were very similar. The excursions of the interface in the synthetic boundary layer were, of

course, periodic and limited in their outward extent in comparison to the natural boundary layer. The flow was intermittent between $0.4 < y/\delta_t < 0.9$ while it is so between $0.4 < y/\delta_t < 1.2$ in the natural boundary layer. Thus in the synthetic turbulent boundary layer all large coherent eddies may be considered equal while they vary in size in the natural case. This inequality may be traced to the various origins of the large eddies which are probably quite randomly located in the turbulent boundary layer.

The engulfment of non turbulent fluid by spanwise oriented vortices was considered. Firstly an attempt was made to estimate the rate of entrainment on a plane of symmetry of an isolated spot from the ensemble-averaged data. Such estimates were made previously by CCD and WSF; the novelty in the present approach stems from the following:

(i) Both streamwise and normal velocity components in the X-Y plane were actually measured, while in previous investigations the normal component was calculated by assuming two dimensional flow.

(ii) The average celerity of the interface was determined in the X and Y directions from a large number of measurements at successive downstream locations.

Previously the celerity of the interface was calculated assuming conical similarity (CCD); it was assumed to be constant across the boundary layer (WSF). The calculations based on the recent data suggest that the leading interface of the isolated spot entrains non turbulent fluid much more vigourously than previously believed. The same entrainment calcula-

tions were applied to the array of interacting spots and were compared to the entrainment required to sustain the overall rate of growth of the spots. It transpires that the two-dimensional calculations of entrainment can account for 20% of the total rate of entrainment necessary to maintain the known rate of growth, the rest has to come from vortices oriented in the streamwise direction, which engulf non turbulent fluid in the X-Z plane. Streamwise vortices are clearly observed by flow visualization (CCD, GBR, Matsui, 1980 and most recently Carlson and Widnall, 1981) they are also observed in a free shear layer (Bridental, 1978) and are largely responsible for the mixing of species.

The use of a hot wire rake which spans across the boundary layer enables one to consider the instantaneous velocity field and compare it to the ensemble average data. It is obvious that considerable amount of information is lost by the averaging process. A single spot contains several large coherent eddies and an array of successive spots after a prolonged interaction contains twice as many eddies as spots in the array. The isolated spot is not equivalent to a single eddy, however, the eddies within the spot must be arranged in some preferred order to give the spot its universal shape.

Spots generated at the same instant at different spanwise locations appear to grow independently of one another and not inhibit each others growth (see also Elder 1960). Successive spots generated from the same source inhibit the growth of one another as a result of the interactions. In terms of ensemble averaged quantities, this inhibition is manifested by

an acceleration of the trailing interfaces in an array of spots relative to the isolated spot surrounded entirely by laminar flow. One may argue that the orientation of the individual eddies in a spot determines the effect of its interaction with surrounding similar structures. Since the eddies are basically oriented longitudinally in the streamwise direction the interaction of successive spots may severely inhibit their growth process, while interaction with neighbouring spots in the spanwise direction represents no restriction on the growth of these eddies.

The conventional statistical methods used presently to describe the mean flow in a transitional spot are inadequate. An attempt to present physically meaningful ensemble averaged turbulent intensities in this flow (see Antonia, Chambers, Sokolov and Van Atta 1981) is even less adequate, because it incorporates errors resulting from variations in the time of arrival of the spot at the measuring location; jitter in the length of the spot etc. Some of these effects have been diagnosed and assessed but there is no clear alternative description. One should define a statistical representation which will reveal the detailed structure of the ensemble averaged spot and at the same time ensure that it is representative of the single realization.

APPENDIX

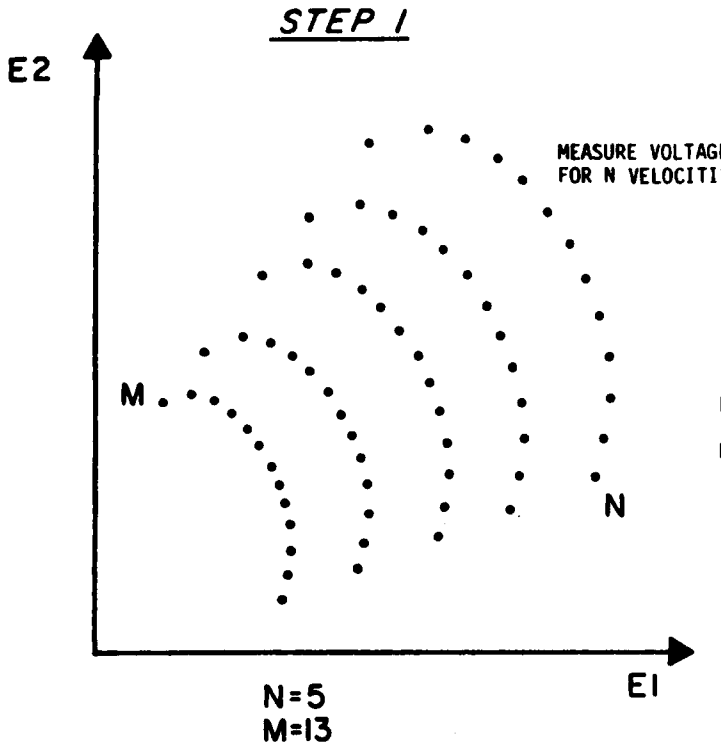
STEP 1
E2
E1
M
N
N=5
M=13
MEASURE VOLTAGES E1 AND E2 OF AN X-WIRE FOR N VELOCITIES AND M ANGLES.
Q(N)
α(M)
SELECTED
E1(N,M)
E2(N,M)
MEASURED

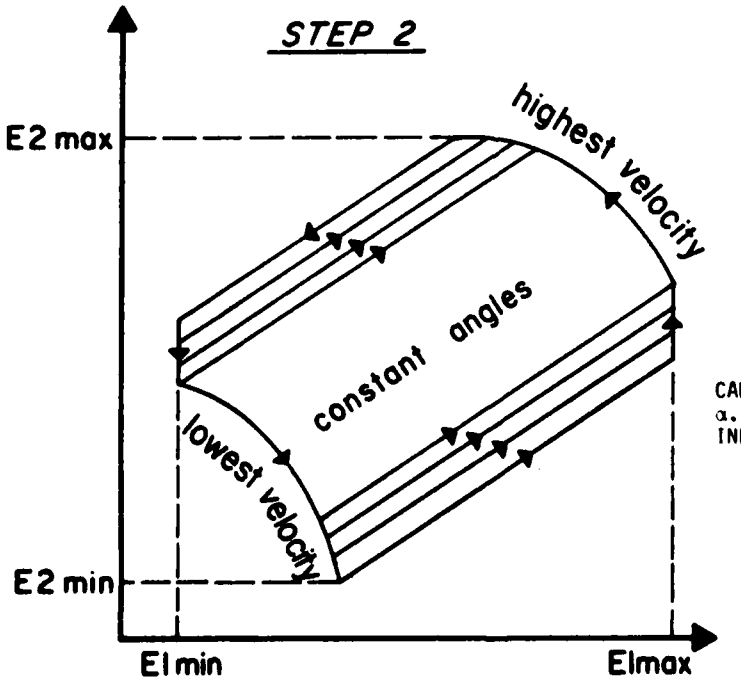
STEP 2
E2 max
E2 min
E1 min
Elmax
highest velocity
constant angles
lowest velocity
CALCULATE SPLINE COEFFICIENTS FOR Q, α, AND E2 ALONG LINES WITH E1 AS INDEPENDENT VARIABLE.

STEP 3

FINDS α, E2 AND Ω FOR EACH DE1 INCREMENT WITHIN CALIBRATION REGION USING COEFFICIENTS OBTAINED IN STEP 2

P=NUMBER OF INCREMENTS

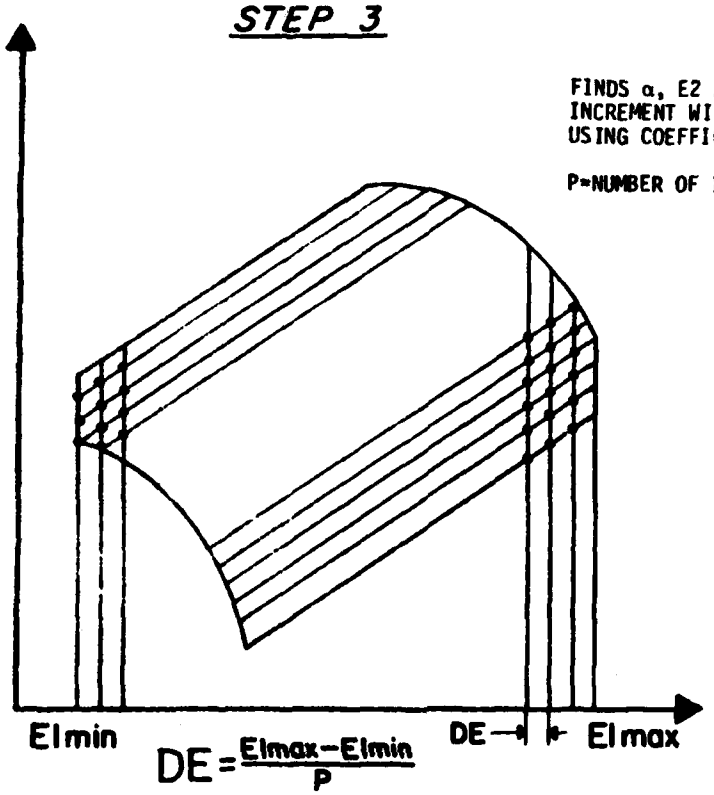

$$DE = \frac{Elmax - Elmin}{P}$$

STEP 4

OBTAIN Q AND α ON EACH GRID POINT WITH E1 AND E2 AS VARIABLES.

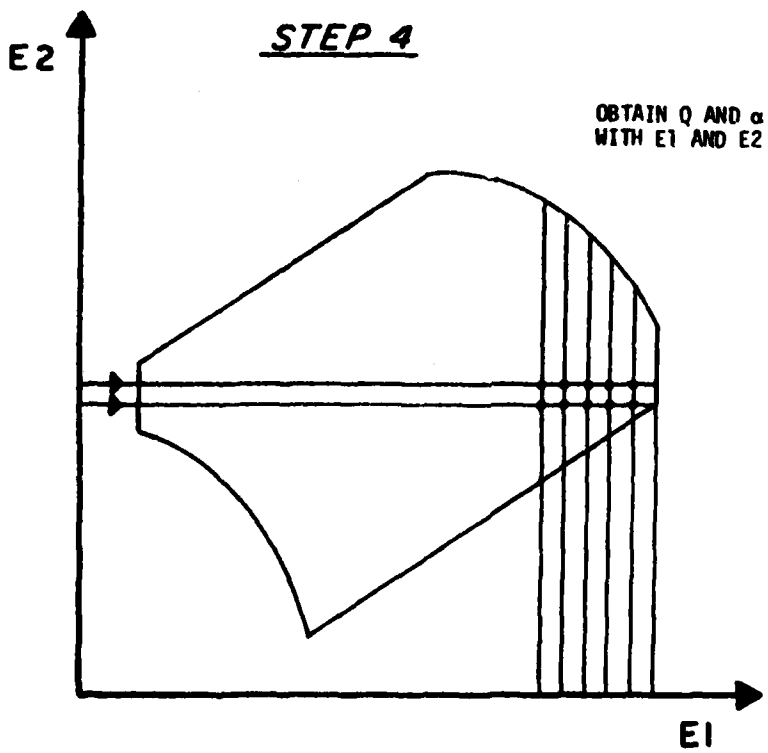

STEP 5

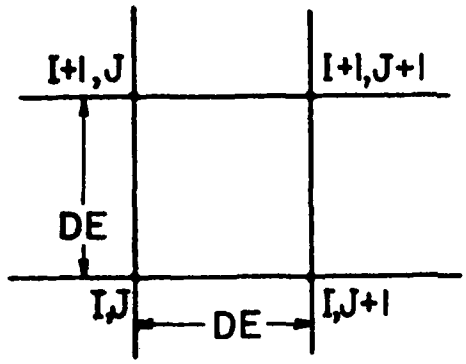

FIND THE FOLLOWING COEFFICIENTS:

A_α, B_α, C_α, A_Q, B_Q AND C_Q, OF A TWO DIMENSIONAL LINEAR POLINOMIAL BY SOLVING SIX EQUATIONS WITH Q AND α KNOWN AT EACH POINT.

THREE EQUATIONS FOR Q

$$Q(I+1,J) = Q(I,J) + DE*B_Q$$

$$Q(I,J+1) = Q(I,J) + DE*A_Q$$

$$Q(I+1,J+1) = Q(I,J) + DE*A_Q + DE*B_Q + DE^2*C_Q$$

THREE EQUATIONS FOR α

$$\alpha(I+1,J) = \alpha(I,J) + DE*B_\alpha$$

$$\alpha(I,J+1) = \alpha(I,J) + DE*A_\alpha$$

$$\alpha(I+1,J+1) = \alpha(I,J) + DE*A_\alpha + DE*B_\alpha + DE^2* C_\alpha$$

STEP 6

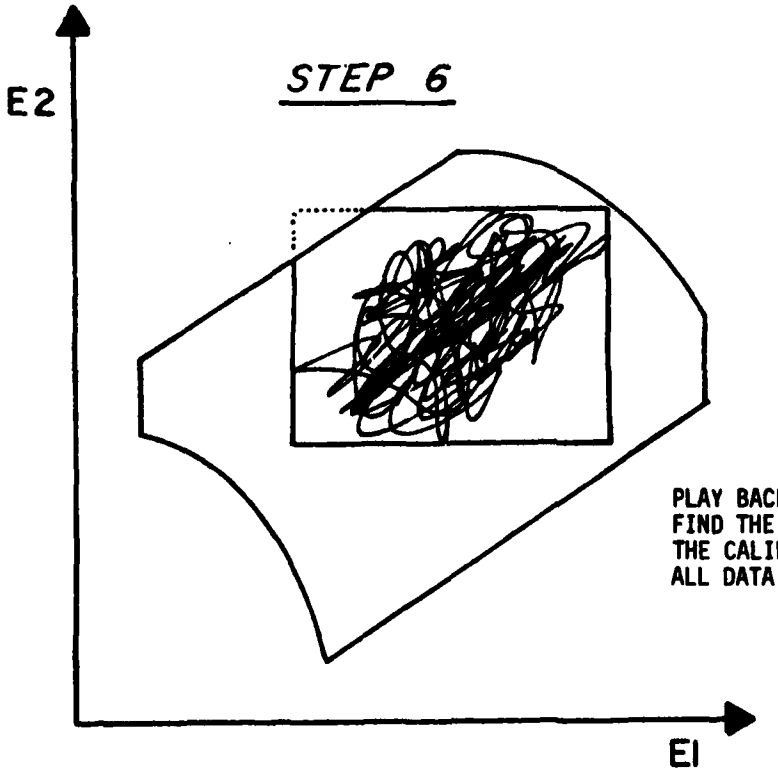

PLAY BACK EACH X-WIRE DATA AND FIND THE NARROWEST WINDOW WITHIN THE CALIBRATION REGION CONTAINING ALL DATA POINTS.

STEP 7

VOLTAGE TO VELOCITY TRANSFORMATION

FIND THE SQUARE IN THE ABOVE WINDOW, CONTAINING EACH MEASURING POINT e_1; e_2.

$I = f(\frac{e_1}{DE})$

$J = f(\frac{e_2}{DE})$

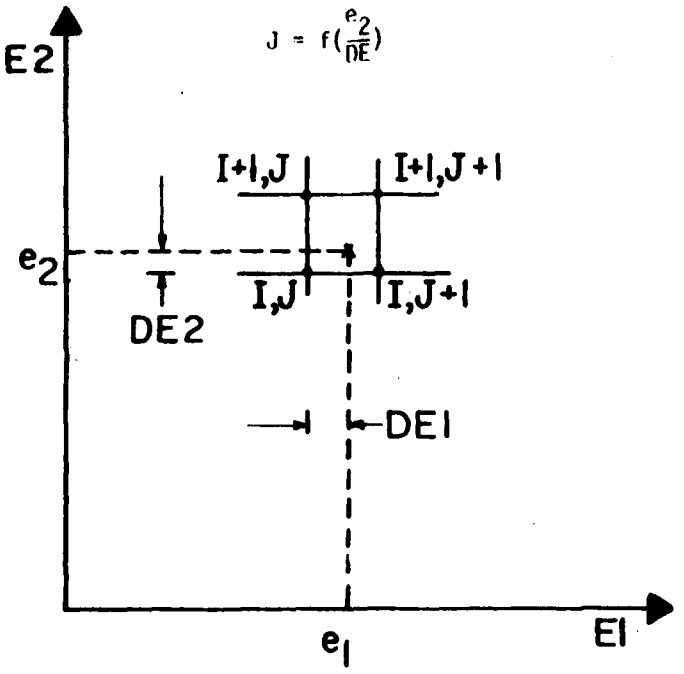

STEP 8

TRANSLATE VOLTAGES TO VELOCITIES AND ANGLES, USING TWO DIMENSIONAL LINEAR POLINOMIAL

$Q = Q_{I,J} + A_Q * DE1 + B_Q * DE2 + C_Q * DE1 * DE2$

$\alpha = \alpha_{I,J} + A_\alpha * DE1 + B_\alpha * DE2 + C_\alpha * DE1 * DE2$

STEP 9

TRANSFORM COORDINATES

$U = Q * COS\alpha$: $V = Q * SIN\alpha$

LIST OF SYMBOLS

$A,B,C,D,$	- Calibration constants of normal hot-wires.
$A_\alpha, B_\alpha, C_\alpha$	- Calibration constants of X-wires.
A_Q, B_Q, C_Q	
E	- Hot-wire voltage.
$E1, E2$	- Voltages of X-wire.
H	- The mean height of a spot in a laminar boundary layer.
I	- Intermittency function.
$(2/\rho U^2)x(dp/dx)$	- Pressure gradient along the flat plate.
Q	- Resultant velocity during X-wire calibration.
q	- Rate of entrainment (velocity times length).
T	- Time.
ΔT	- Time interval between successive sparks.
$Tn=\Delta T x U_\infty / X_s$	- Dimensionless interval between sparks.
U,V,W	- Components of instantaneous velocity.
u,v,w	- Components of velocity fluctuations.
$\bar{U}=U-u$	- Mean value of streamwise velocity component.
$Uint, Vint$	- Streamwise and normal components of the celerity of the interface.
$\tilde{U}_1, \bar{V}_1$	- Mean value of streamwise and normal velocity in the laminar neighbourhood.
U_{le}, V_{le}	- Two components of the celerity of the leading edge.
U_p, V_p	- Two components of perturbation velocity.

U_τ	- Friction velocity.
$U/U_\tau = U^+$	- Dimensionless velocity.
$\langle U \rangle$	- Ensemble averaged velocity.
u', v'	- R.M.S of u and v fluctuations.
$\langle u' \rangle, \langle v' \rangle$	- R.e.m.s (root ensemble mean square) of the fluctuations.
$\overline{u'v'}$	- Mean product of uv.
$\langle uv \rangle$	- Ensemble-averaged of uv product.
$\bar{\bar{u}}', \bar{\bar{v}}'$	- Turbulent zone-averaged of the fluctuations u and v.
$\overline{\overline{u'v'}}$	- Turbulent zone-averaged of uv product.
U_∞	- Free stream velocity.
X,Y,Z	- Directions in Cartesian coordinates.
x,y,z	- Distances along three directions.
X_s	- Streamwise distance from the spark generator.
$yU_\tau/\nu = y^+$	- Normal distance from the surface in wall coordinates.
α	- Direction of flow during X-wire calibration.
γ	- Intermittency.
δ	- Boundary layer thickness.
δ_l	- Laminar boundary layer thickness.
δ_t	- Turbulent boundary layer thickness.
δ^*	- Displacement thickness.
θ	- Momentum thickness.
$Re\delta^*$	- Reynolds number based on displacement thickness.
$Re\theta$	- Reynolds number based on momentum thickness.

REFERENCES

1. Amini, J. 1978 Ph.D Thesis, Institute de Mecanique de Grenoble.

2. Antonia, R.A., Chambers, A.J., Sokolov, M. and Van Atta, C.W. 1981 JFM, Vol. 108, p. 317.

3. Blackwelder, R.F. 1970 Ph.D Thesis, The Johns Hopkins University.

4. Blackwelder, R. F. 1978 Coherent Structure of Turbulent Boundary Layers, (C.R Smith and D.E Abbott, eds.) AFOSR/Lehigh University Workshop, p. 168.

5. Blackwelder, R.F. and Kaplan, R.E. 1972 NATO-AGARD Conf. Proc No. 93 London Technical Editing and Reproduction Ltd.

6. Bridental, R.E.J. 1978 Ph.D Thesis, California Institute of Technology.

7. Brown, G.L. and Thomas A.S.W. 1978 Coherent Structure of Turbulent Boundary Layers, AFOSR/Lehigh University Workshop, p. 243.

8. Cantwell, B., Coles, D., Dimotakis, P. (1978) JFM, Vol. 87, p. 641.

9. Carlson, D.R. and Widnall, S.E. 1981 (to be published).

10. Coles, D. 1964 Physics of Fluids, 7, p. 1403.

11. Coles, D., and Barker, S.J., (1975) in Proceedings of Project SQUID Workshop on Turbulent Mixing in Non-reactive and Reactive Flows, edited by S.N.B. Murthy, Plenum Press, N.Y.

12. Coles, D., Cantwell, B. and Wadcock, A. 1978 NASA Contructor, Report 3066.

13. Elder, J.W. (1960) JFM, Vol. 9, p. 235.

14. Emmons, H.W. (1951) J. Aero. Sc. 18, 490.

15. Falco, R.E. 1977 Physics of Fluids, Vol. 20, Num. 10, Part II S124.

16. Falco, R.E. 1978 Coherent Structure of Turbulent Boundary Layers, (C.R. Smith and D.E. Abbott eds.) AFOSR/Lehigh University Workshop, p. 448.

17. Gad el Hak, M., Blackwelder, R.F. and Riley, J.J. 1980 Submitted to JFM.

18. Gaster, M. 1968 JFM, Vol. 32, p. 173.

AD-A133 808 ON THE RELATIONSHIP BETWEEN TRANSITIONAL AND FULLY TURBULENT SHEAR FLOW..(U) TEL-AVIV UNIV (ISRAEL) DEPT OF FLUID MECHANICS AND HEAT TRANS.. I WYGNANSKI ET AL. 2/2

UNCLASSIFIED MAY 82 AFOSR-TR-83-0806 AFOSR-77-3275 F/G 20/4 NL

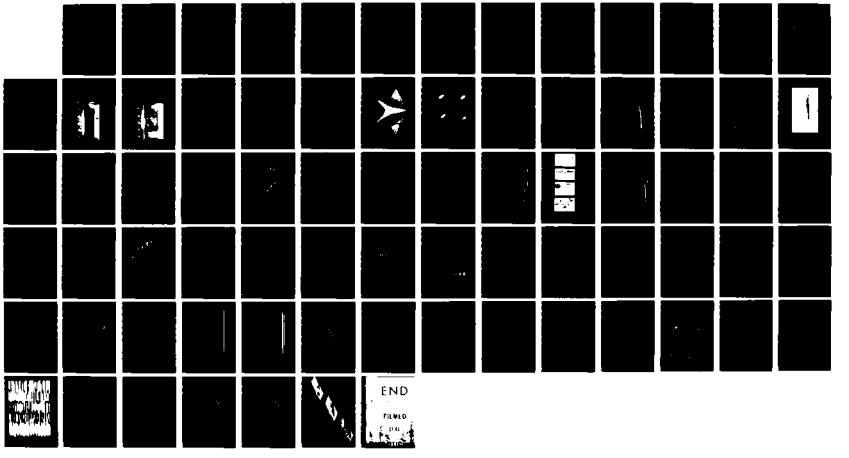

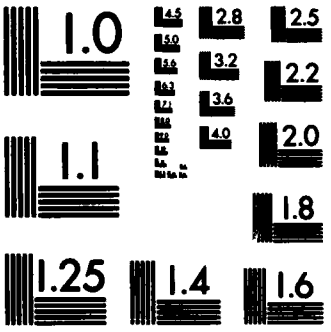

MICROCOPY RESOLUTION TEST CHART
NATIONAL BUREAU OF STANDARDS-1963-A

19. Gupta, A.K, Laufer, J. and Kaplan, R.E. 1971 JFM, Vol. 50, p. 493.

20. Haritonidis, J.H., Kaplan, R.E. and Wygnanski, I. 1977 Lecture Notes in Physics; Structures and Mechanism of Turbulence-I, Proceedings, Berlin, p. 234

21. Head, M.R. 1958 Aero. Res. Coun. R and M no. 3152.

22. Kim, H.T., Kline, S.J. and Reynolds, W.C. 1971 JFM, 50, p. 133

23. Klebanoff, P.S., Tidstrom, K.D. and Sargent, L.M. 1962 JFM, 12, p. 1.

24. Kline, S.J. 1978 Coherent Structure of Turbulent Boundary Layers, AFOSR/Lehigh University Workshop, p. 1

25. Kovasznay, L.S.G., Kibens, V. and Blackwelder, R.F. 1970 JFM, Vol. 41, p. 283.

26. Kovasznay, L.S.G., Komoda, H. and Vasudeva, B.R. 1962 Proc. Heat Trans. and Fluid Mechanics Inst., Stanford University Press.

27. Laufer, J.1975 Annual Review of Fluid Mechanics, Vol.7, p.307.

28. Laufer, J. and Narayanan, B.M.A. 1970 Physics of Fluids Vol.14, Num 1 p. 182.

29. Leonard, A. 1979 NASA Technical Memorandum 78579.

30. Matsui, T. 1980 IUTAM-SYMPOSIUM ON LAMINAR-TURBULENT TRANSITION, STUTTGART.

31. Rao, N.K., Narasimha, R. and Badri Narayanan, M.S. 1971 JFM, VOL. 48, p. 339.

32. Savas, O. 1979 Ph.D Thesis, California Institute of Technology.

33. Schubauer, G.B. and Klebanoff, P.S. (1956) NACA Rep. 1289.

34. Van Atta, C.W. and Helland, K.N. (1980) JFM, VOL. 100, P. 243.

35. Van Atta, C.W., Sokolov, M., Antonia, R.A. and Chambers A.J. 1981 (to be published in the Physics of Fluids).

36. Willmarth, W. W. 1975 Advances in Applied Mechanics, Vol. 15, p. 159.

37. Willmarth, W. W. and Bogar, T. J. 1977 Physics of Fluids Vol. 20, Num. 10, Part II S9.

38. Wygnanski, I. 1978 Coherent Structure of Turbulent Boundary Layers, (C.R. Smith and D.E. Abbott, eds.) AFOSR/Lehigh University Workshop, p. 448.

39. Wygnanski, I. 1980 Lecture Notes in Physics 136, Springer Verlag-Berlin, (Proceeding, Madrid 1980).

40. Wygnanski, I., Sokolov, M. and Friedman, D. (1976) JFM, Vol. 78, p. 785.

41. Wygnanski, I., Haritonidis, J.H. and Kaplan, R.E. (1979) JFM, Vol. 92, p. 505.

42. Zilberman, M., Wygnanski, I., Kaplan, R.E. (1977) Physics of Fluids, Vol. 20, Num. 10, Part II S258.

LIST OF FIGURES

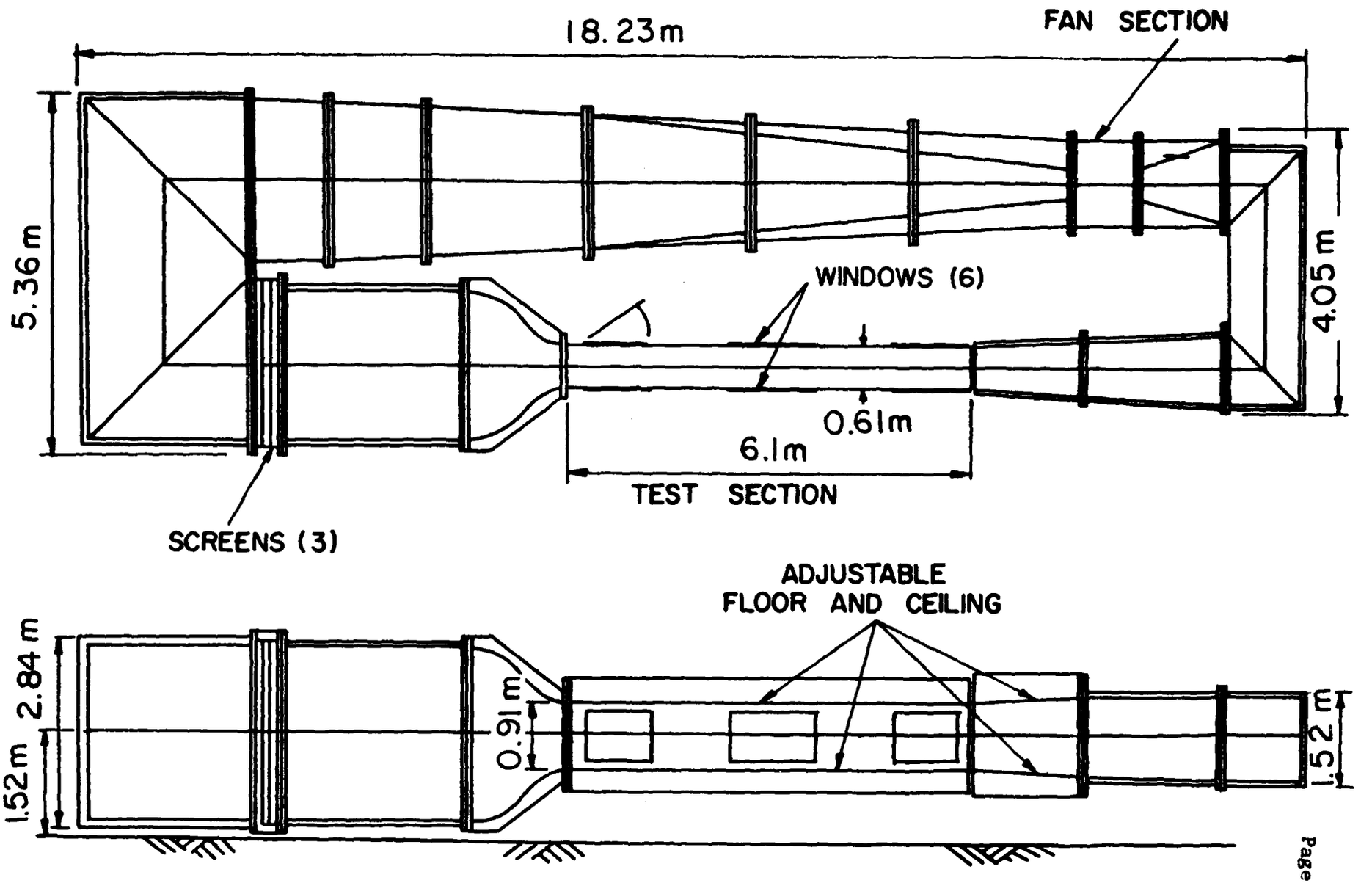
18.23m
FAN SECTION
5.36m
4.05m
WINDOWS (6)
0.61m
6.1m
TEST SECTION
SCREENS (3)
ADJUSTABLE
FLOOR AND CEILING
2.84m
1.52m
0.91m
1.52m

FIGURE B.1.1

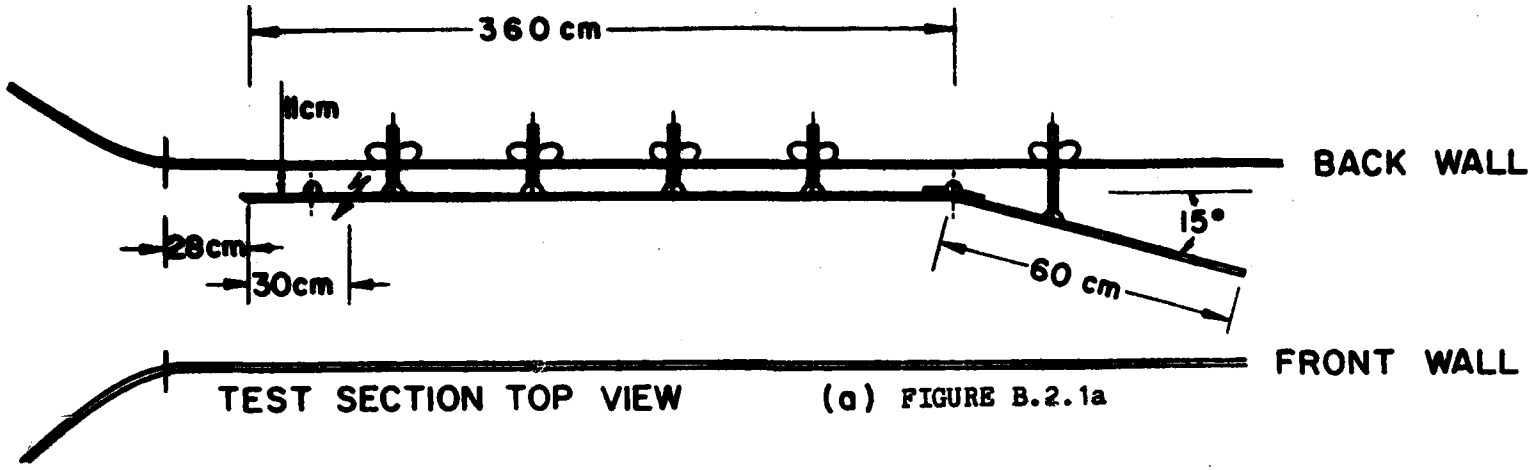

(a) FIGURE B.2.1a

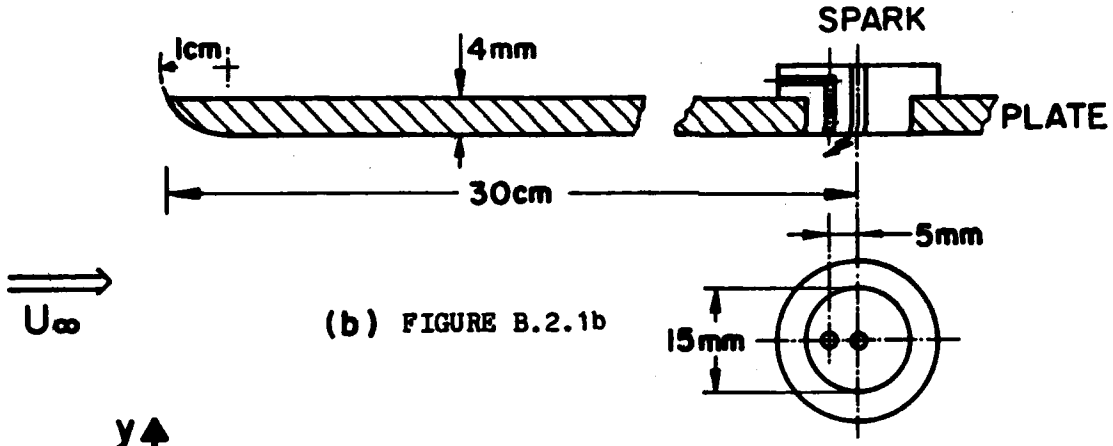

(b) FIGURE B.2.1b

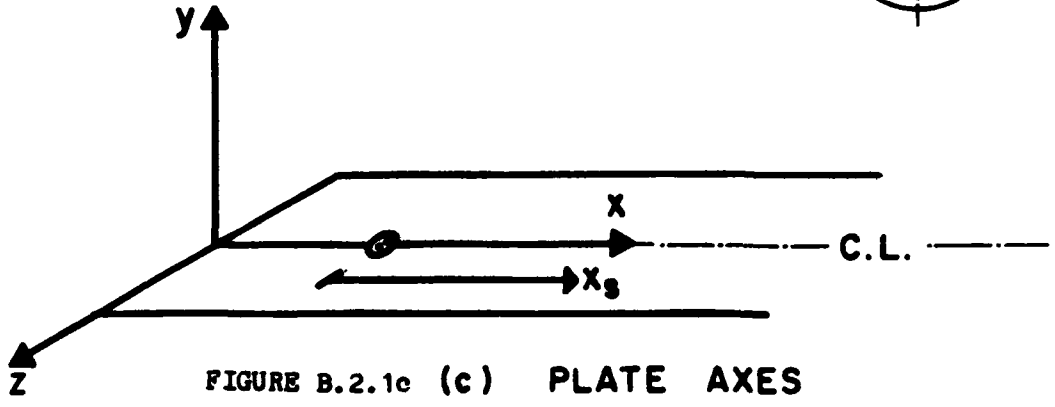

FIGURE B.2.1c (c) PLATE AXES

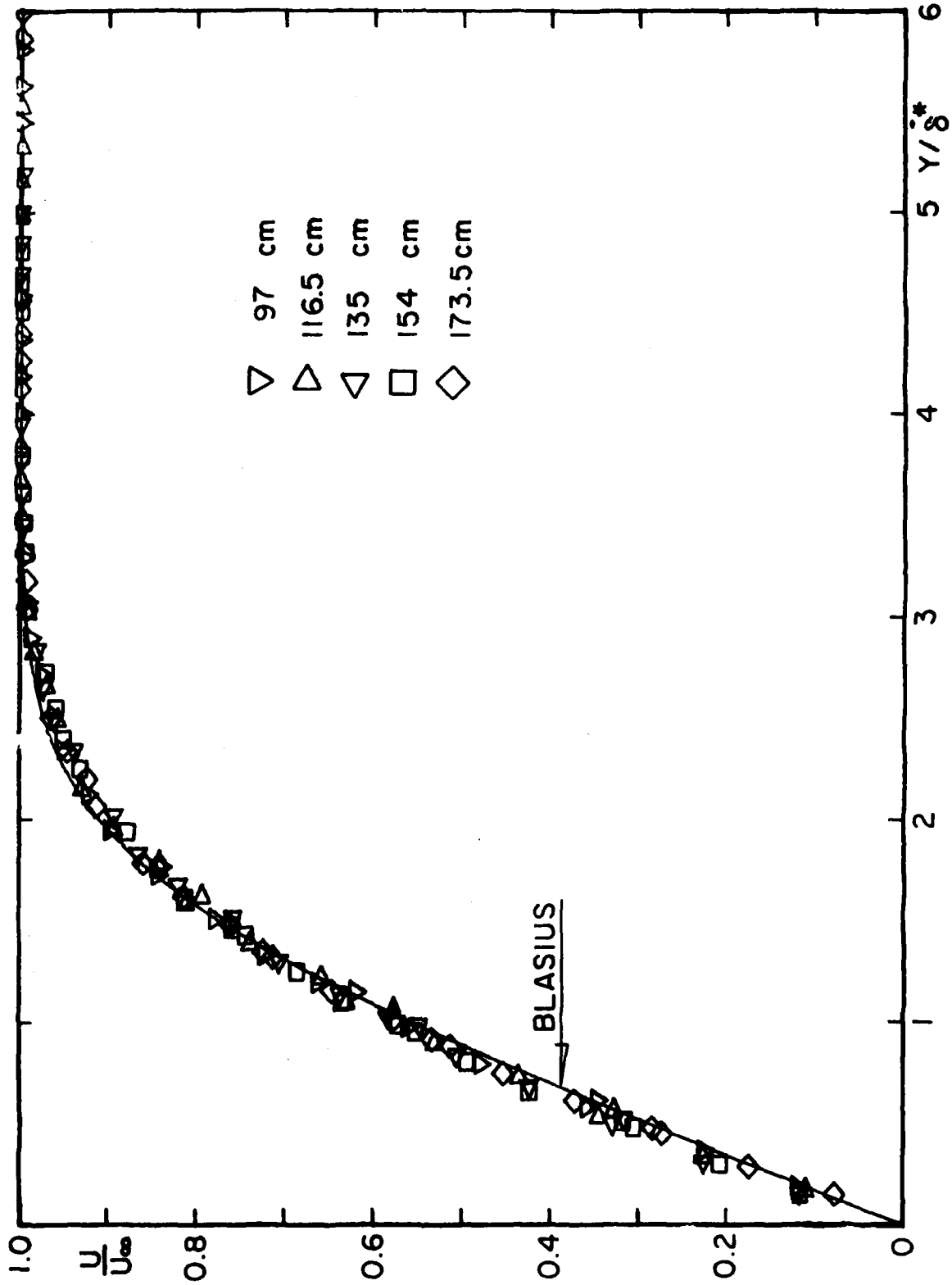
97 cm
116.5 cm
135 cm
154 cm
173.5cm
BLASIUS
$\frac{u}{U_\infty}$
1.0
0.8
0.6
0.4
0.2
0
1
2
3
4
5
6
Y/δ^*

FIGURE B.2.2

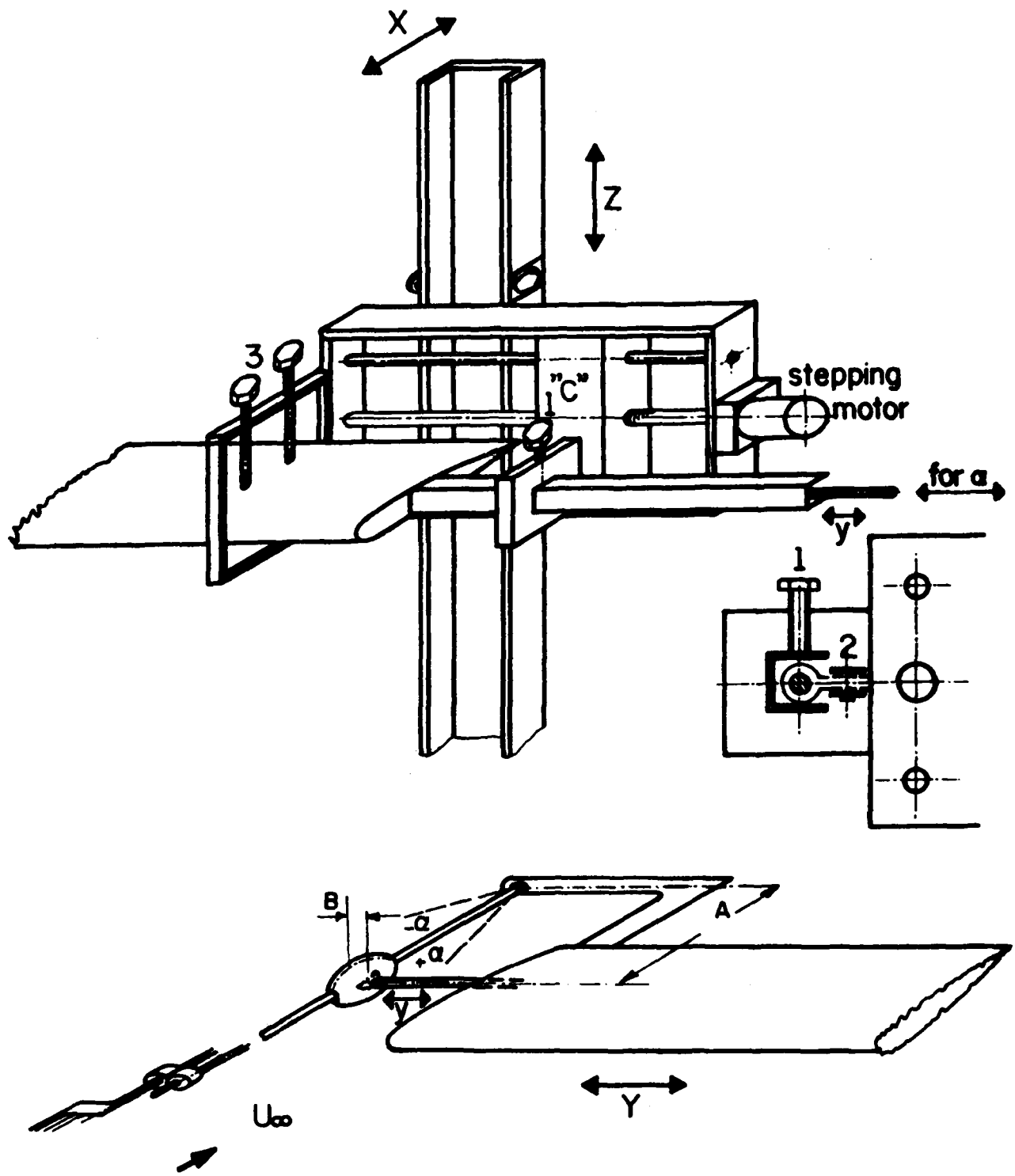

FIGURE B.3.1

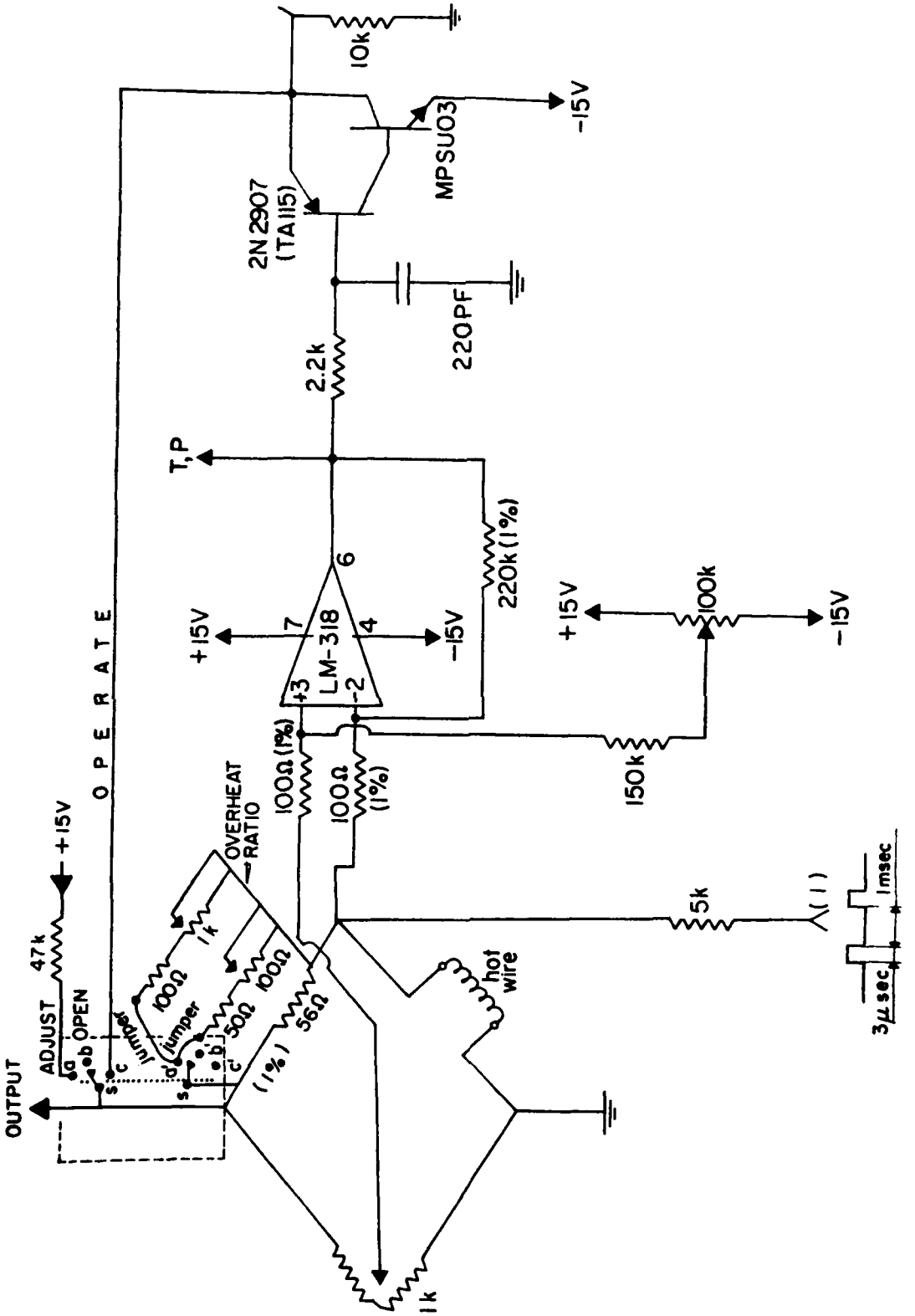
10k
-15V
MPSU03
2N 2907
(TA115)
220PF
2.2k
T,P
220k(1%)
+15V
7
4
-15V
6
LM-318
+3
-2
+15V
100k
-15V
150k
100Ω (1%)
100Ω
(1%)
OVERHEAT
RATIO
OPERATE
+15V
47k
ADJUST
OUTPUT
a
b OPEN
c
s
d
jumper
1k
100Ω
100Ω
500Ω
560Ω
(1%)
b'
c'
s'
hot
wire
1k
5k
1msec
3μsec

FIGURE B.4.1

NORMAL— WIRE RAKE

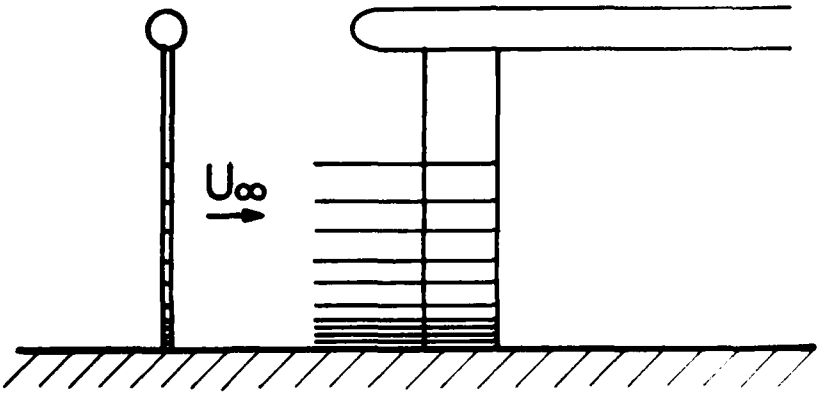

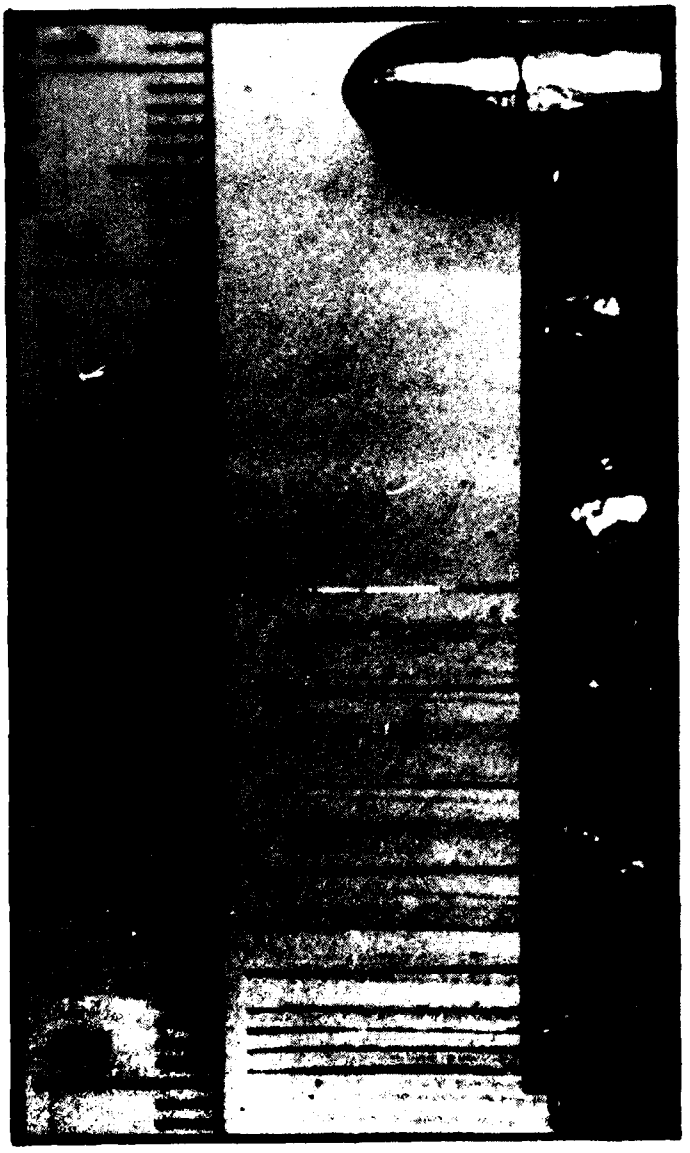

FIGURE B.5.1

X-WIRE RAKE

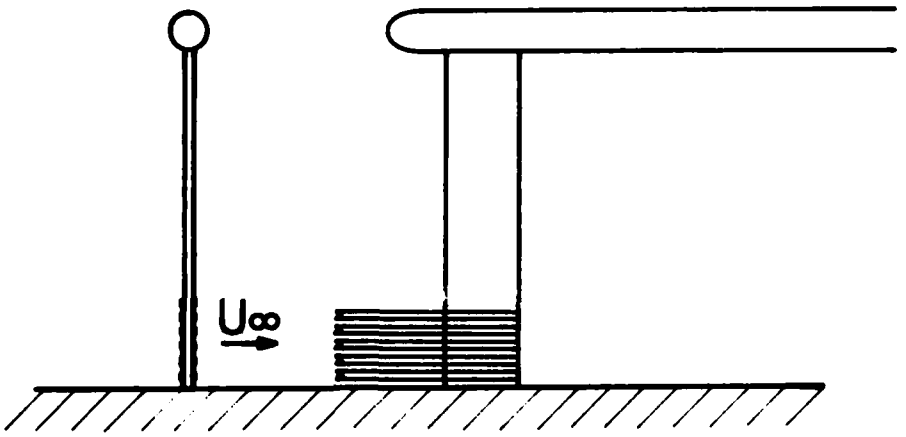

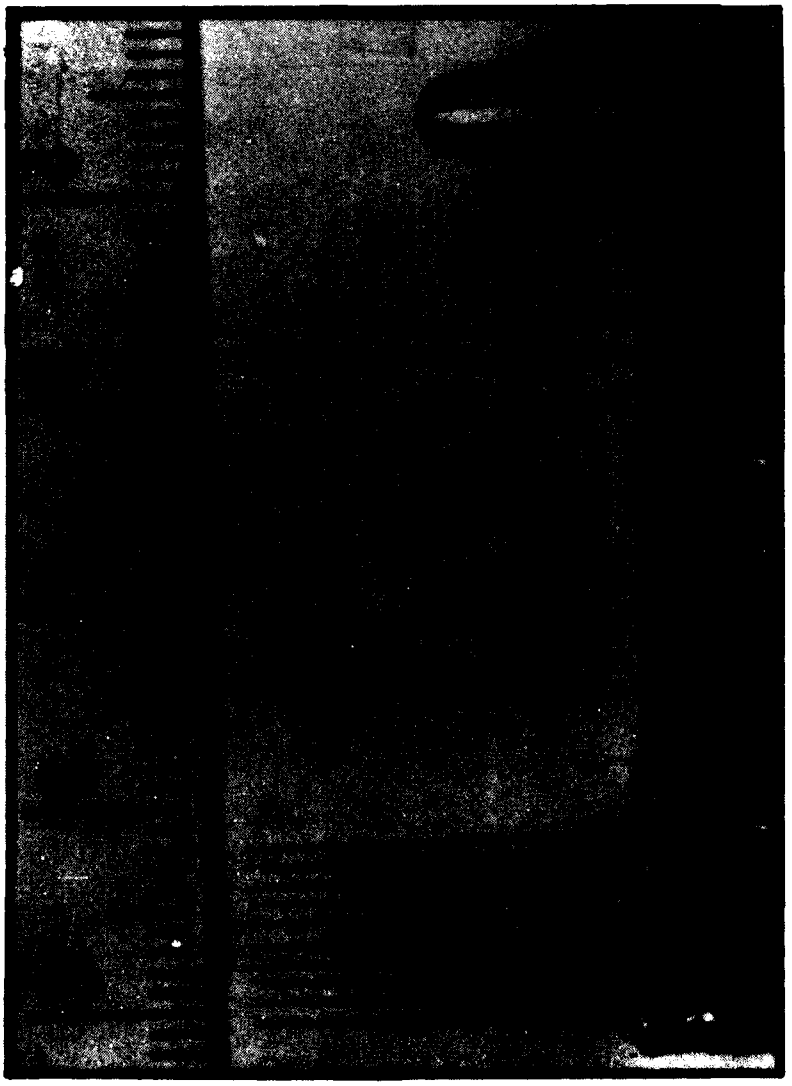

FIGURE B.5.2

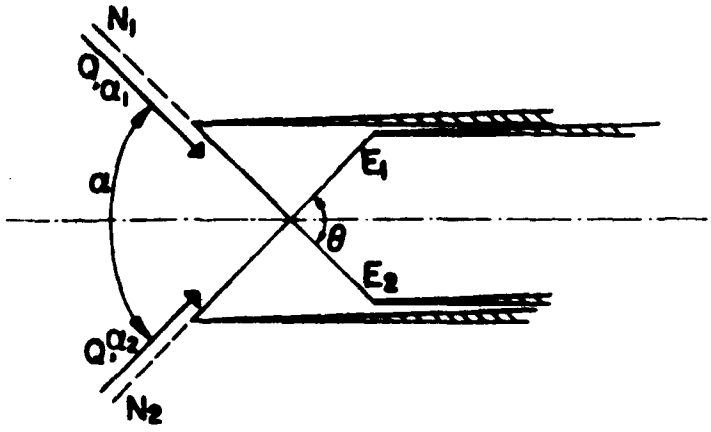

CASE 1: $\alpha \cong \theta$, $\theta = 90°$

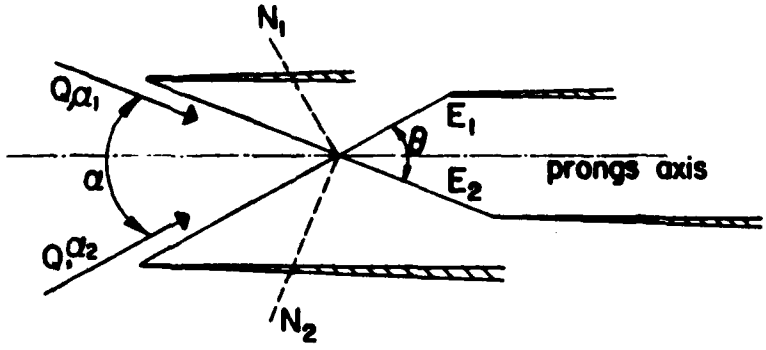

CASE 2: $\alpha \cong \theta$, $\theta < 90°$

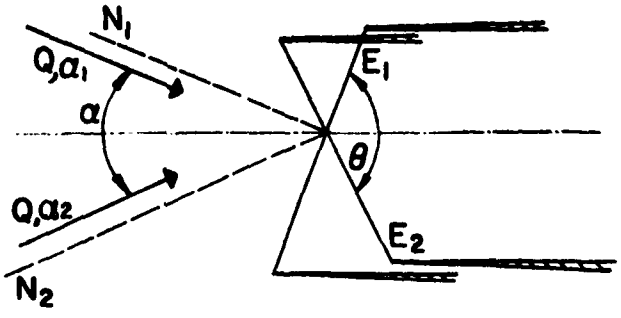

CASE 3: $\alpha \cong \pi - \theta$, $\theta > 90°$

FIGURES C.3.1a,b,c

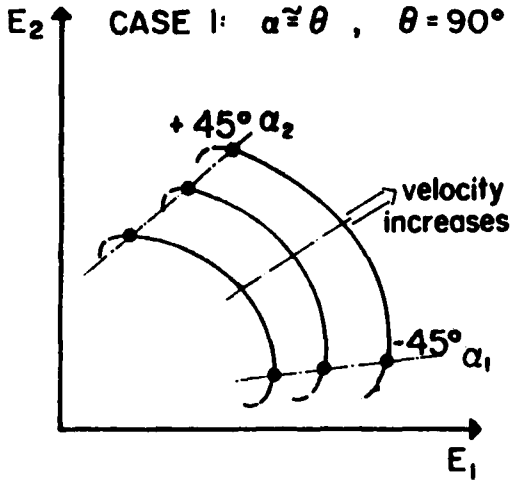

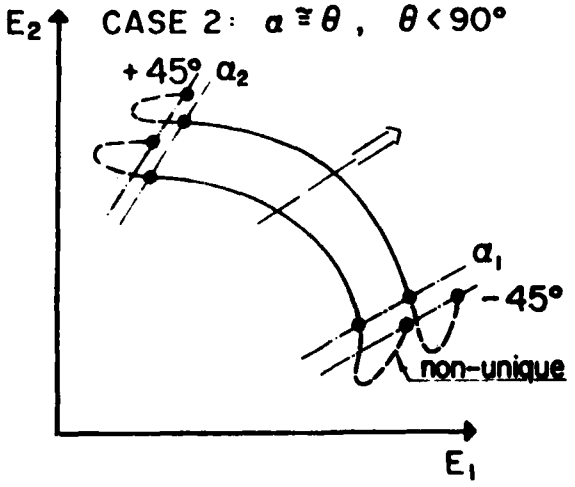

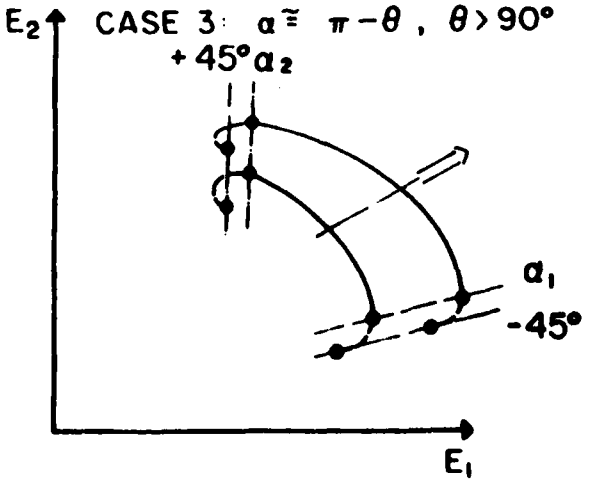

FIGURES C.3.2a,b,c

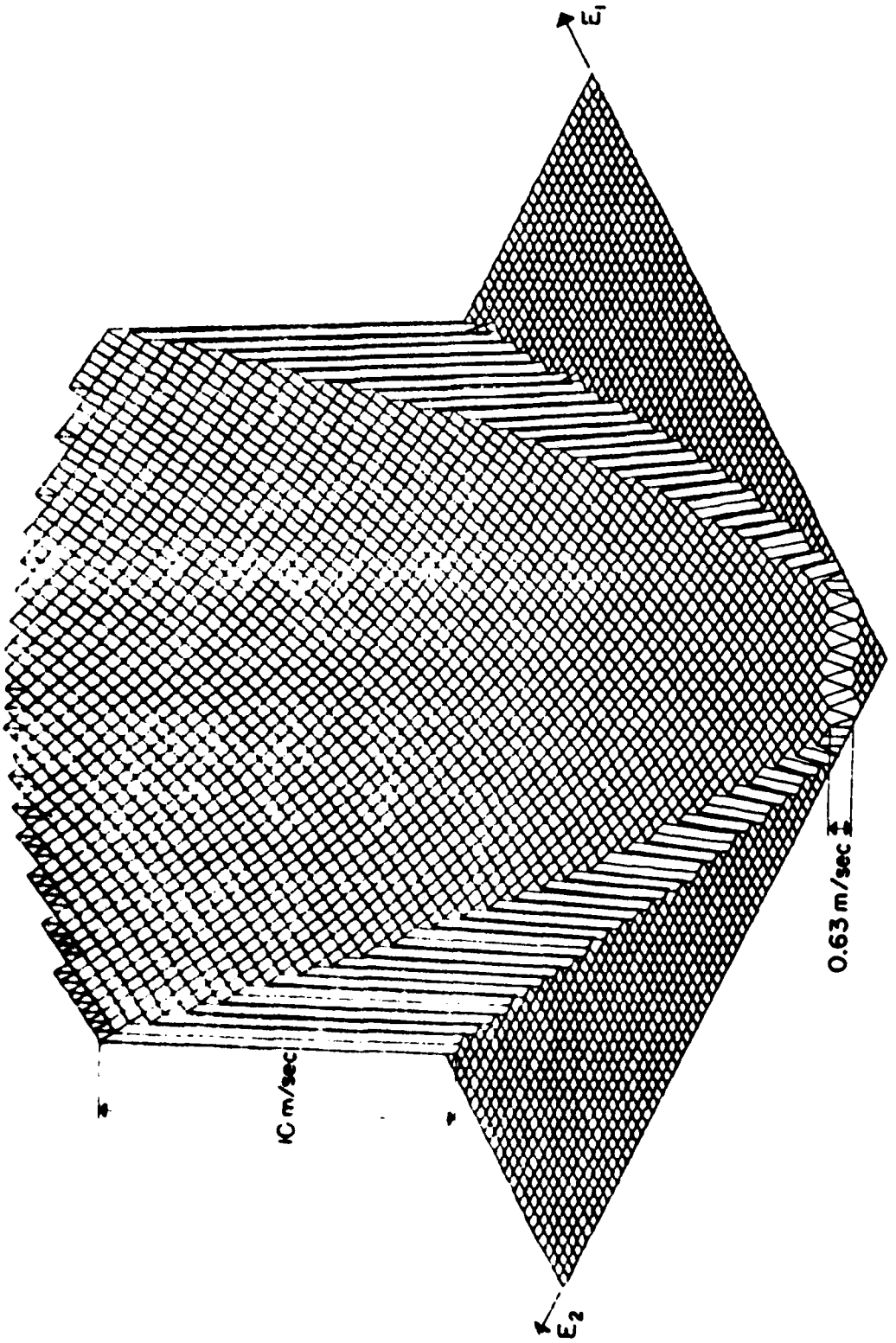

FIGURE C.3.3a

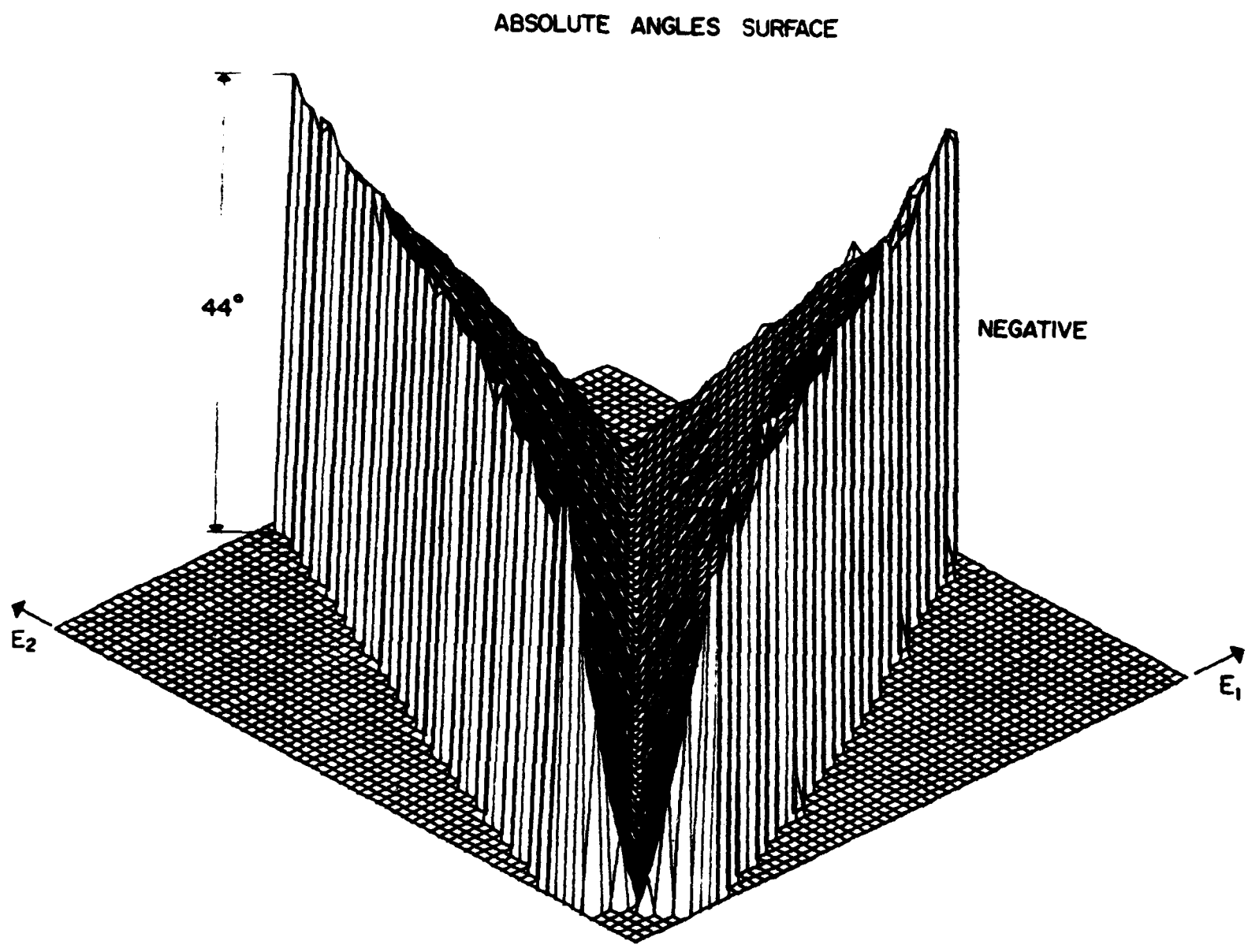

FIGURE C.3.3b

FIGURE C.3.4a

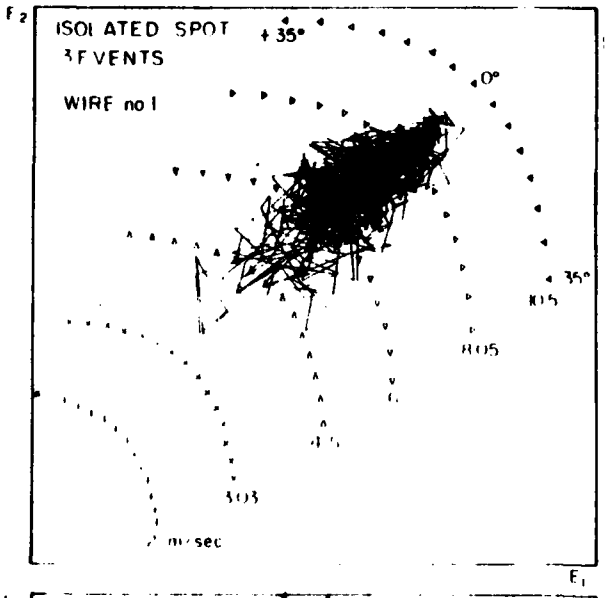

FIGURE C.3.4b

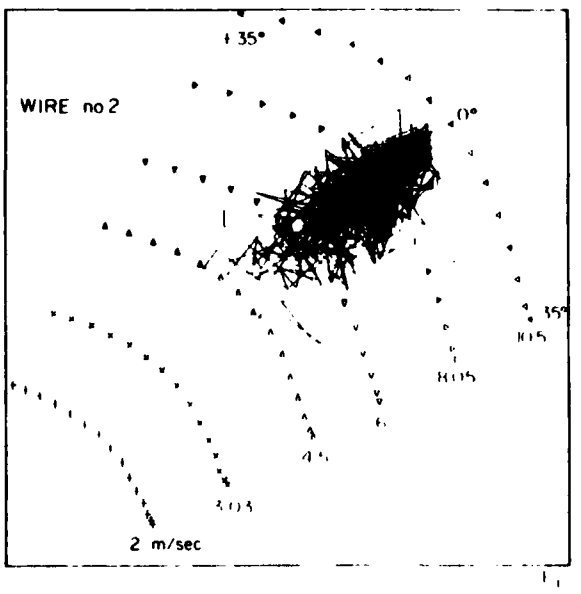

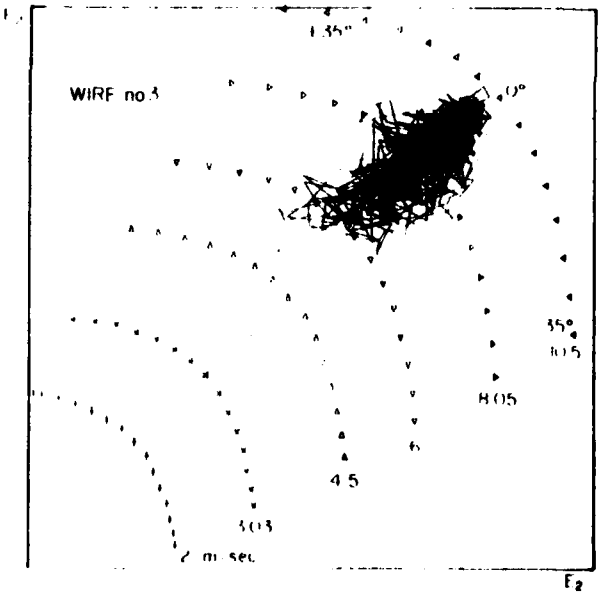

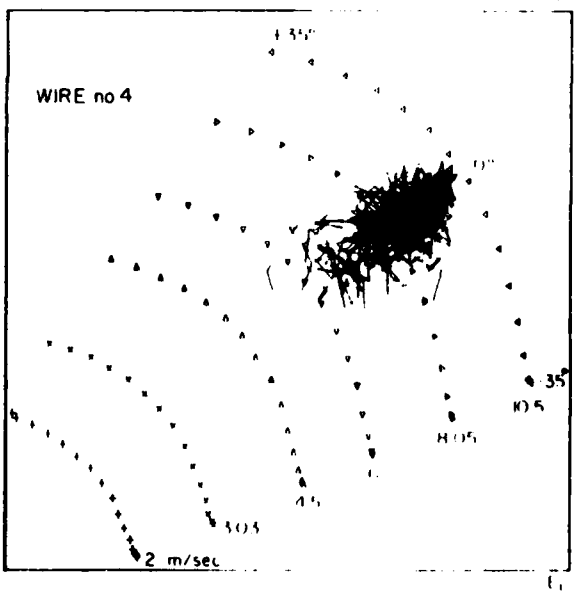

FIGURE C.3.4c

FIGURE C.3.4d

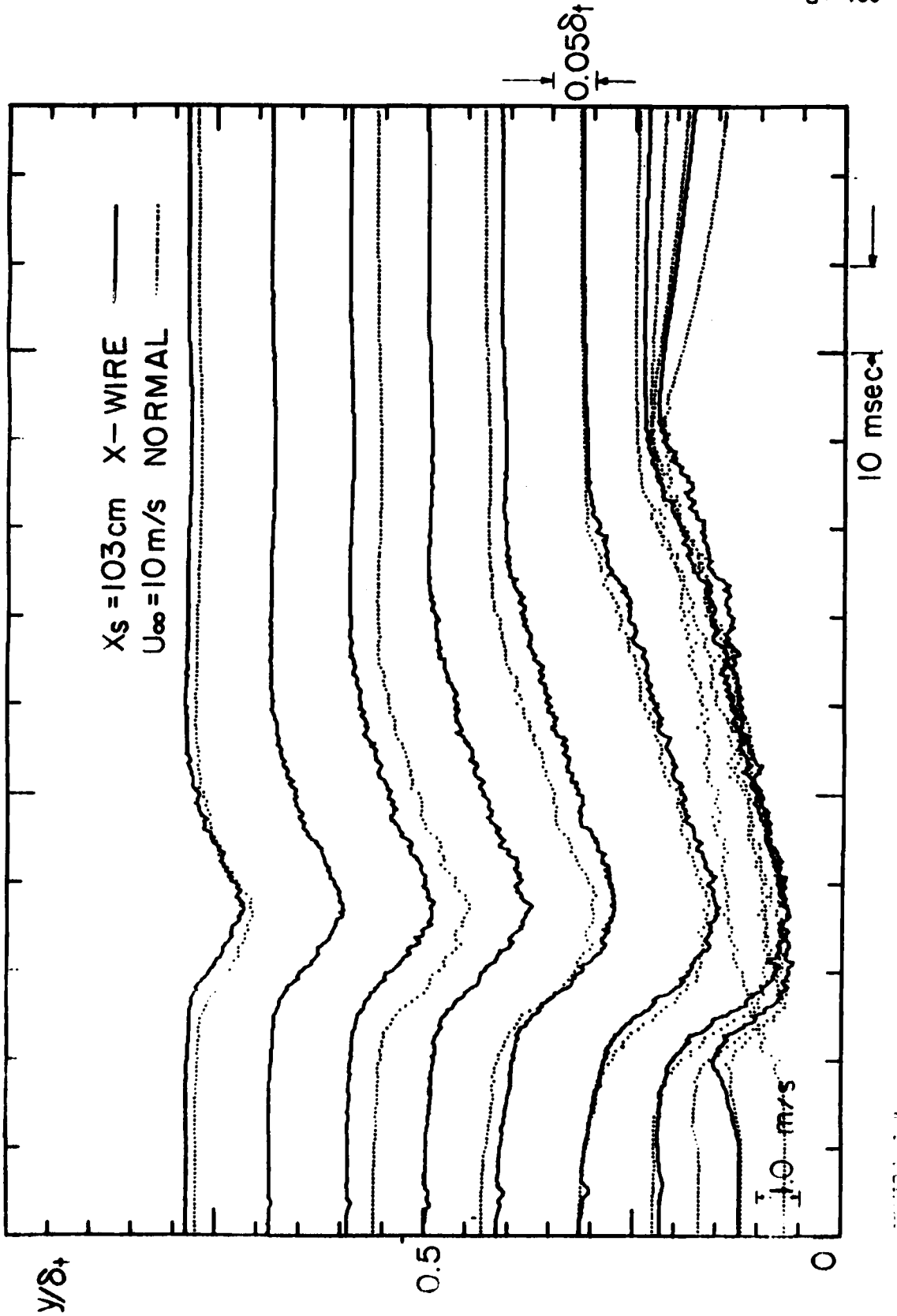
X_S =103cm X-WIRE
U_∞=10 m/s NORMAL
0.05δ_+
10 msec
±1.0 m/s
y/δ_+
0.5
0

FIGURE 3.4.

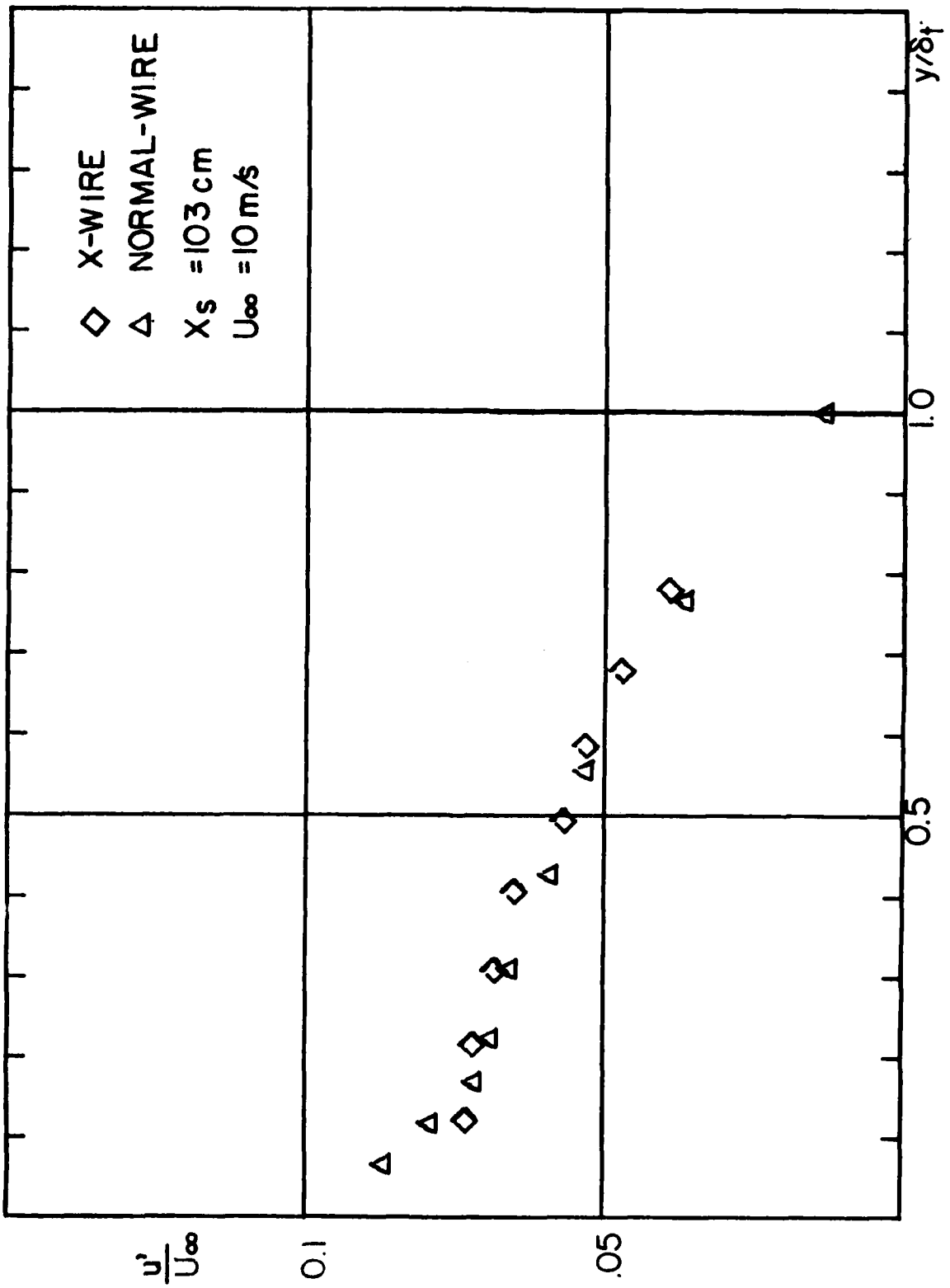

FIGURE C.4.2

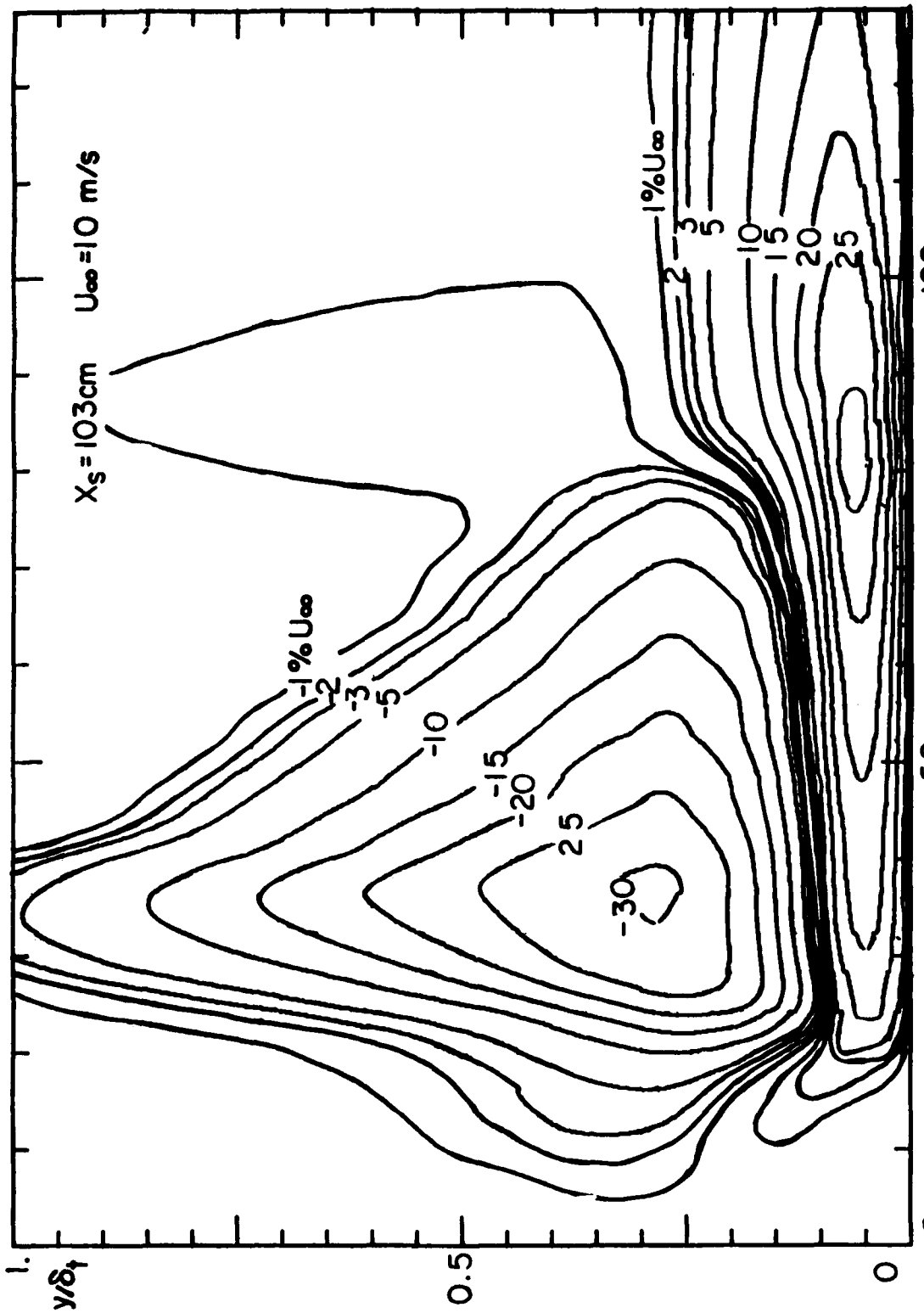
X_s=103cm U_∞=10 m/s
-1%U_∞
-2
-3
-5
-10
-15
-20
25
-30
1%U_∞
2
3
5
10
15
20
25
1.
0.5
0
y/δ_1
0
50
100
msec

FIGURE D.1.1

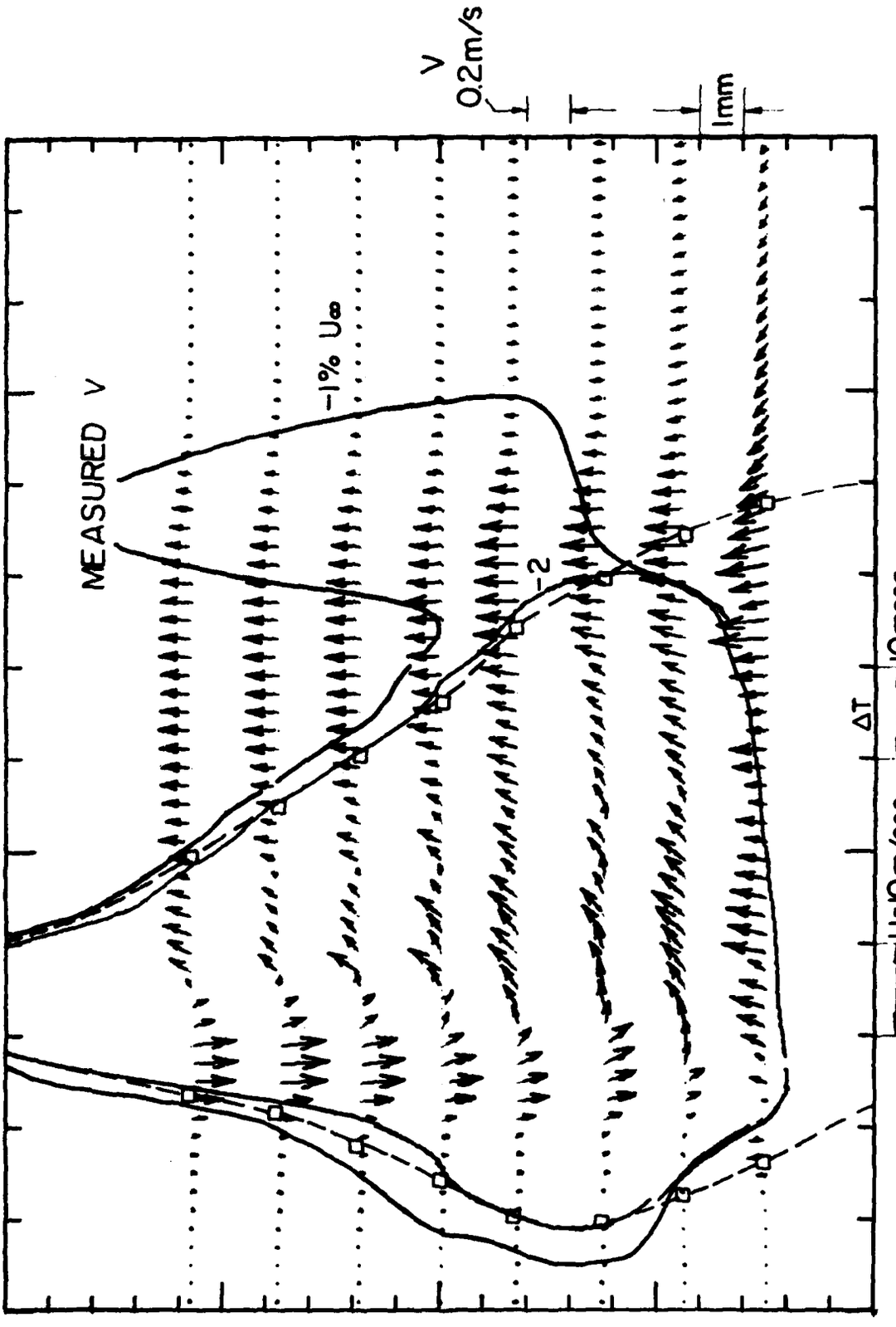

FIGURE D.1.2a

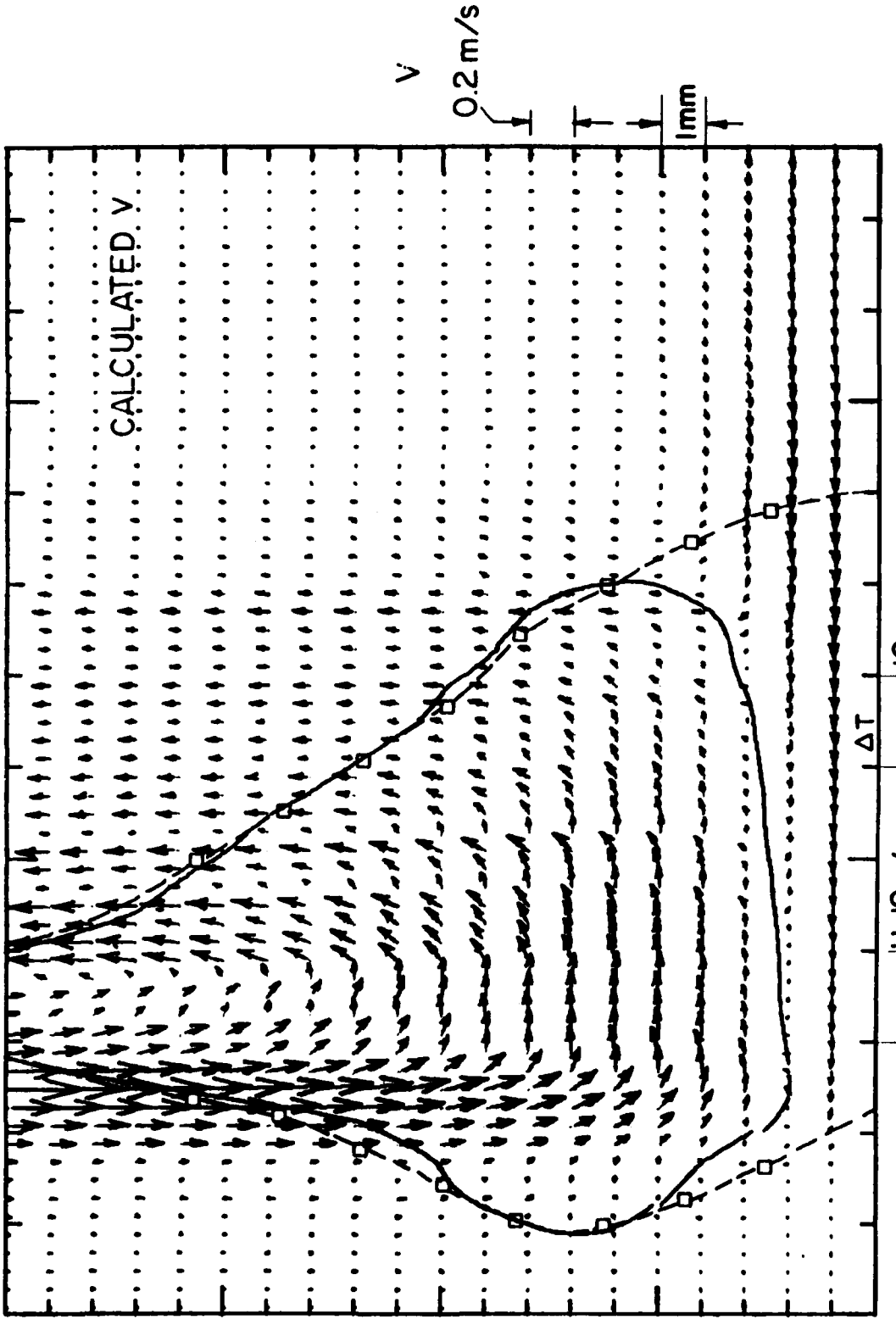

FIGURE D.1.2b

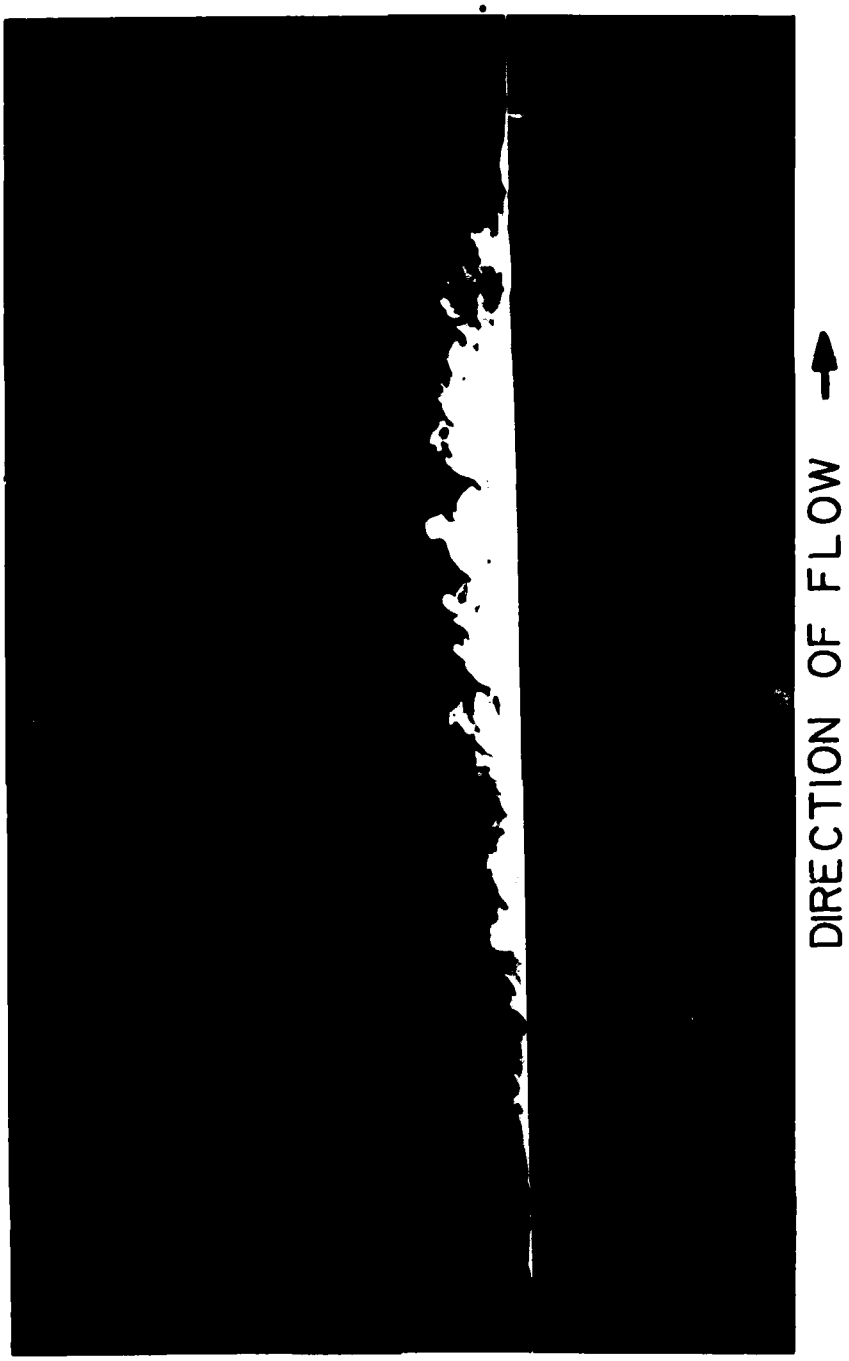

FIGURE D.2.1

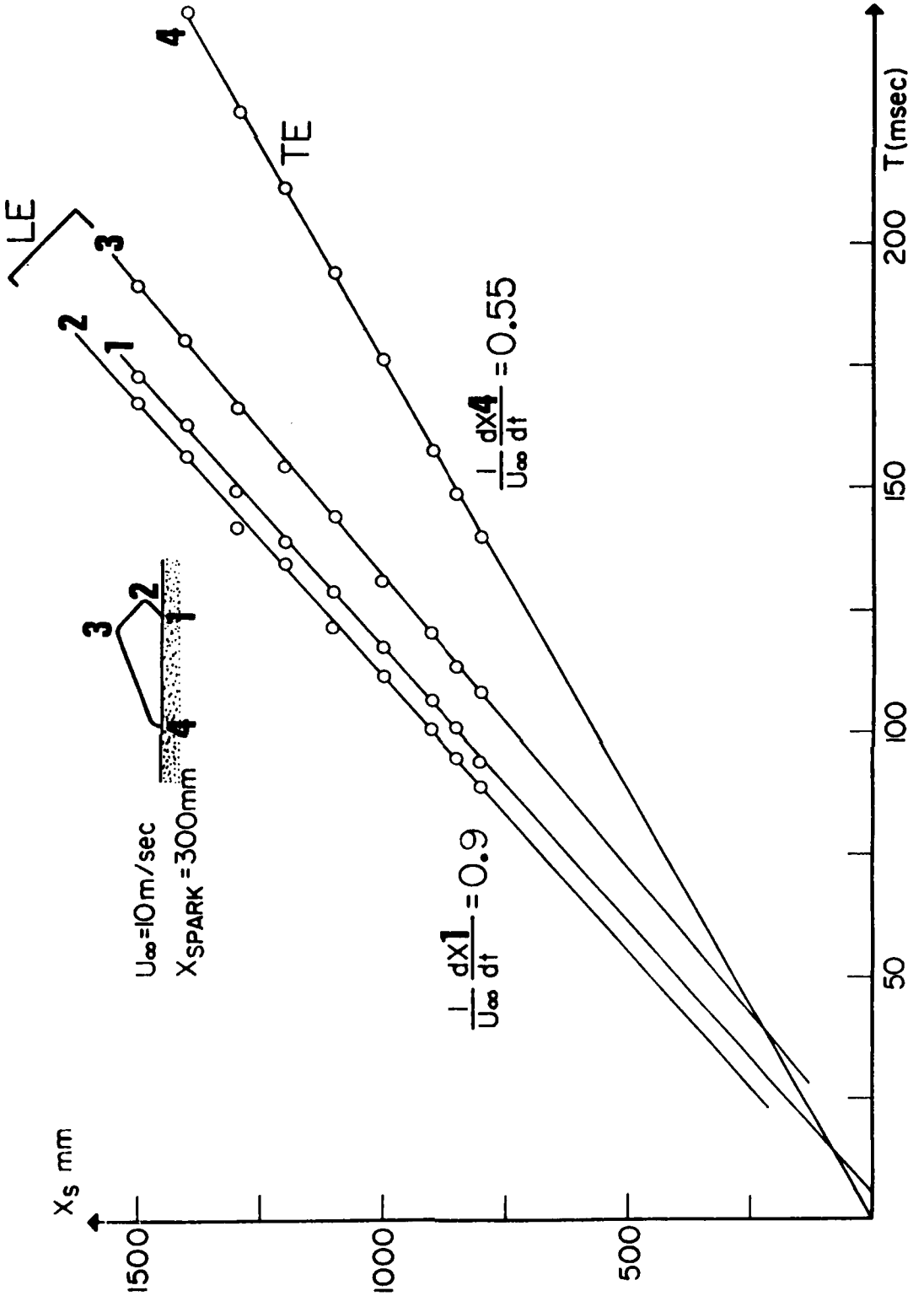
LE
TE
1
2
3
4
U_∞=10 m/sec
X_{SPARK} = 300mm
$\frac{1}{U_\infty}\frac{dX1}{dt}$ = 0.9
$\frac{1}{U_\infty}\frac{dX4}{dt}$ = 0.55
X_s mm
1500
1000
500
50
100
150
200
T(msec)

FIGURE D.2.2

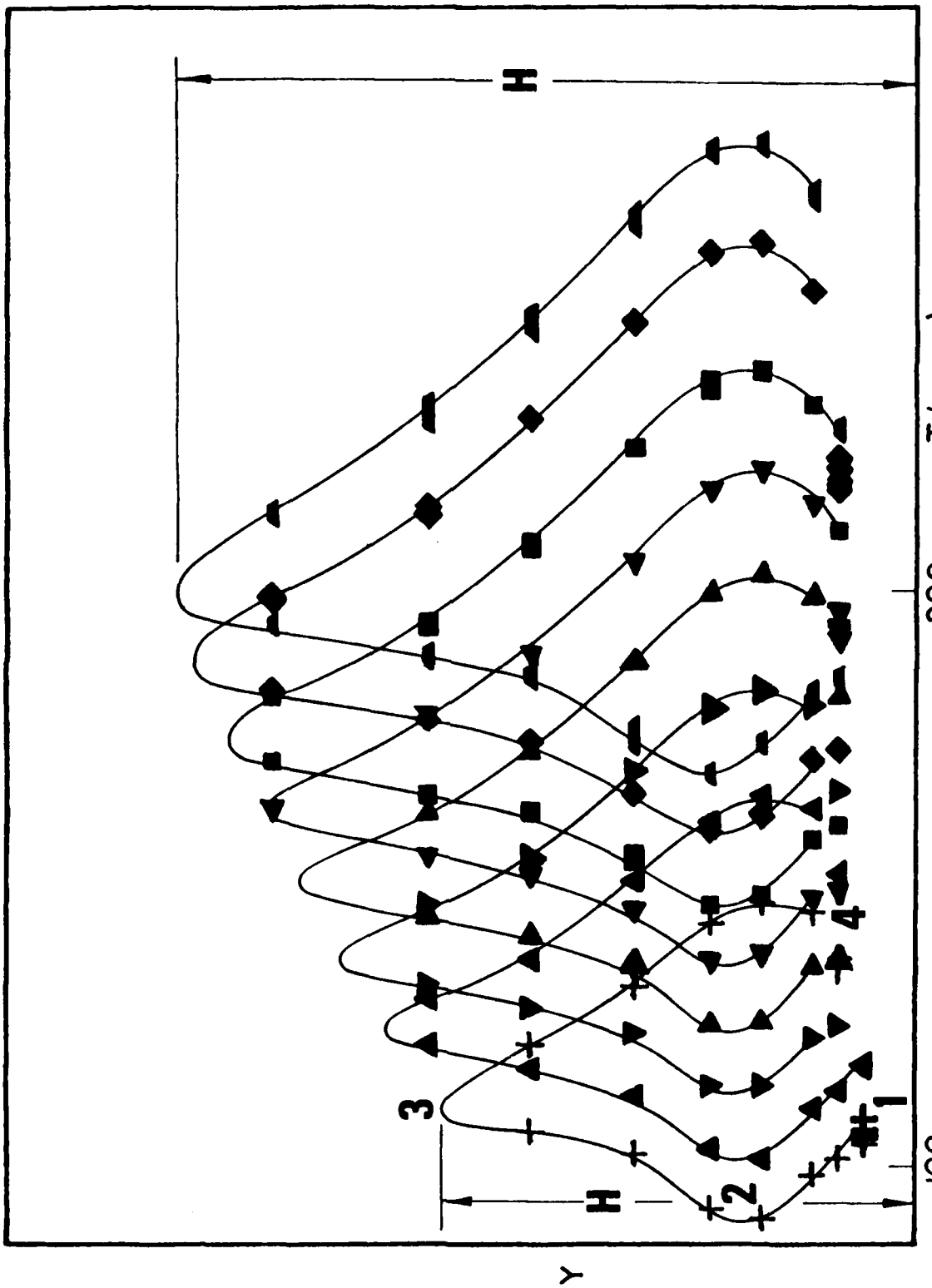

FIGURE D.2.3

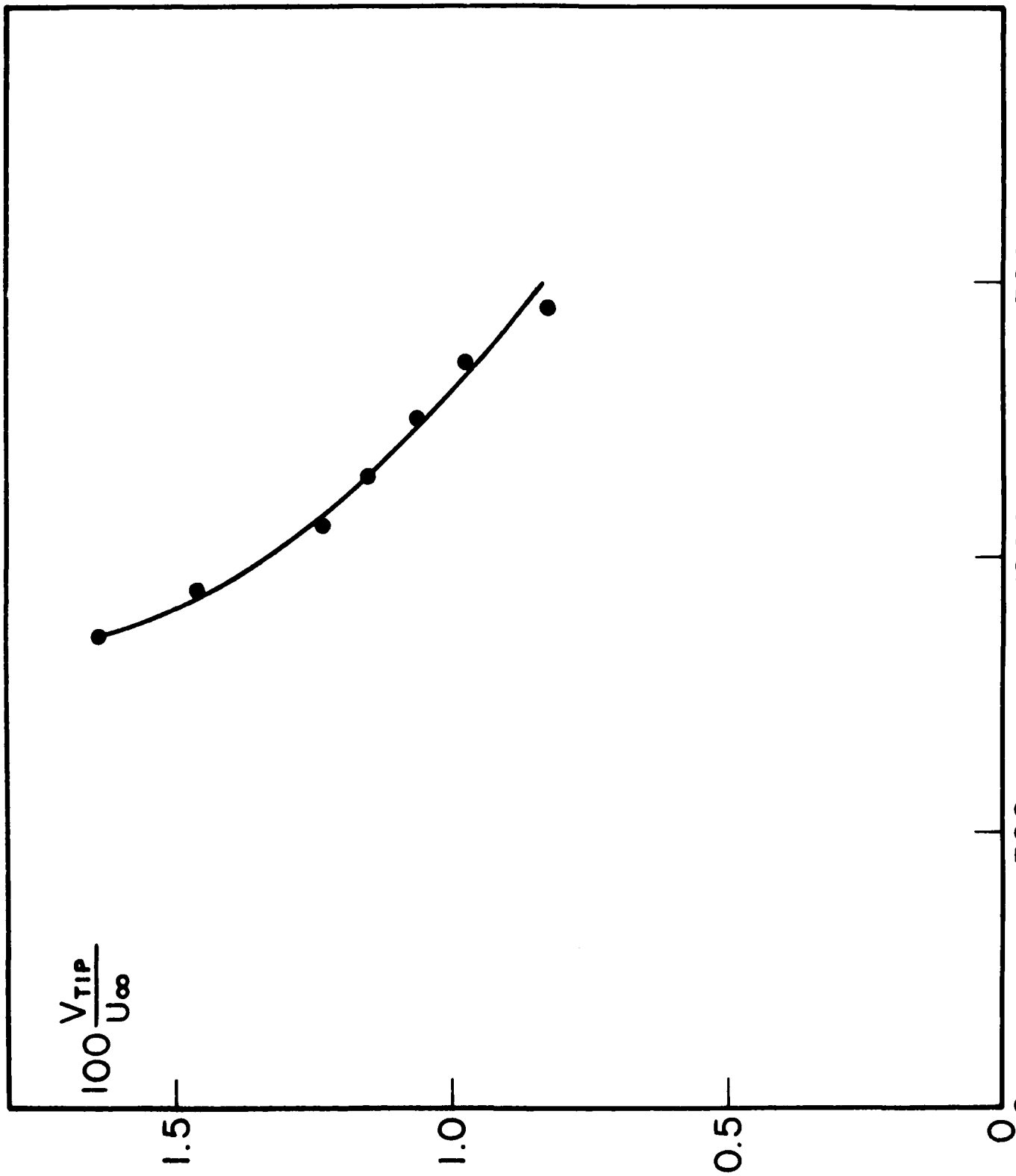

FIGURE D.2.4

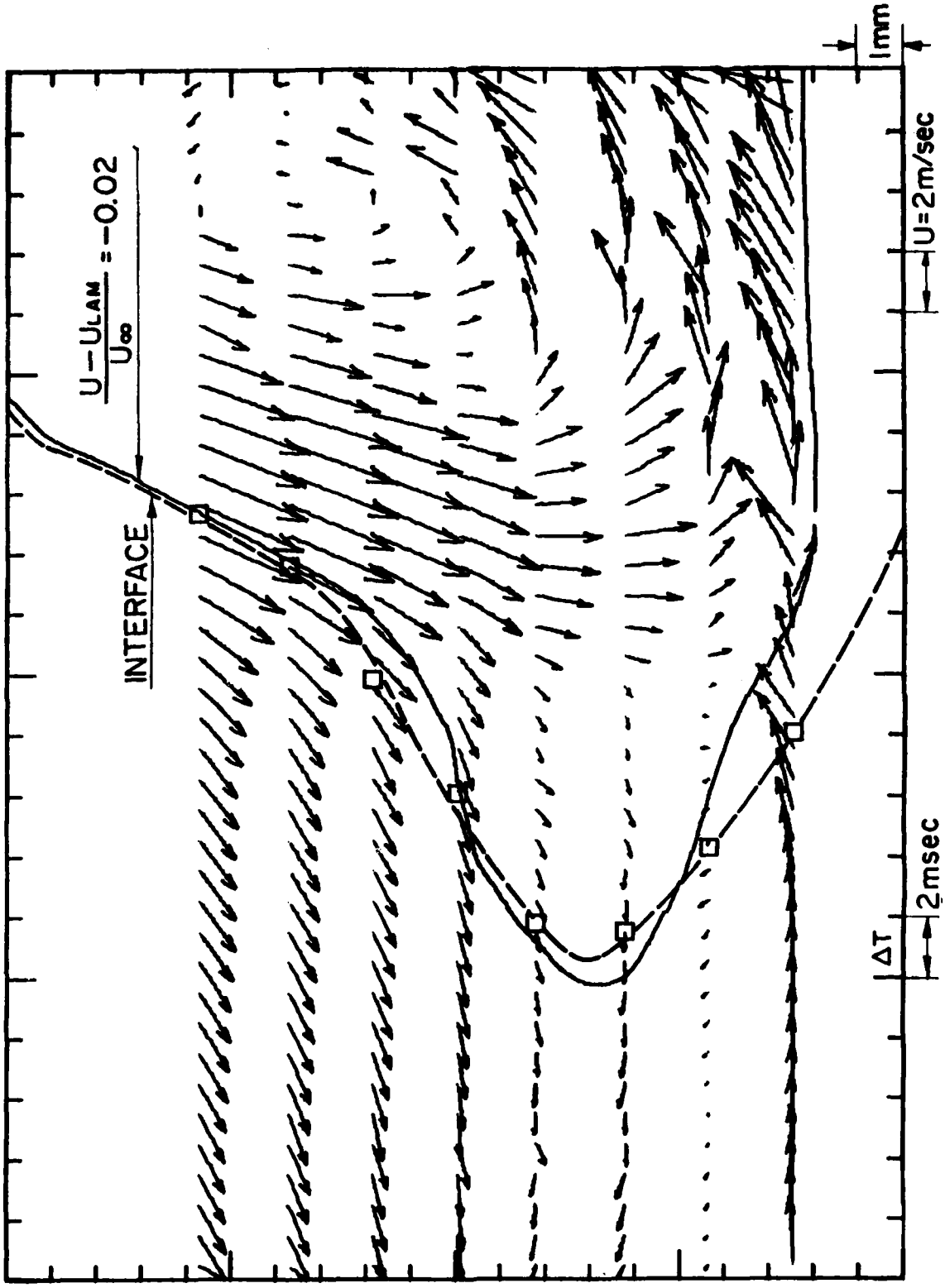

FIGURE D.2.5a

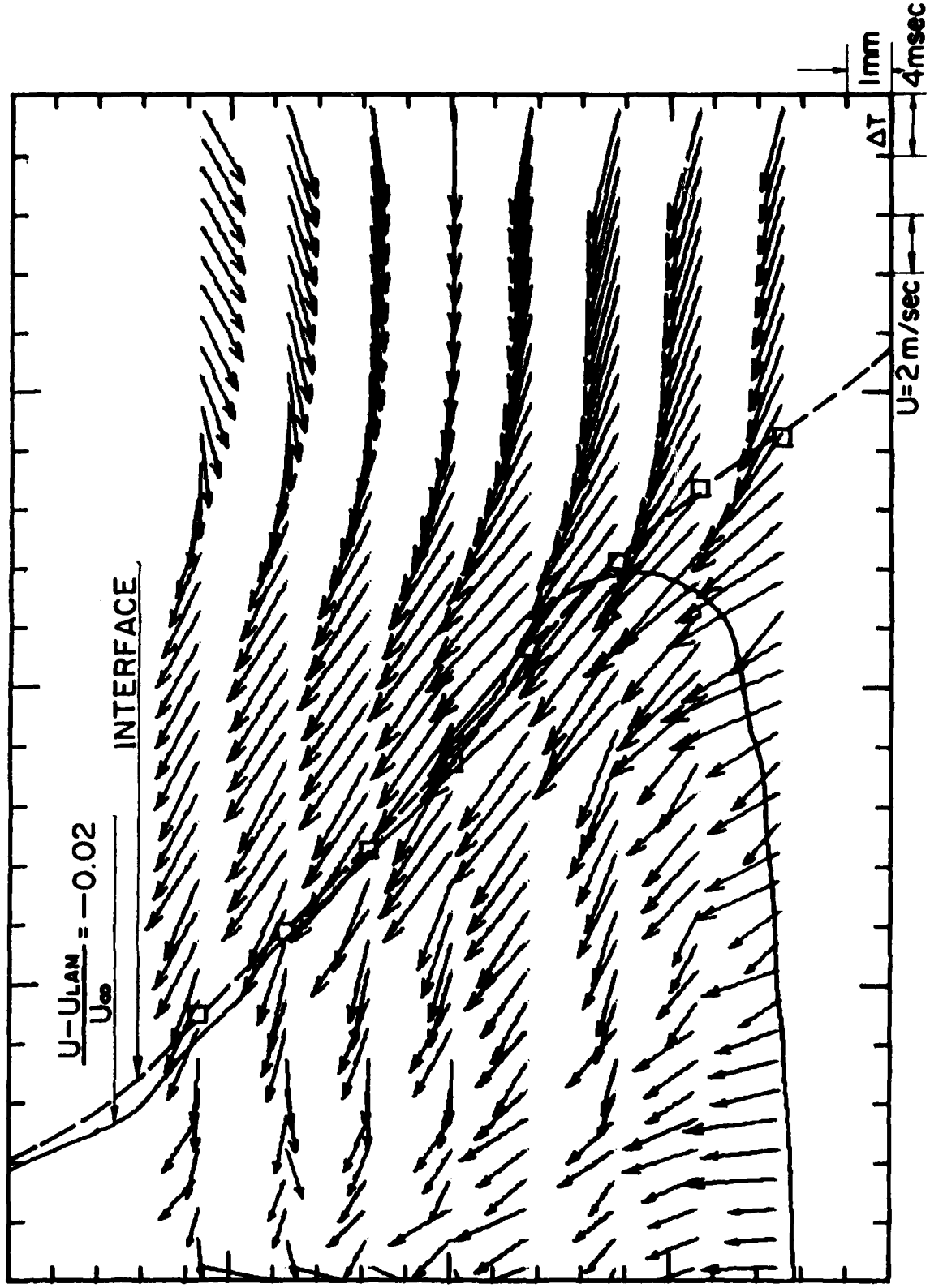

FIGURE D.2.5b

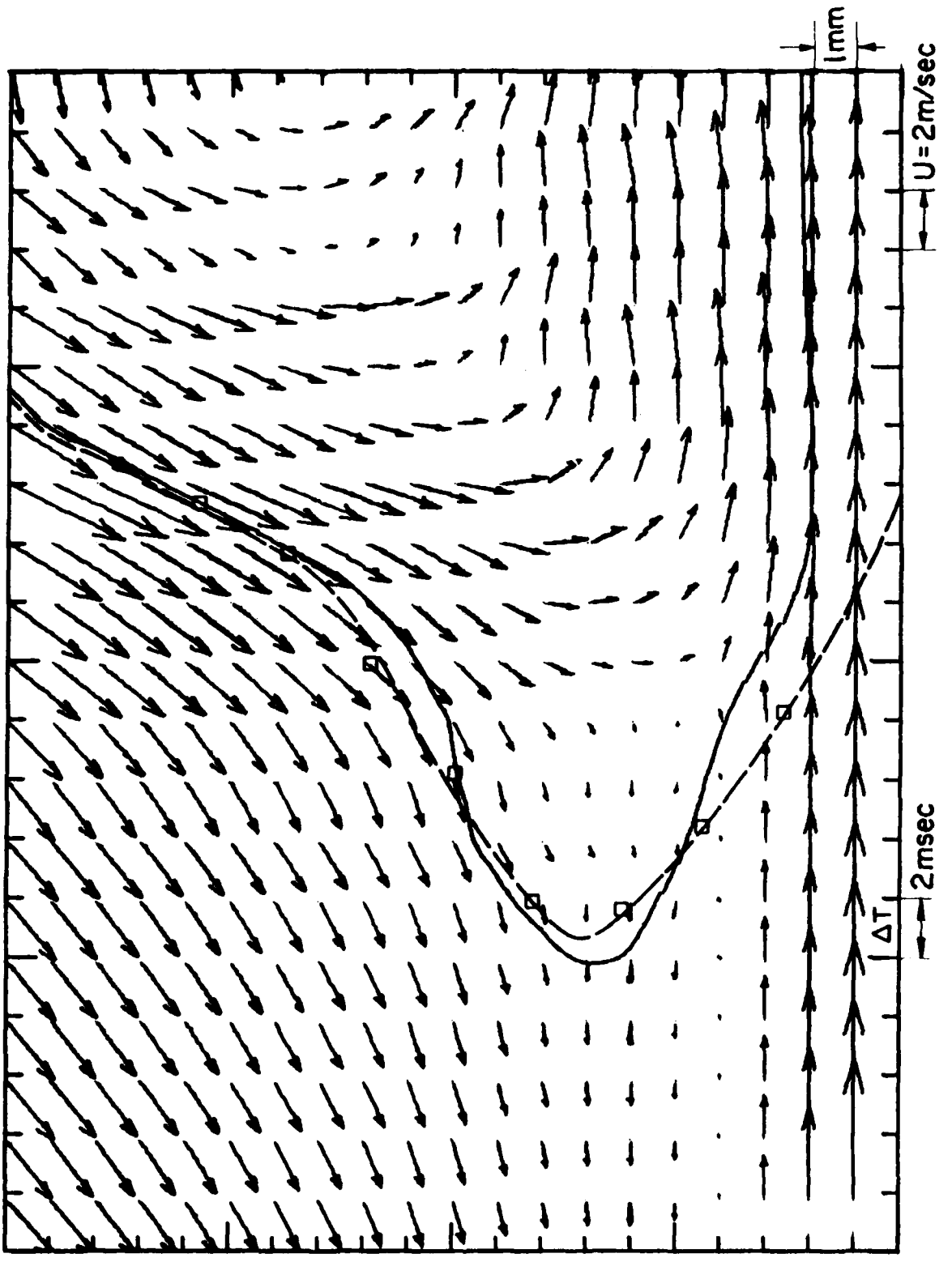

FIGURE D.2.5c

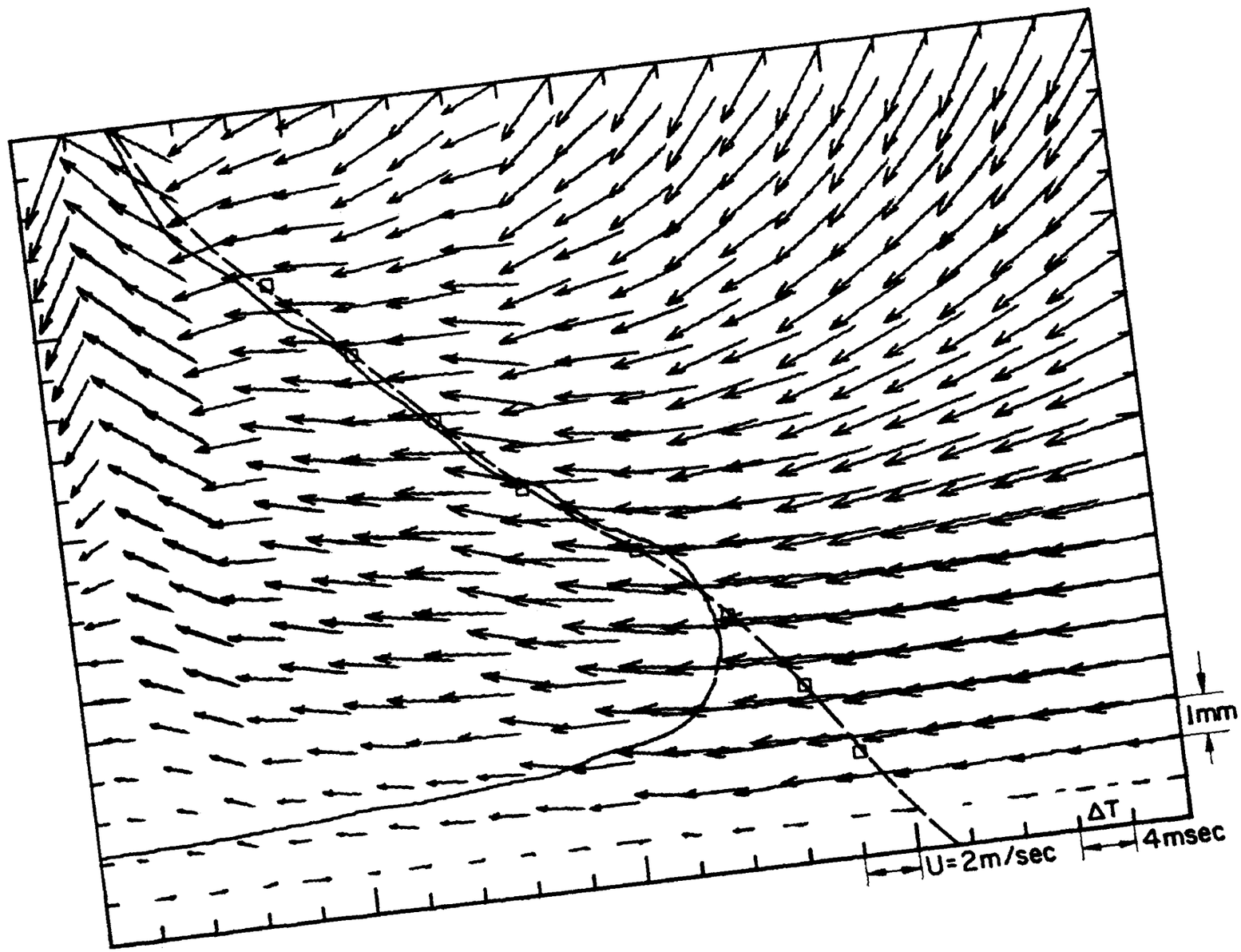

FIGURE D.2.5d

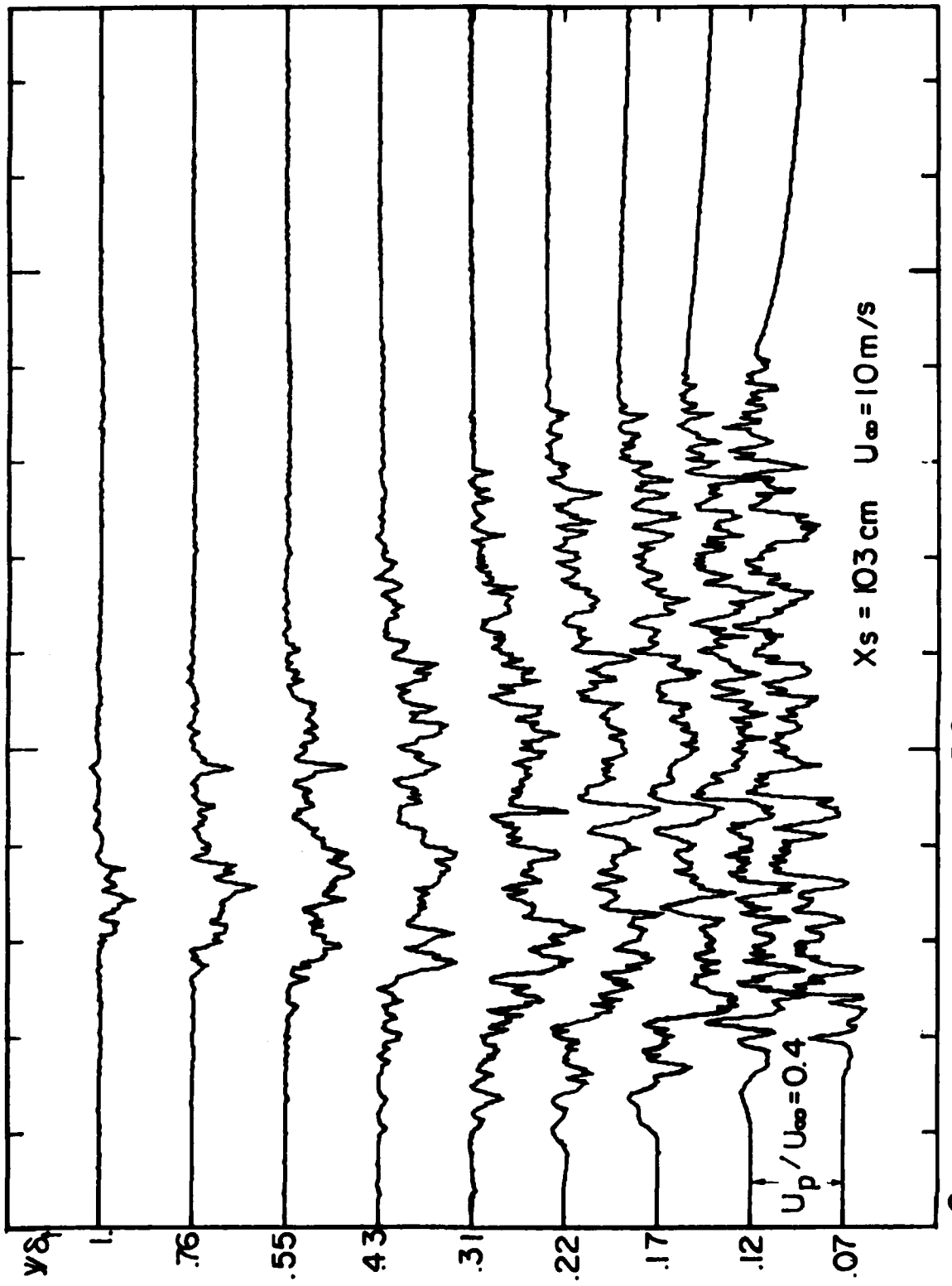
y/δ
1.
.76
.55
.43
.31
.22
.17
.12
.07
$U_p / U_\infty = 0.4$
Xs = 103 cm U_∞ = 10 m/s
0
50
100
msec

FIGURE D.3.1

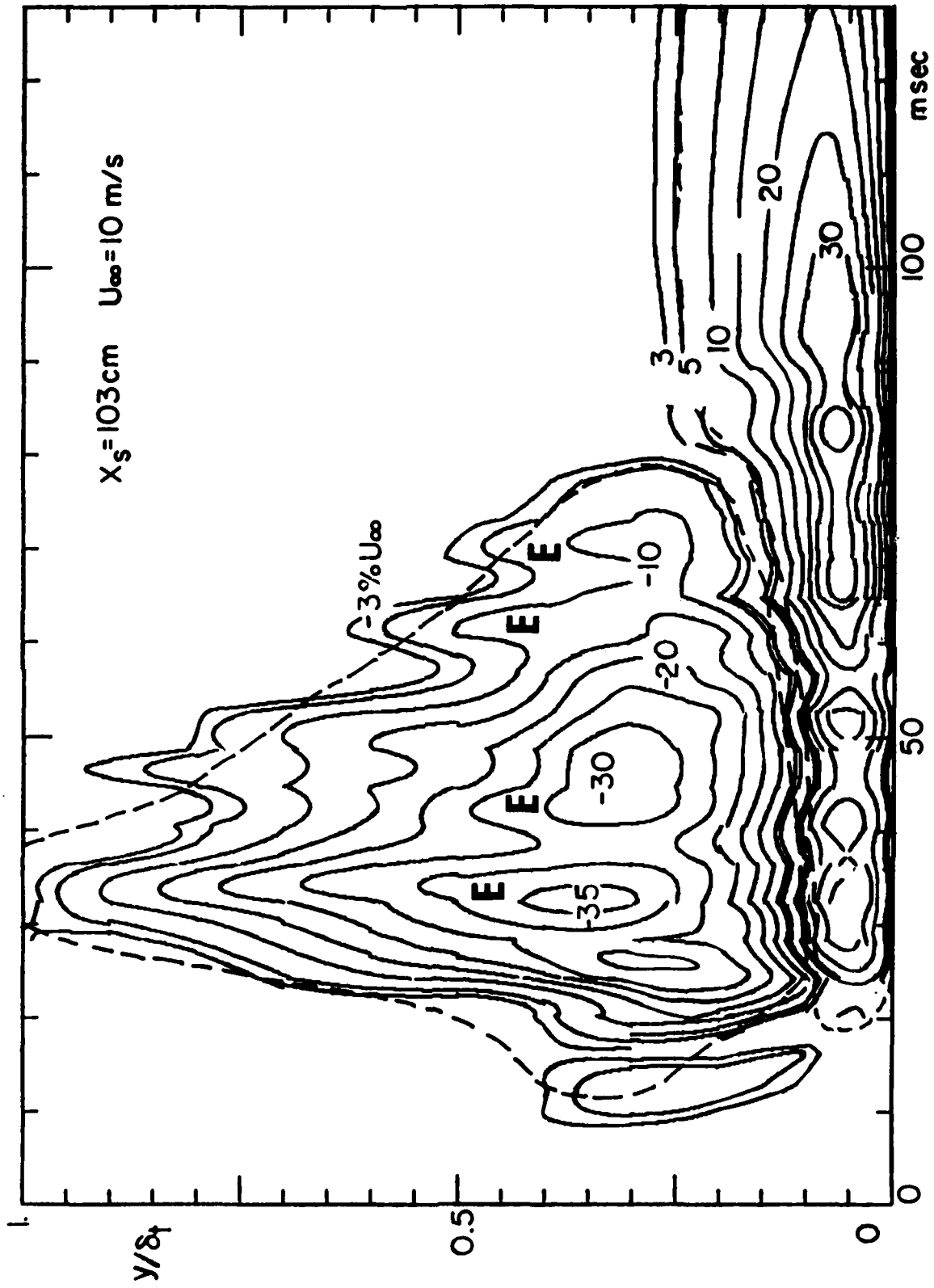
X_s=103cm U_∞=10 m/s
-3%U_∞
E
E
E
E
-10
-20
-30
-35
3
5
10
20
30
50
100
msec
y/δ_1
1.
0.5
0

FIGURE D.3.2

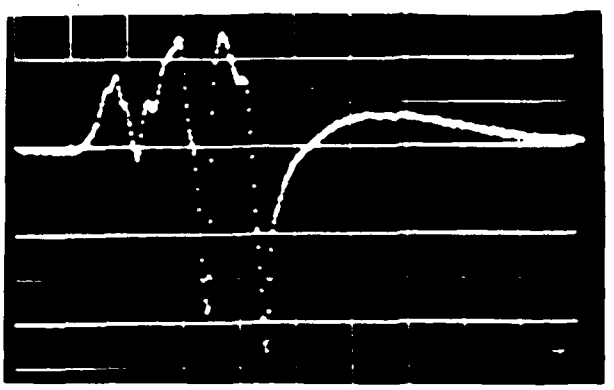

X_S =20cm

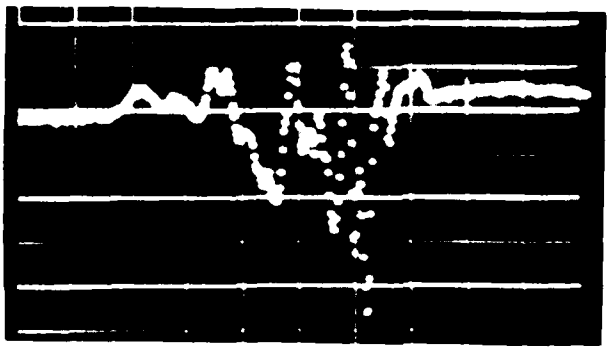

X_S=30cm

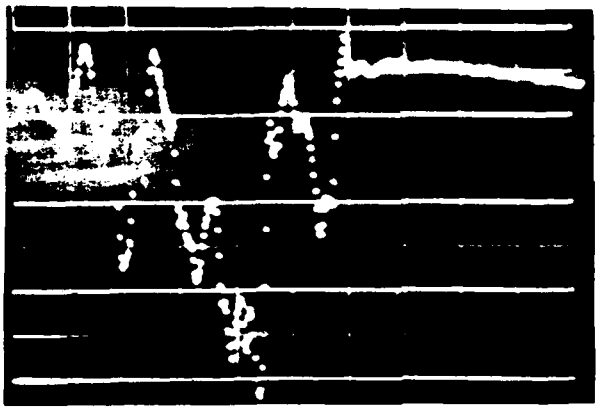

X_S=40cm

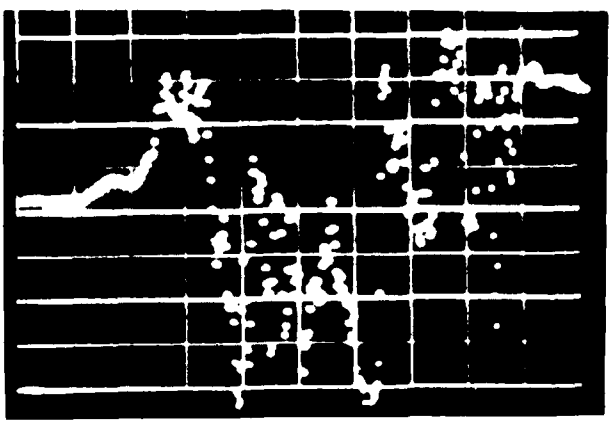

X_S=50cm

6 msec

FIGURE D.3.3

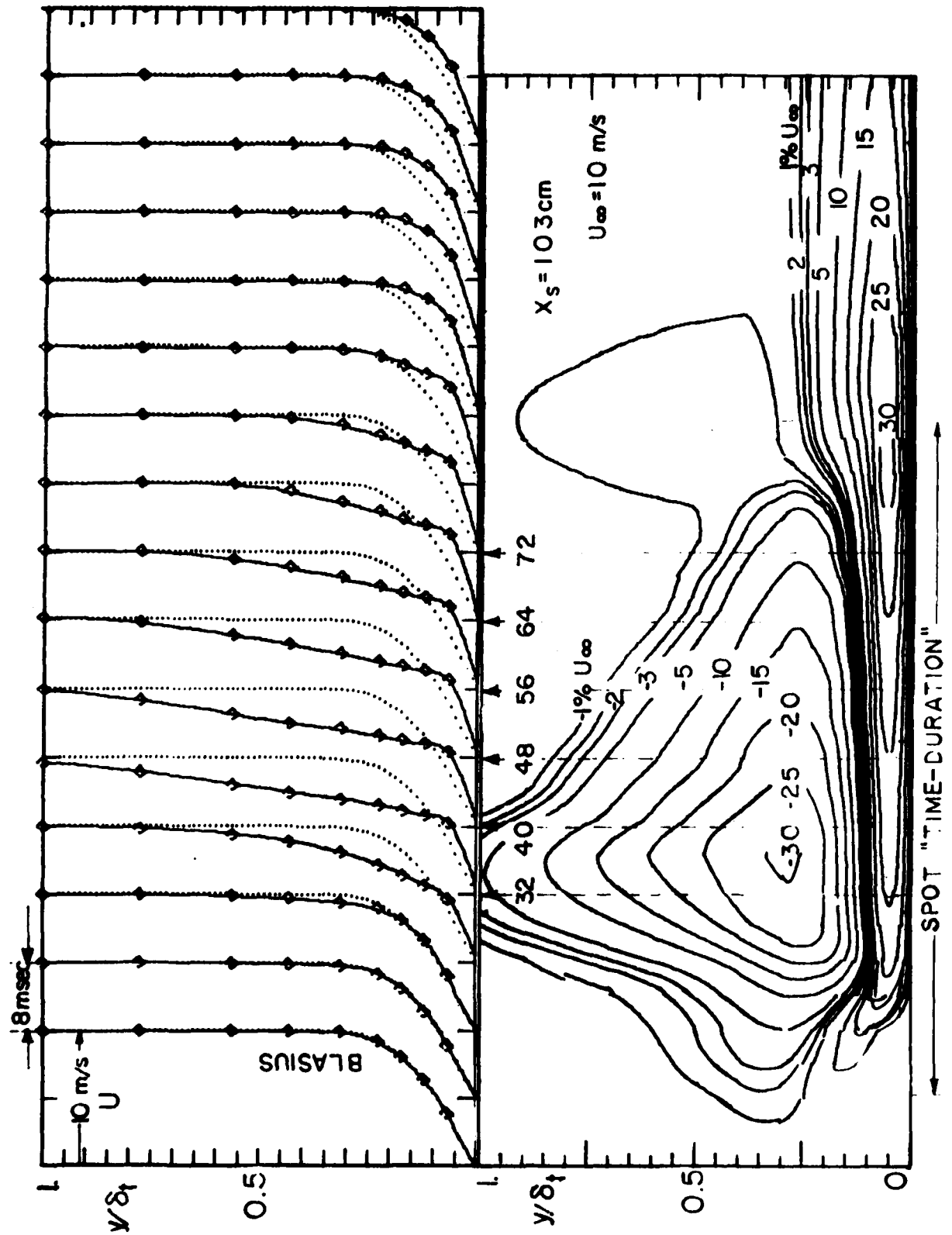
BLASIUS
U
10 m/s
18msec
y/δ1
0.5
1
X_s=103cm
U_∞=10 m/s
1% U_∞
-1% U_∞
-2
-3
-5
-10
-15
-20
-25
-30
2
3
5
10
15
20
25
30
32
40
48
56
64
72
SPOT "TIME-DURATION"

FIGURE D.4.1

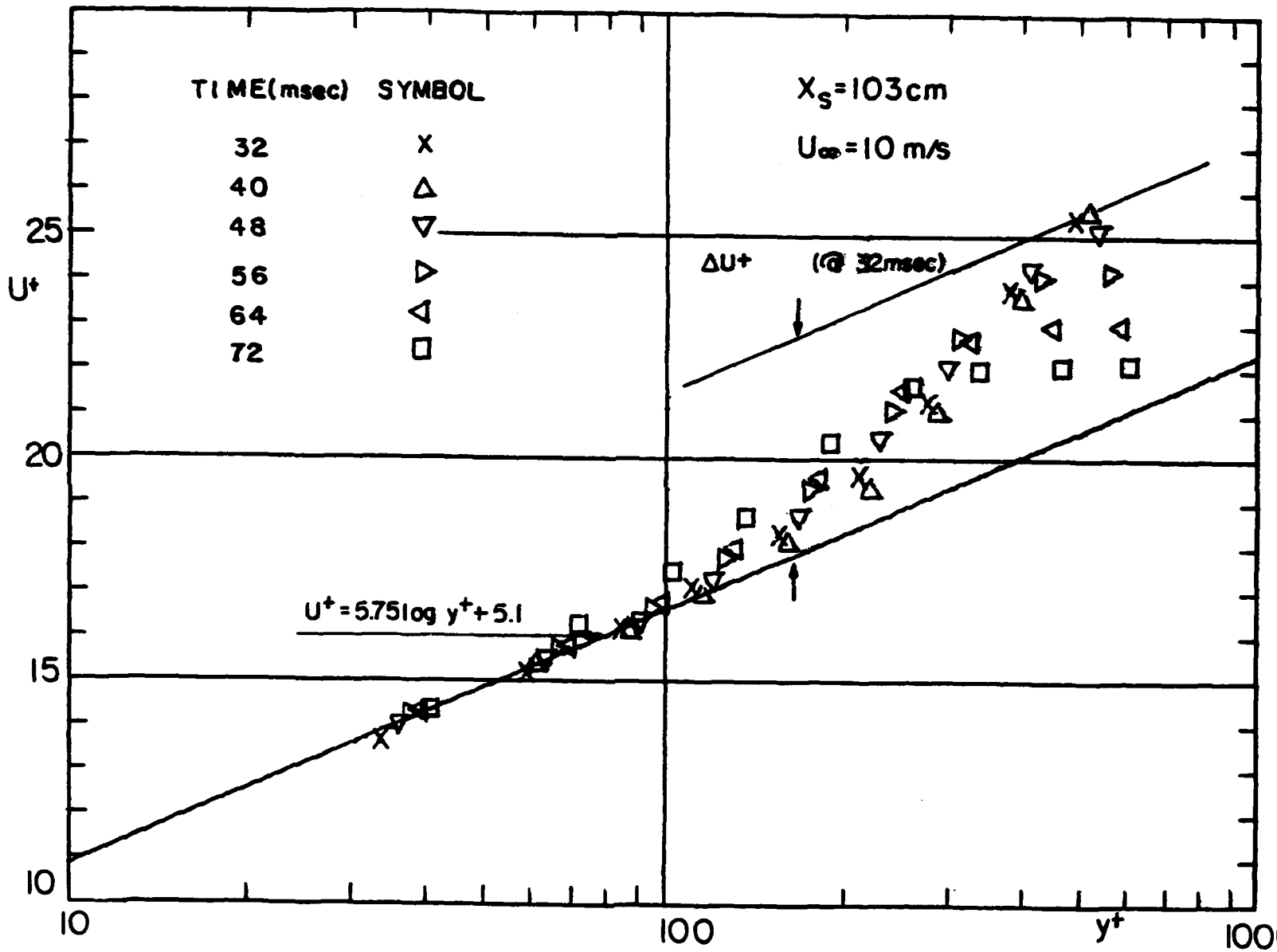
TIME(msec) SYMBOL
32 X
40 Δ
48 ▽
56 ▷
64 ◁
72 □
X_s=103cm
U_∞=10 m/s
ΔU+ (@ 32msec)
$U^+ = 5.75 \log y^+ + 5.1$
U^+
y^+
25
20
15
10
10
100
1000

FIGURE D.4.2

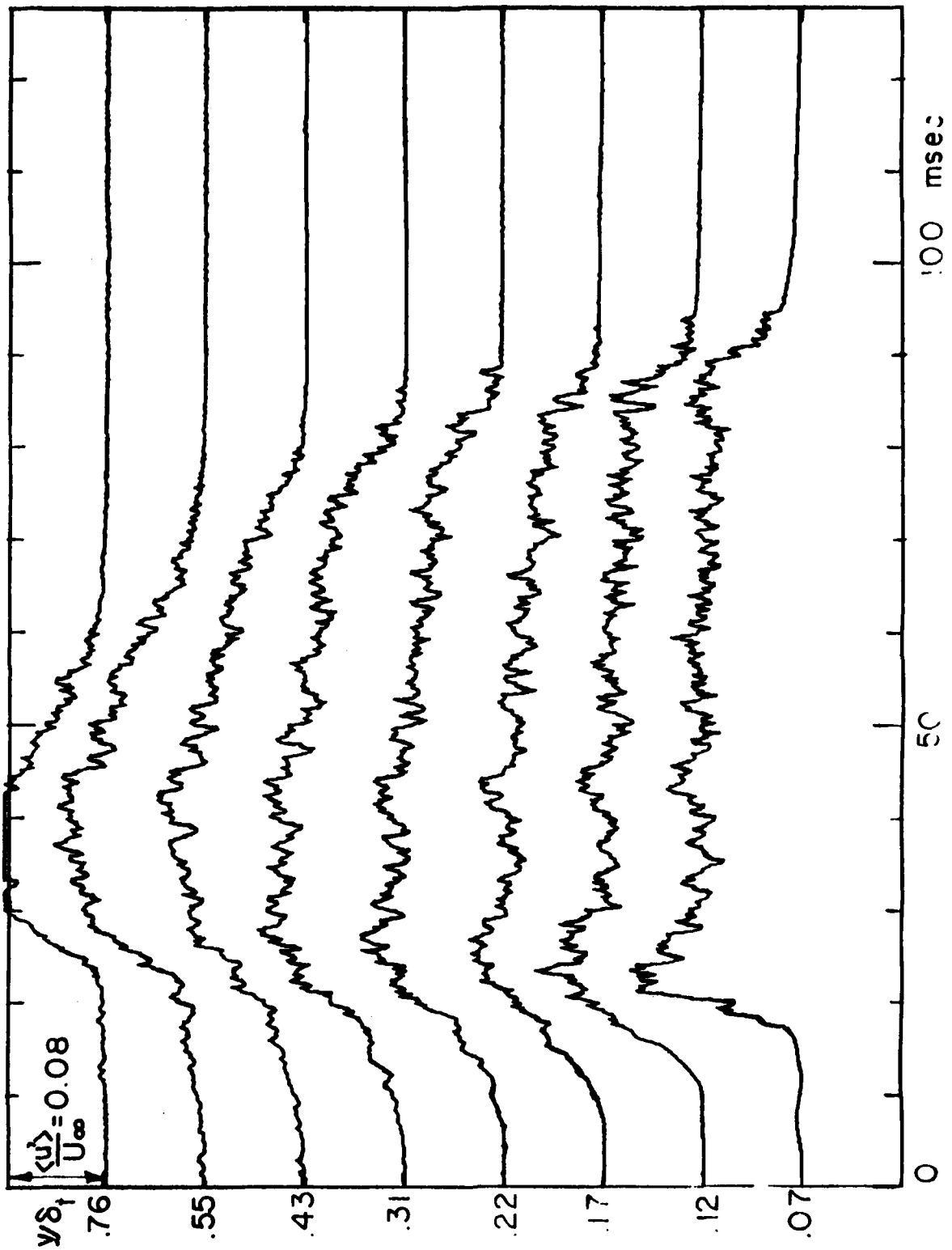
$\frac{\langle u \rangle}{U_\infty}$=0.08
y/δ
.76
.55
.43
.31
.22
.17
.12
.07
0
50
100 msec

FIGURE 5.5.1

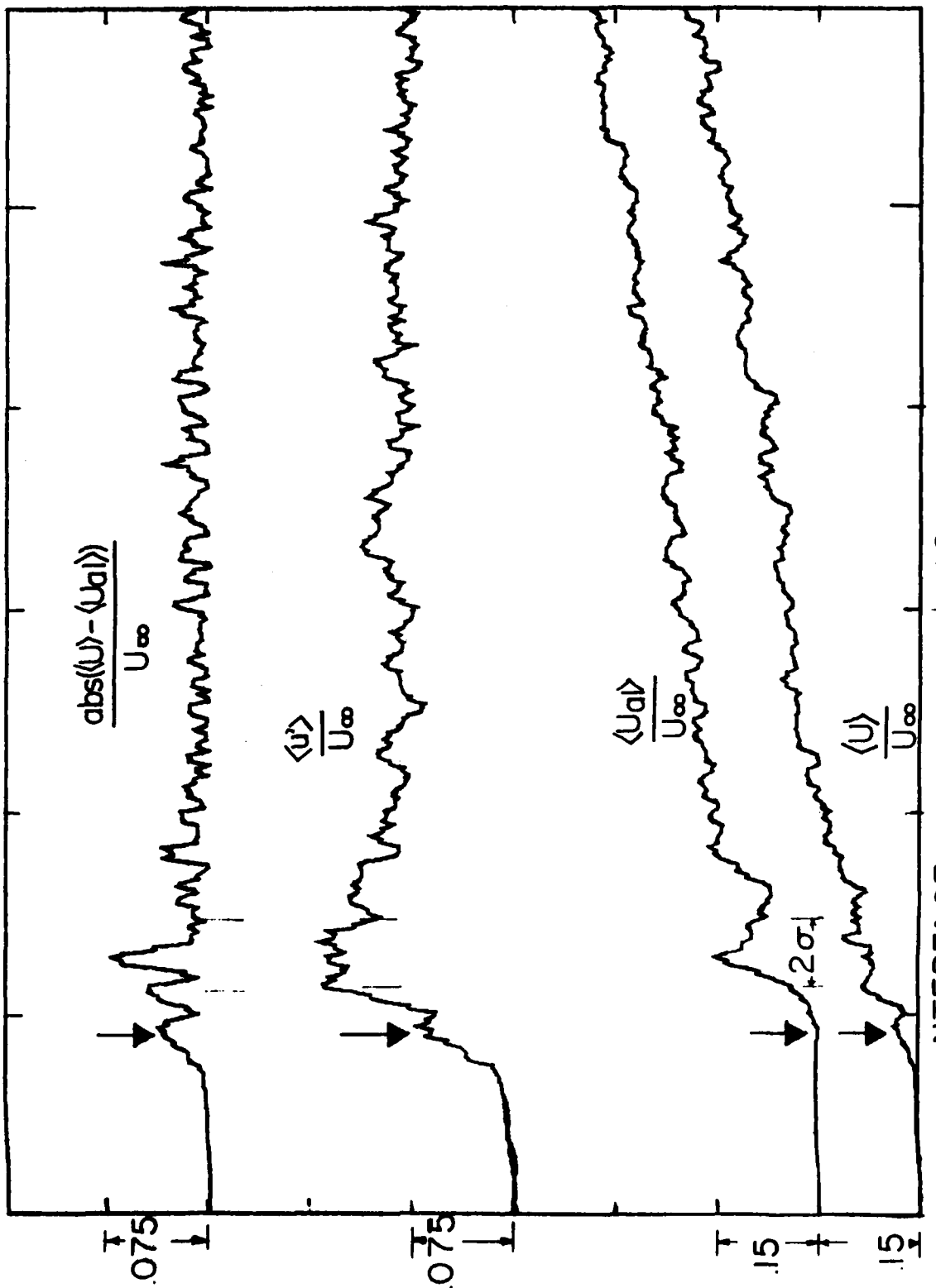

FIGURE D.5.2

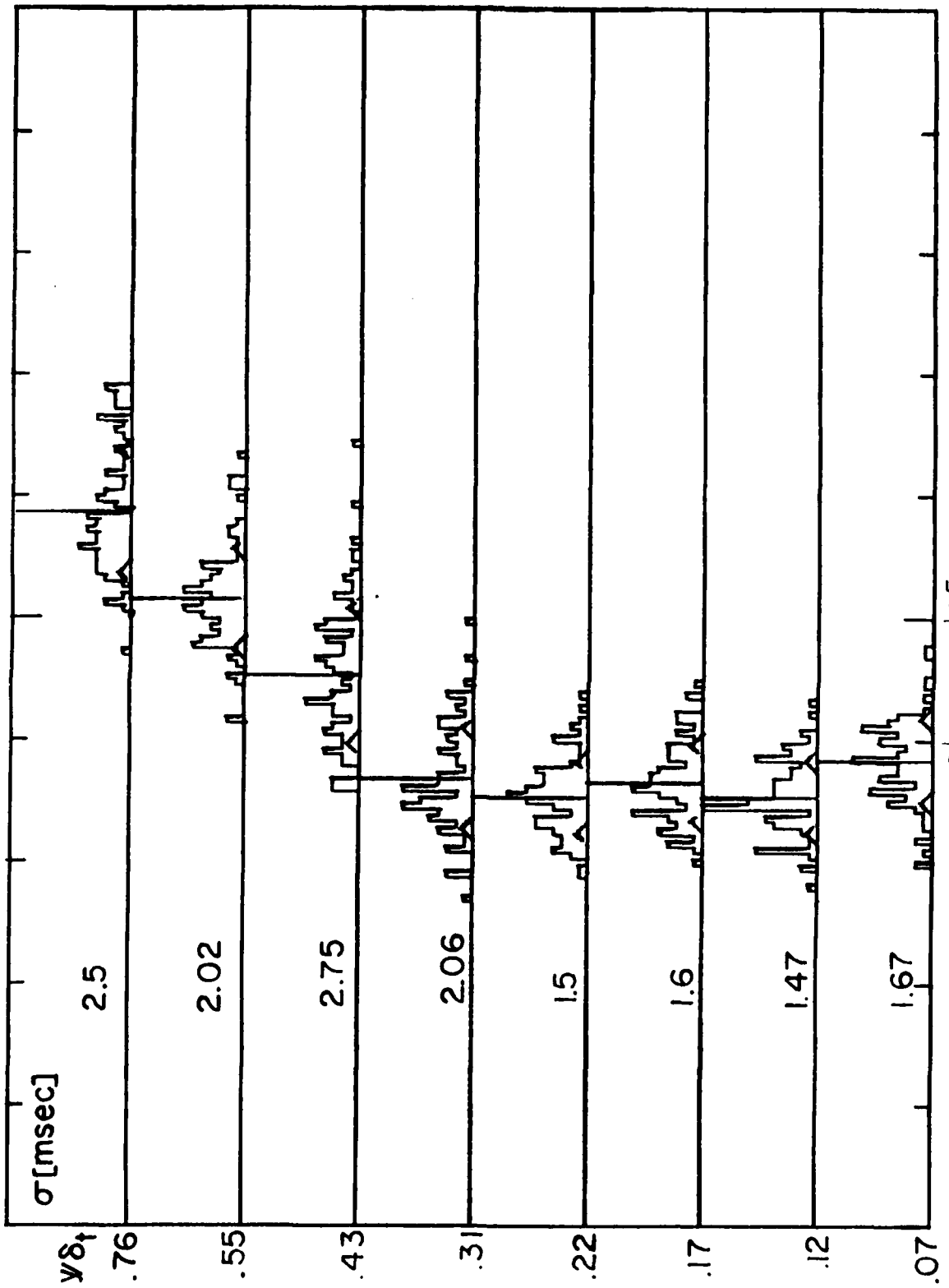
σ[msec]
y/δ1
.76
.55
.43
.31
.22
.17
.12
.07
2.5
2.02
2.75
2.06
1.5
1.6
1.47
1.67
5 msec

FIGURE D.5.3a

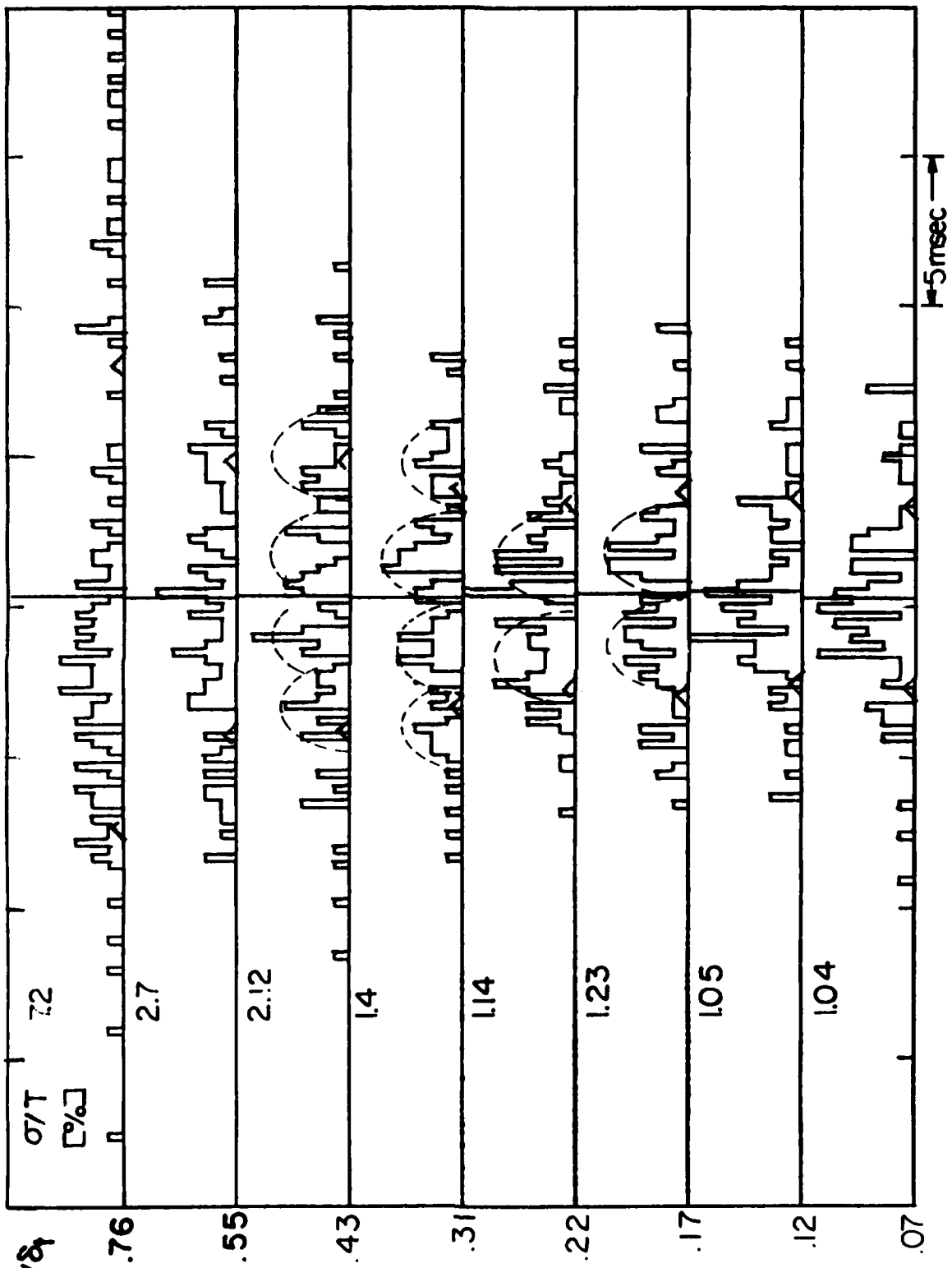
$w\delta_q$
.76
.55
.43
.31
.22
.17
.12
.07
σ/T [%]
7.2
2.7
2.12
1.4
1.14
1.23
1.05
1.04
5msec

FIGURE D.5.3b

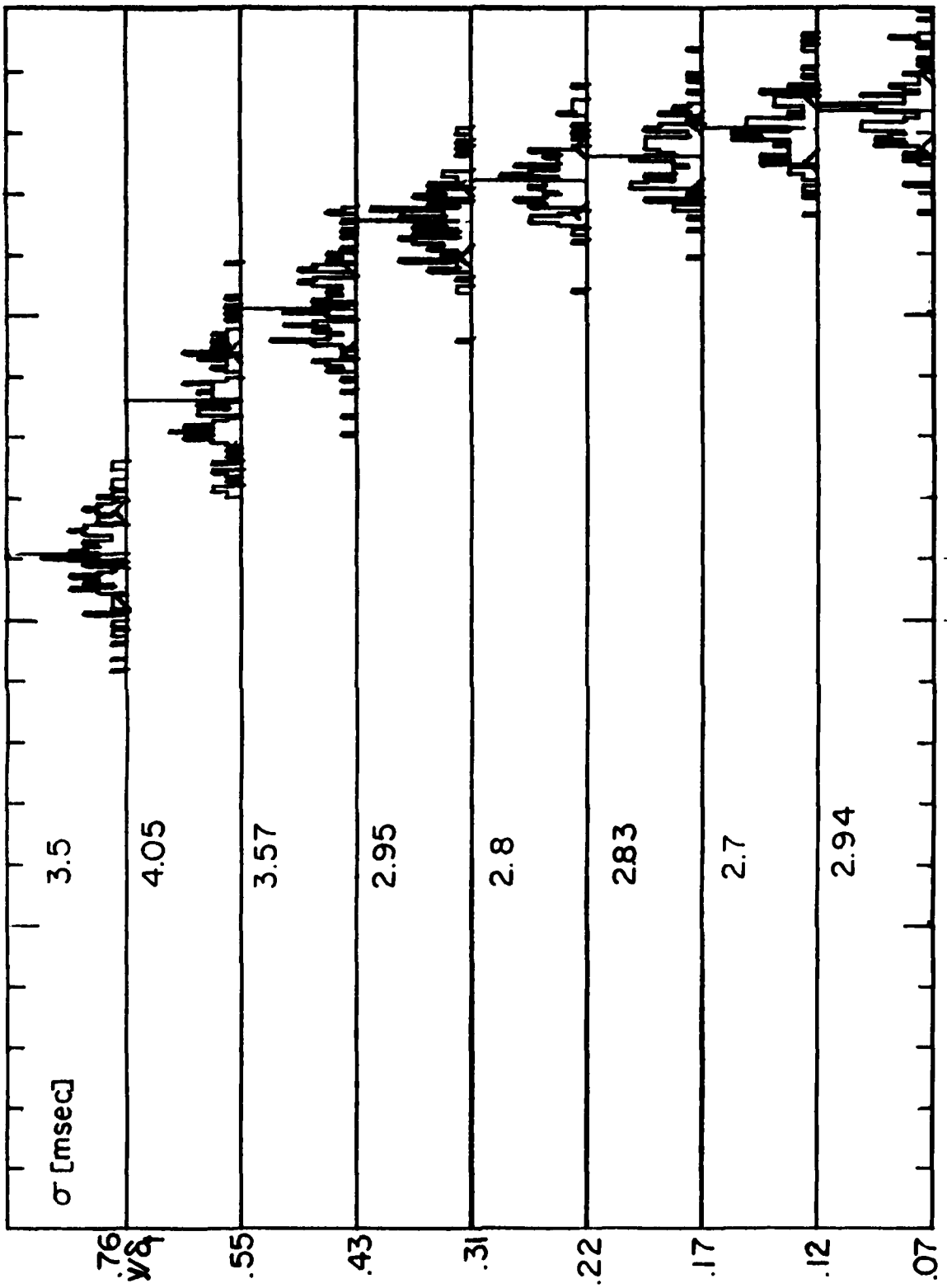

FIGURE D.5.3c

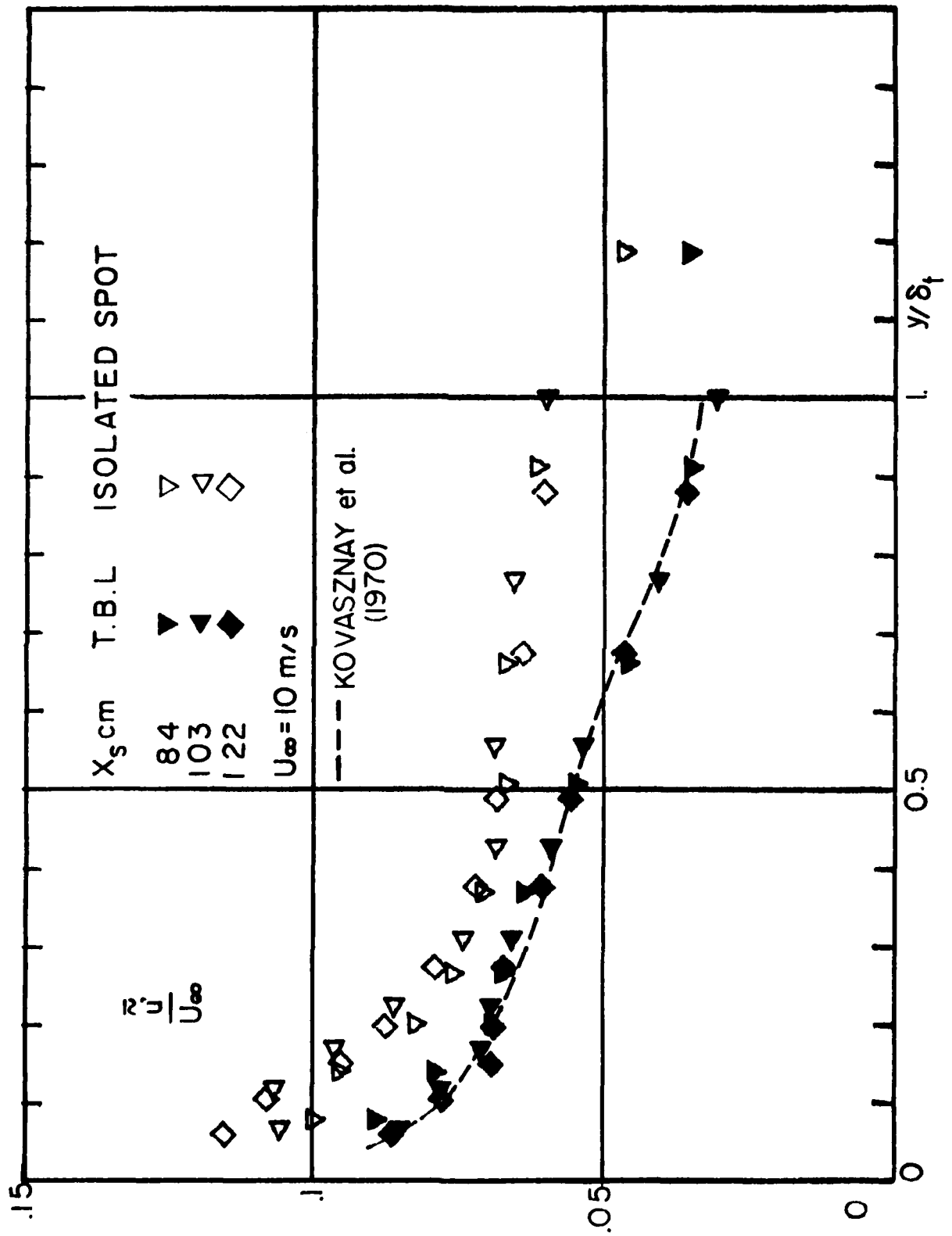
ISOLATED SPOT
T.B.L
X_s cm
84
103
122
U_∞=10 m/s
KOVASZNAY et al.
(1970)
$\overline{u}/U_\infty$
y/δ_1
.15
.1
.05
0
0
0.5
1

FIGURE D.6.1

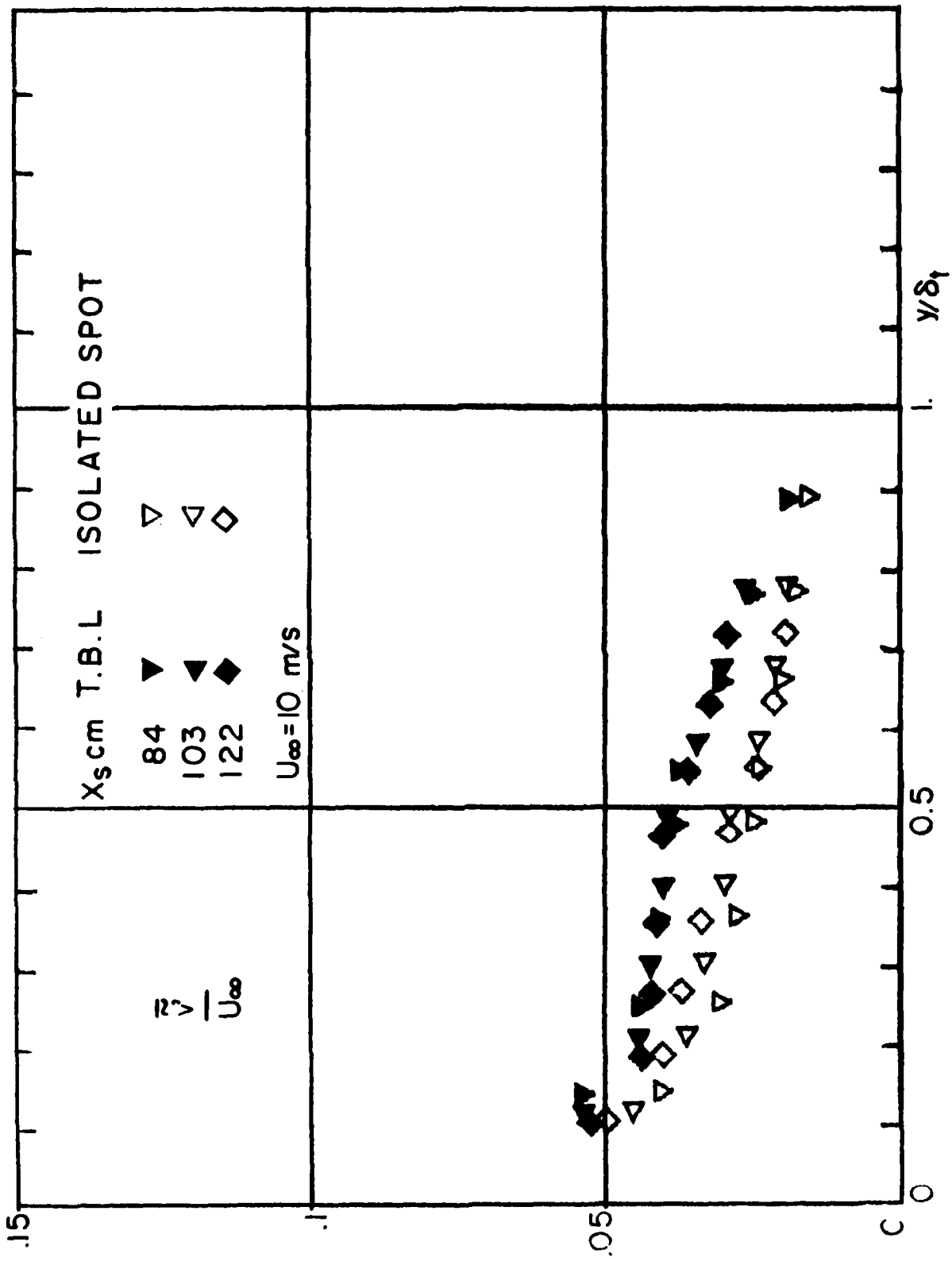
ISOLATED SPOT
X_s cm T.B.L
84
103
122
U_∞=10 m/s
$\overline{R'} / U_\infty$
.15
.1
.05
0
0.5
1.
y/δ_1

FIGURE D.2.2

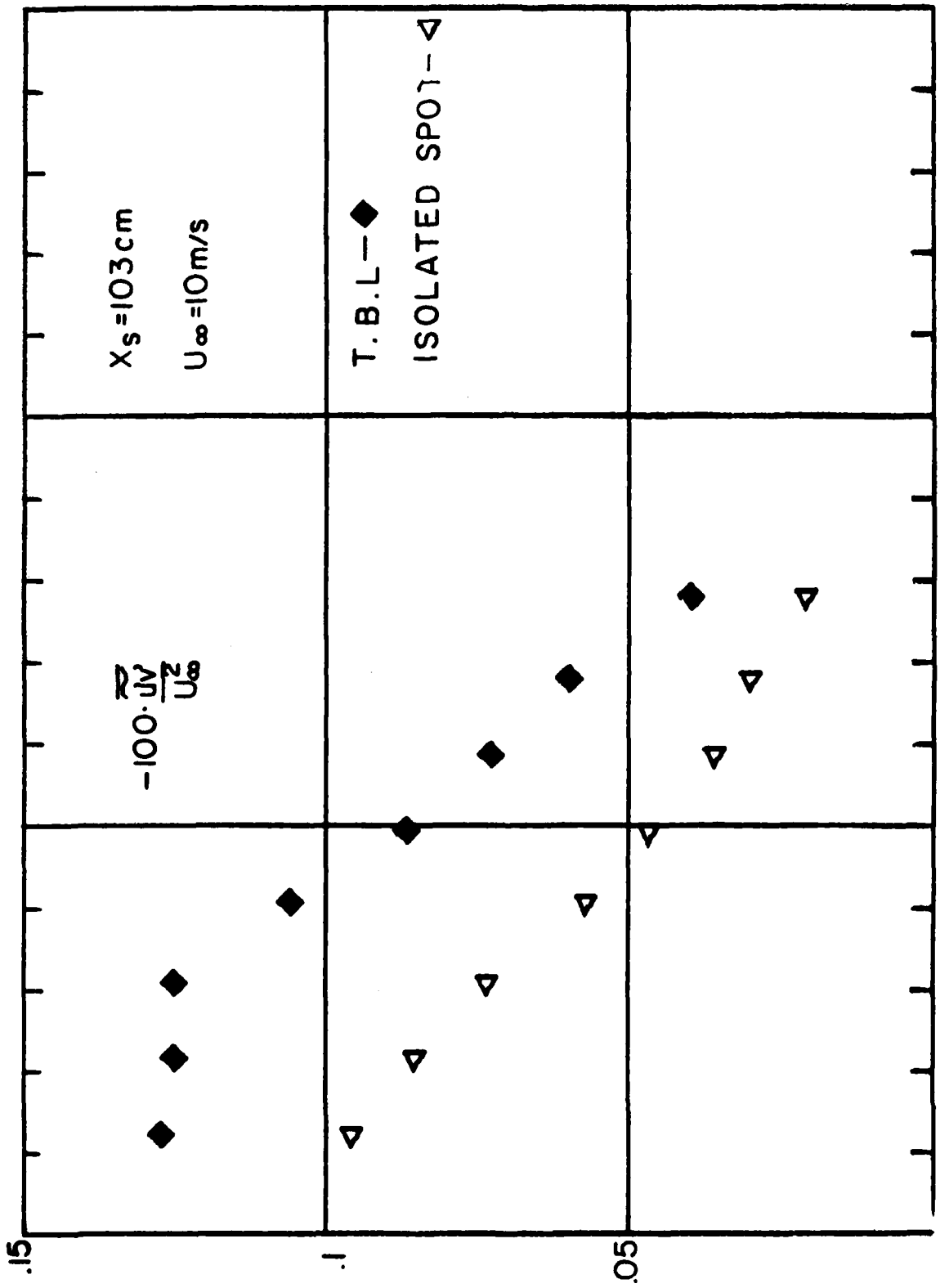
X_s=103cm
U_∞=10m/s
T.B.L—◆
ISOLATED SPOT—▽
$-100\cdot\frac{\overline{uv}}{U_\infty^2}$
.15
.1
.05
0
0.5
1.
y/δ_t

FIGURE D.6.3

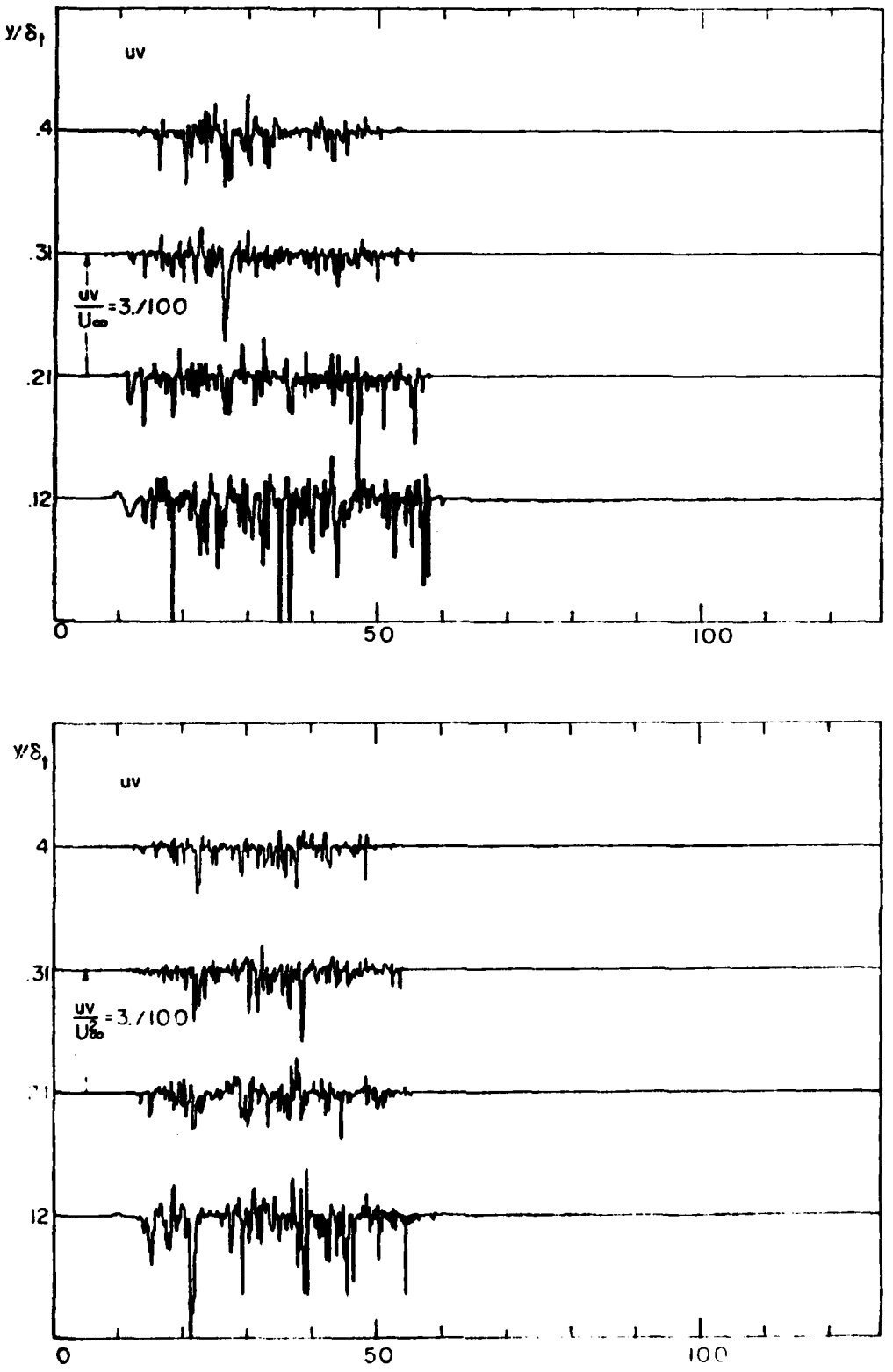

FIGURES D.7.1a,b

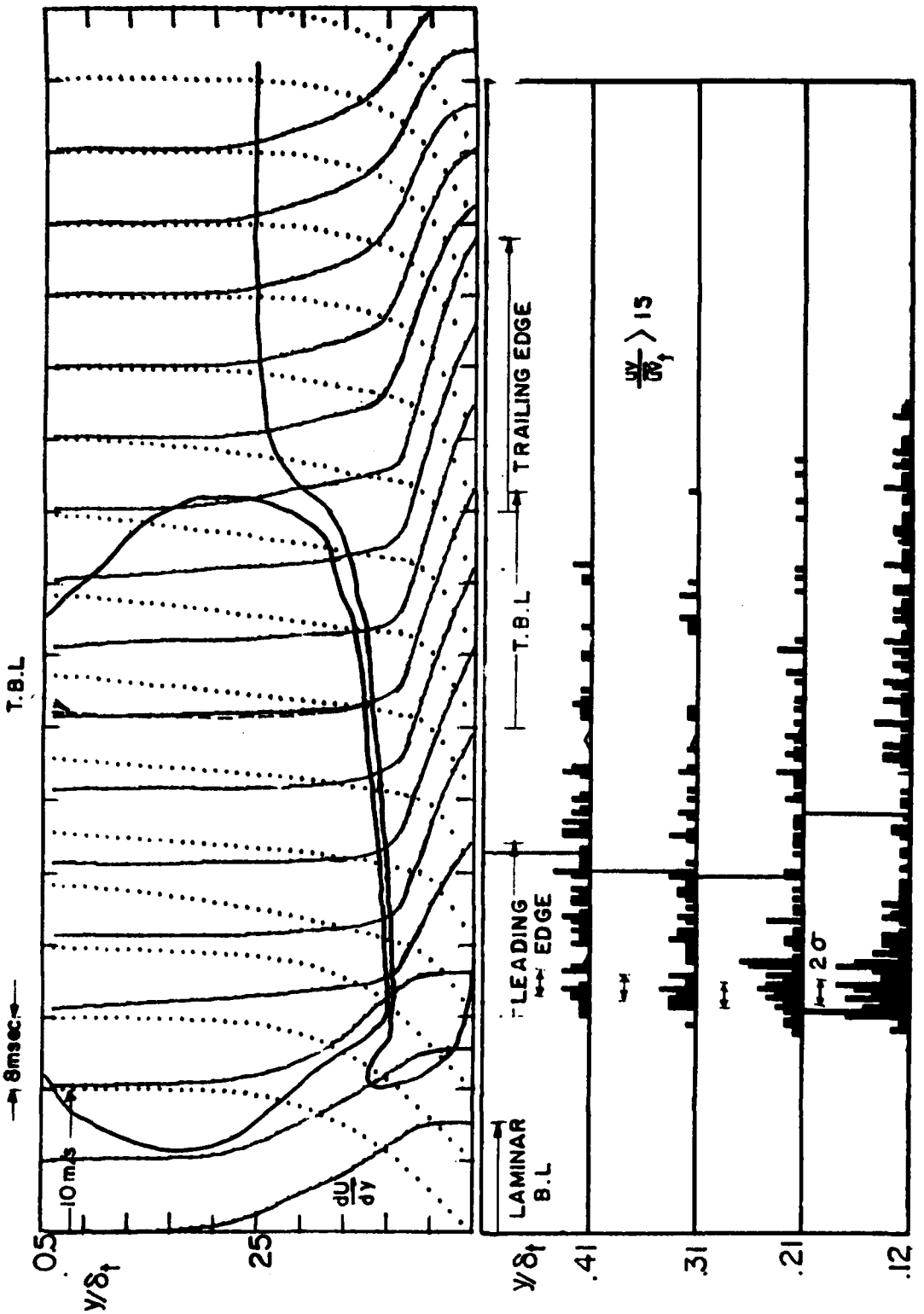
T.B.L
8msec
10 m/s
$\frac{dU}{dy}$
0.5
2.5
y/δ_t
LAMINAR B.L
LEADING EDGE
T.B.L
TRAILING EDGE
$\frac{uv}{(u^2)_t} > 15$
2σ
.41
.31
.21
.12
y/δ_t

FIGURE D.7.2

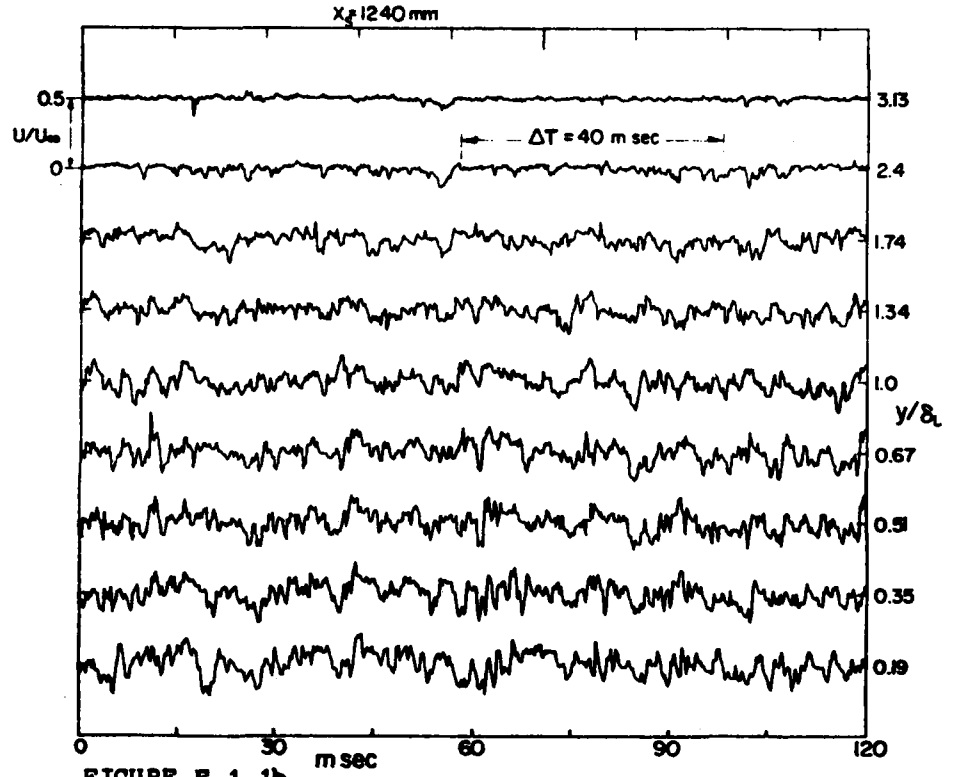

FIGURE E.1.1b

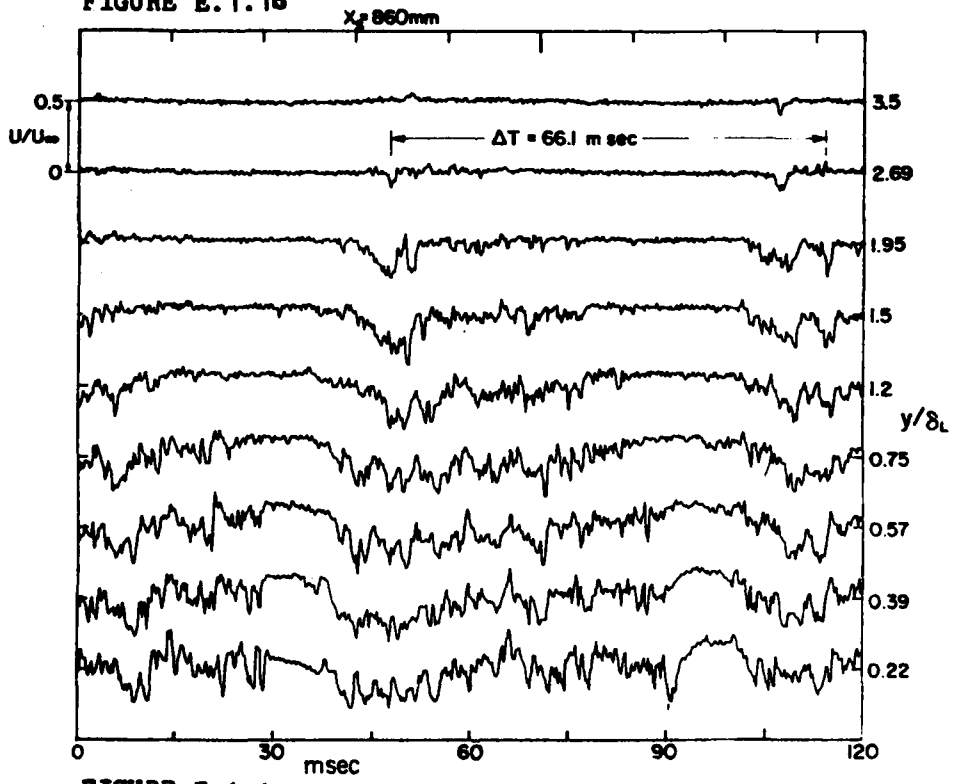

FIGURE E.1.1a

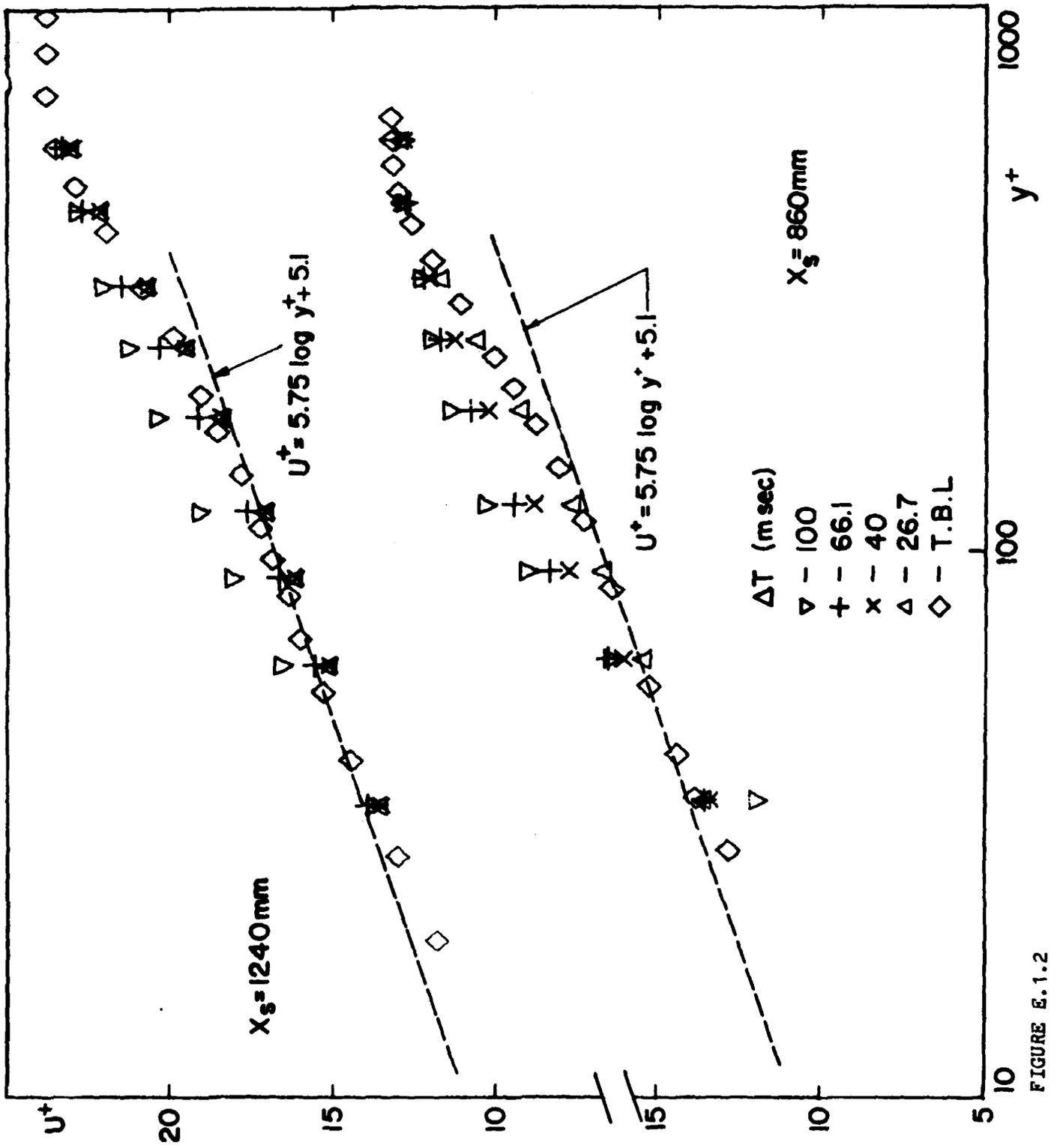
U+
20
15
10
15
10
5
10
100
1000
y+
U+= 5.75 log y+ + 5.1
U+= 5.75 log y+ + 5.1
Xs= 1240mm
Xs= 860mm
ΔT (m sec)
▽ – 100
+ – 66.1
x – 40
△ – 26.7
◇ – T.B.L

FIGURE E.1.2

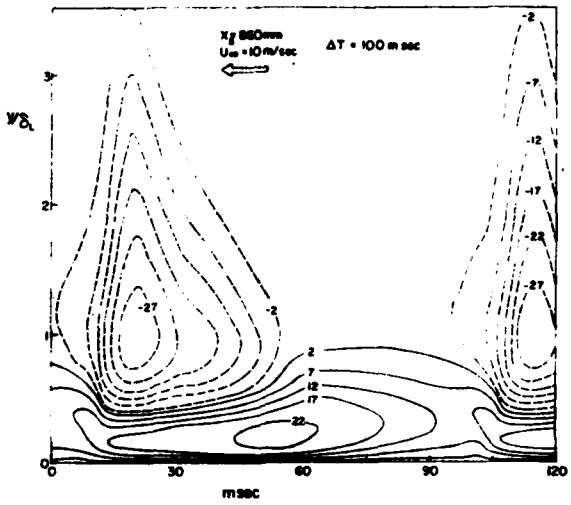

FIGURE E.1.3a

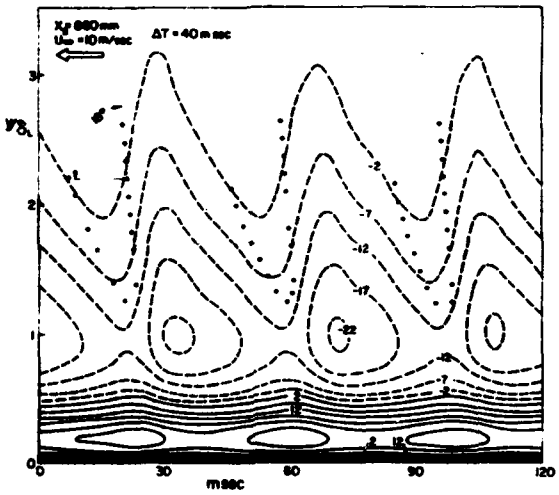

FIGURE E.1.3b

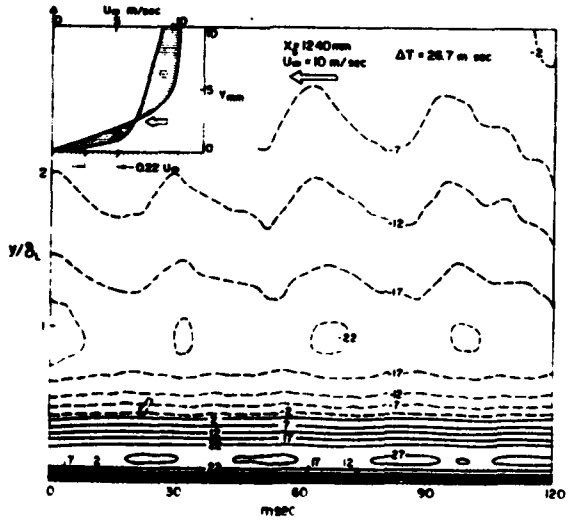

FIGURE E.1.3c

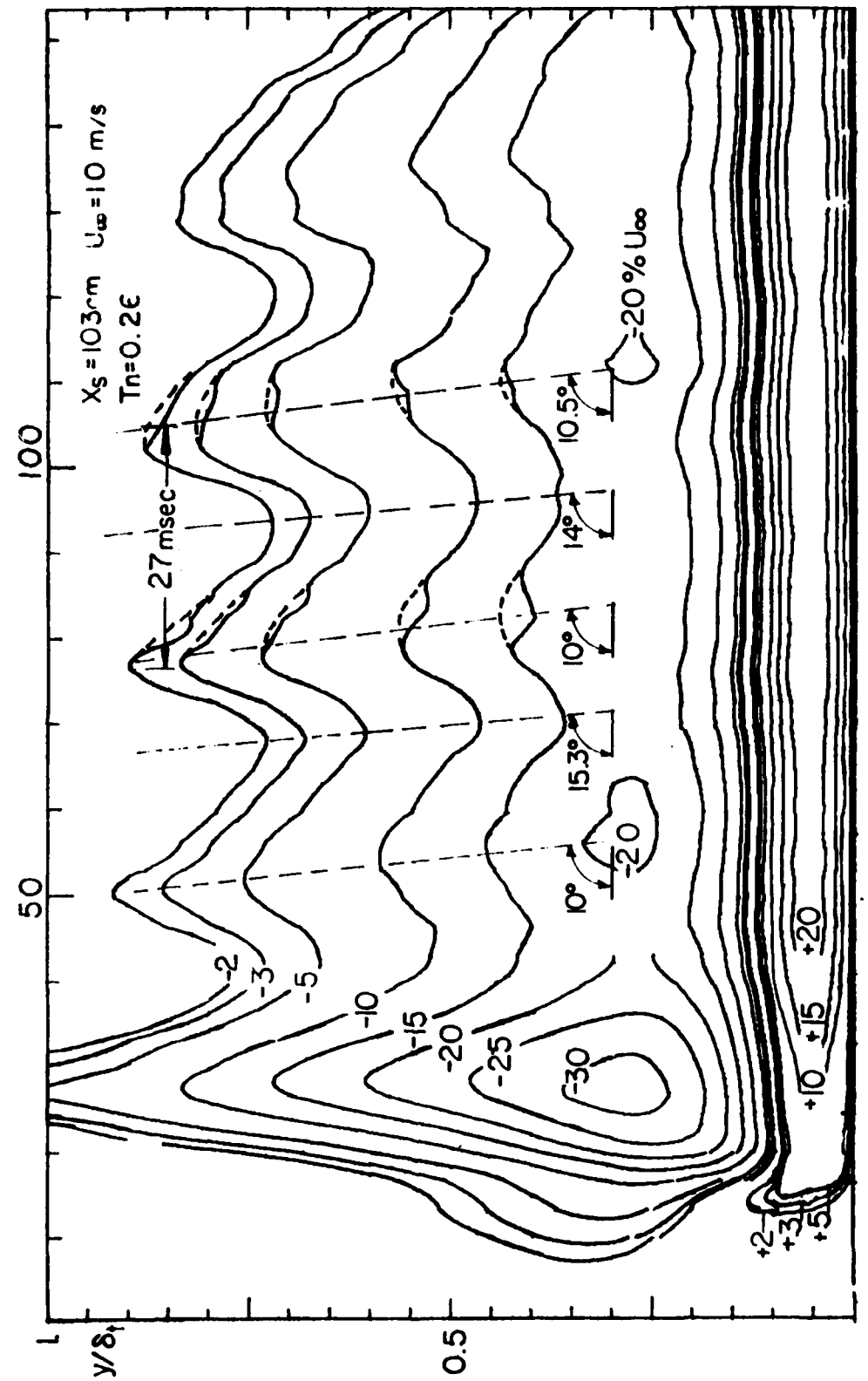
X_s=103cm U_∞=10 m/s
Tn=0.2ε
27 msec
10.5°
14°
10°
15.3°
10°
20 % U_∞
-2
-3
-5
-10
-15
-20
-25
-30
-20
+2
+3
+5
+10
+15
+20
100
50
1
0.5
y/δ_1

FIGURE E.2.1

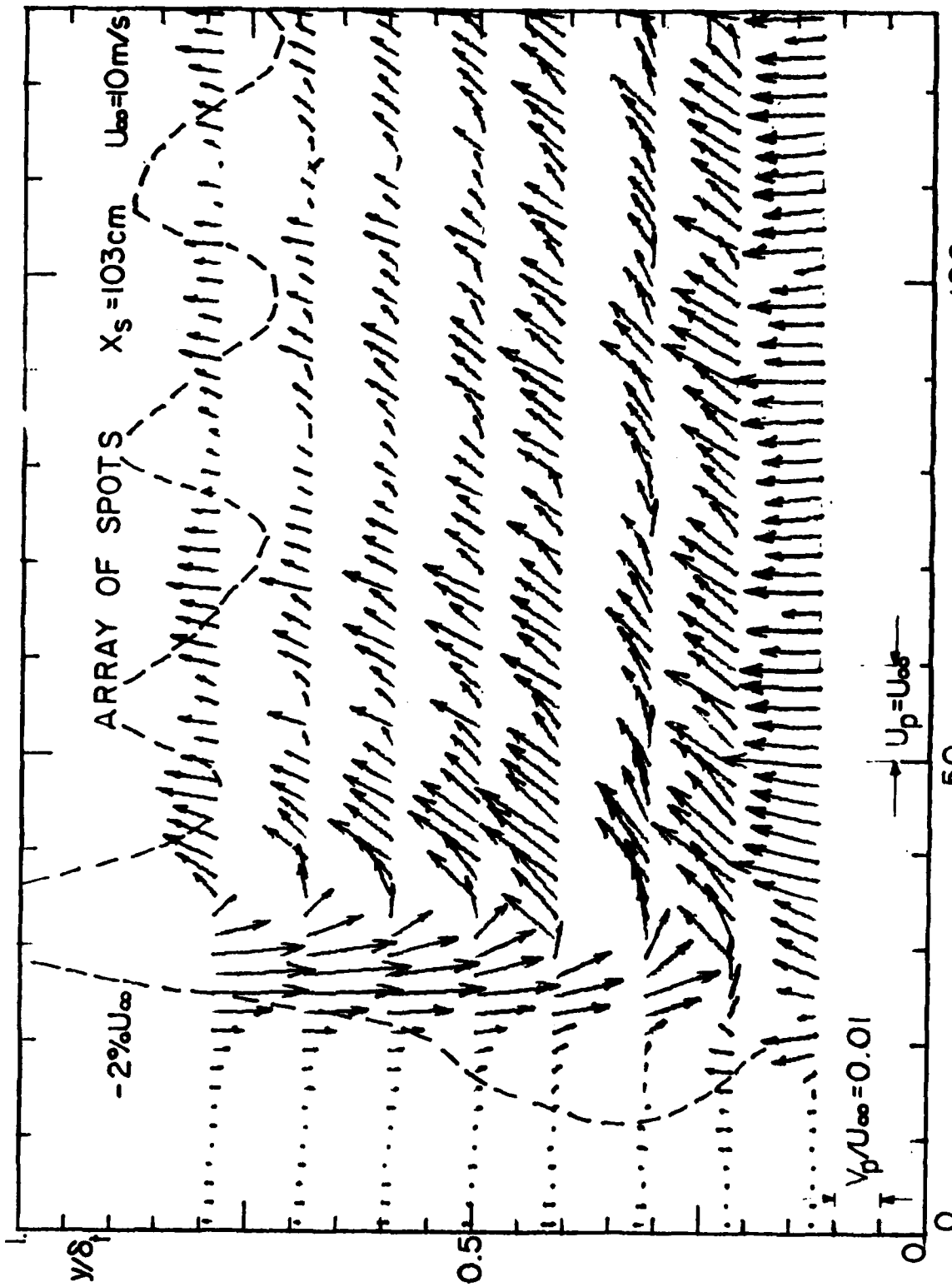
ARRAY OF SPOTS
X_s =103cm
U_∞=10m/s
-2%U_∞
y/δ
0.5
0
50
100
msec
$U_p=U_\infty$
V_p/U_∞=0.01

FIGURE E.2.2

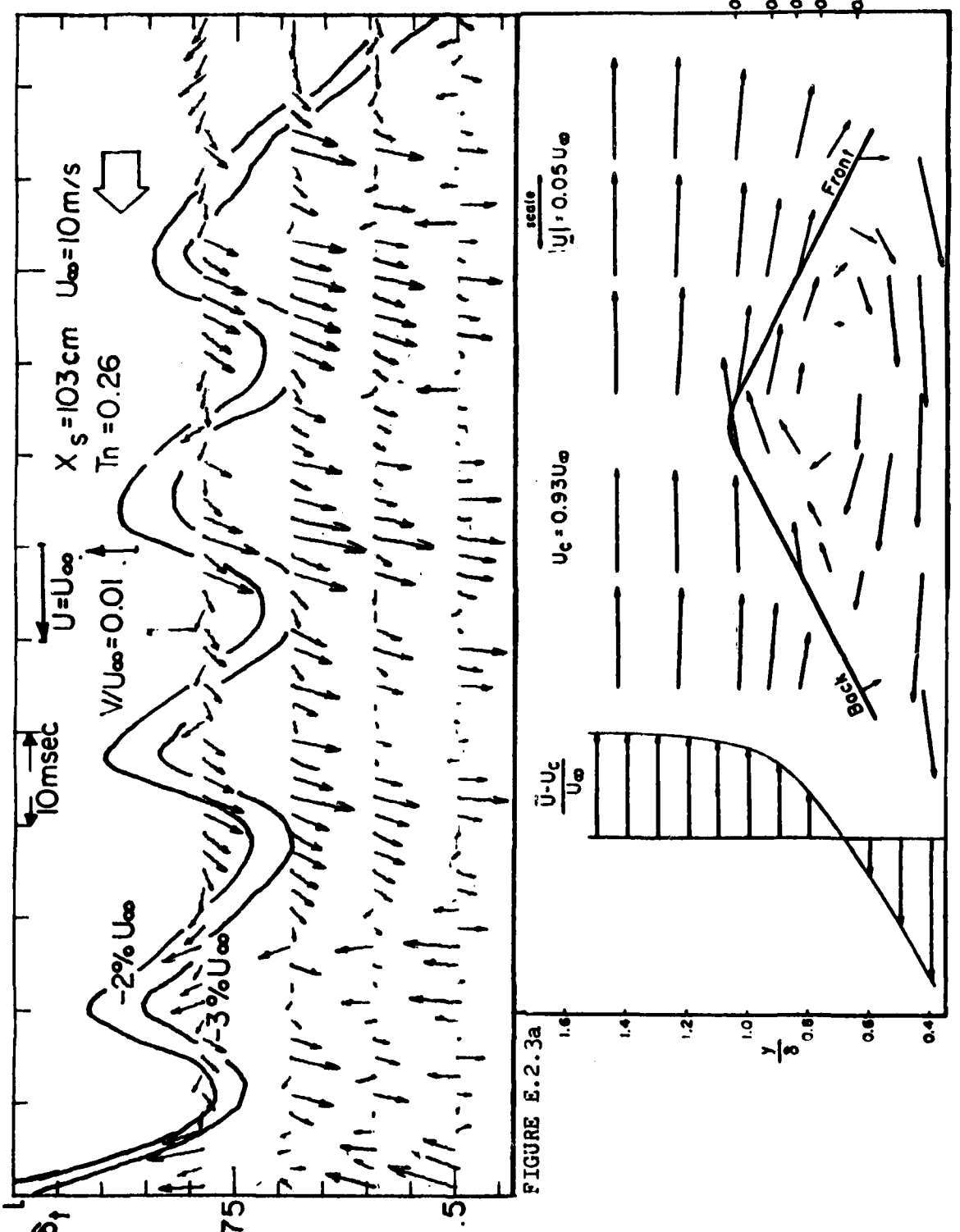

FIGURE E.2.3a

FIGURE E.2.3b

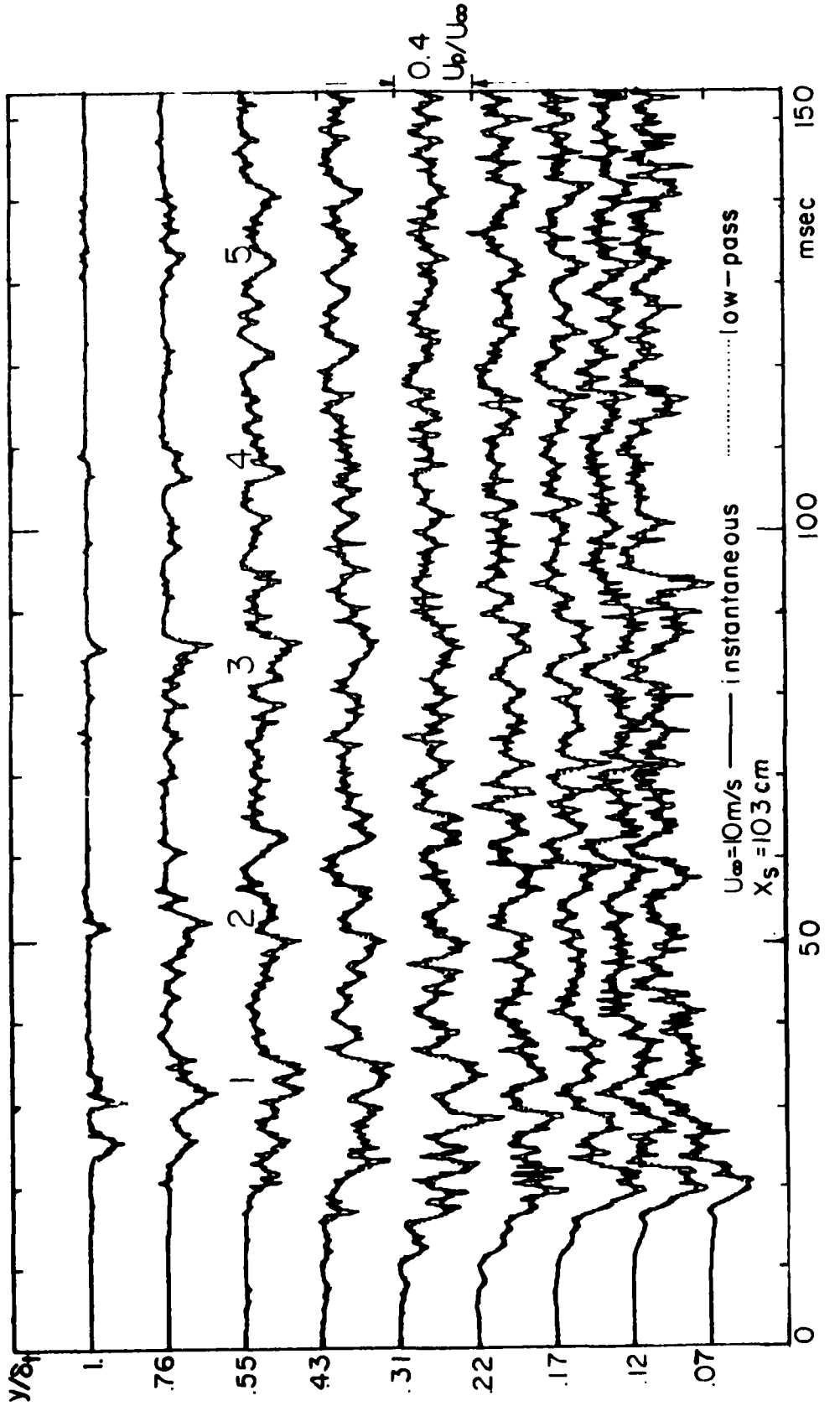
y/δ
1.
.76
.55
.43
.31
.22
.17
.12
.07
1
2
3
4
5
0.4
Ub/U∞
0
50
100
150
msec
U∞=10m/s —— instantaneous ..... low-pass
Xs =103 cm

FIGURE E.3.1

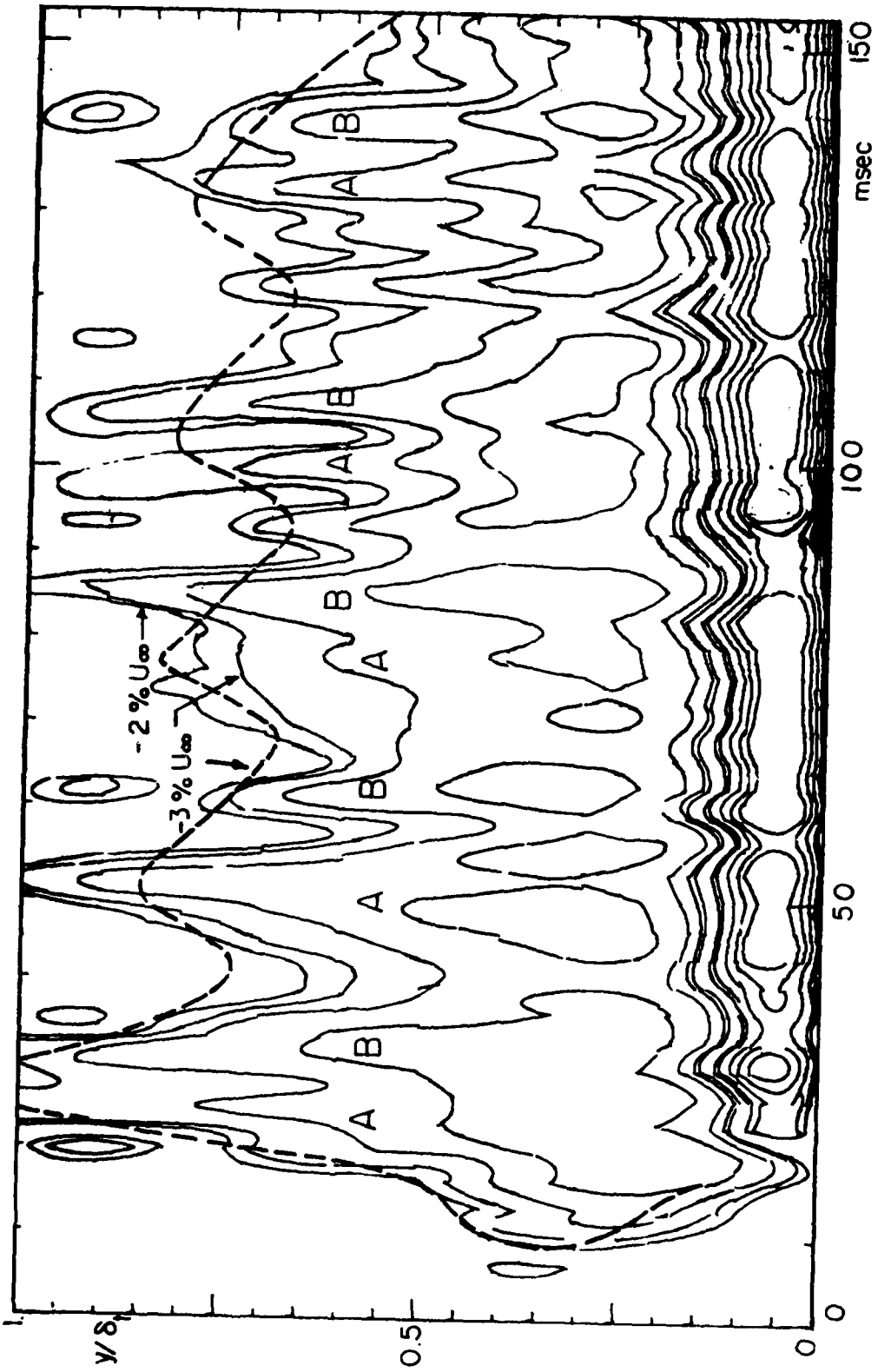

FIGURE E.3.2

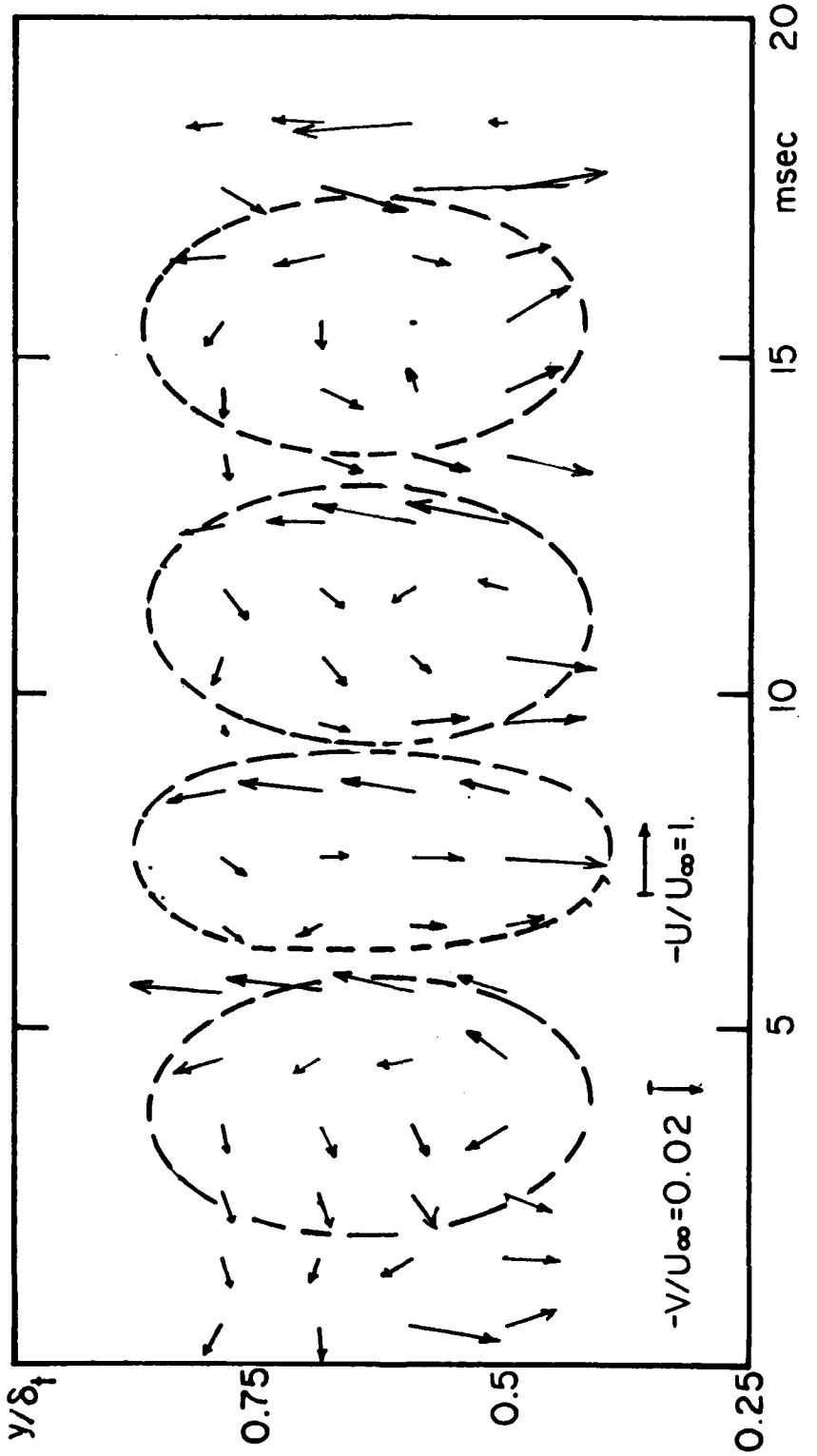

FIGURE E.3.3

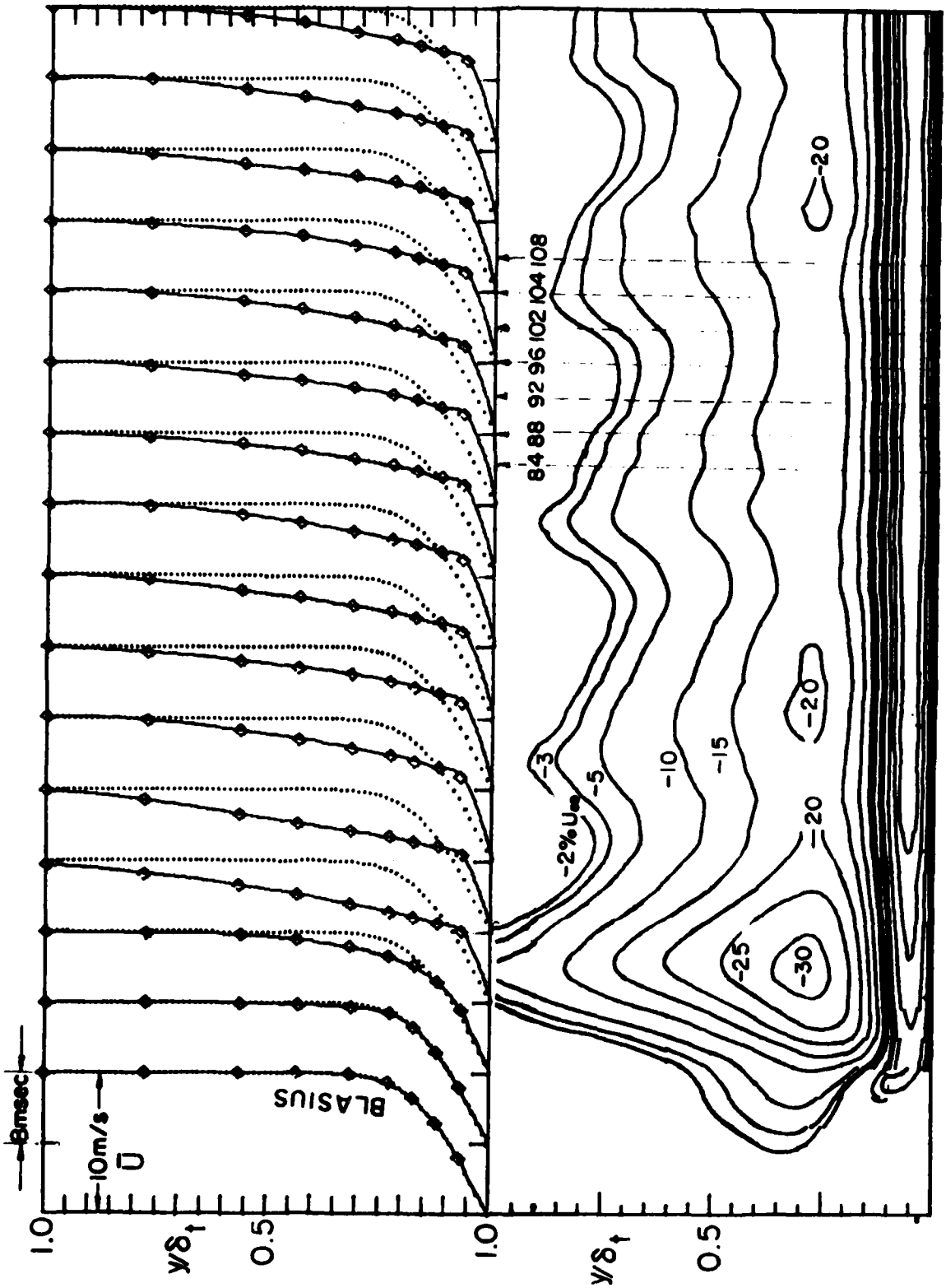
8msec
10m/s
Ū
BLASIUS
1.0
0.5
y/δ1
84 88 92 96 102 104 108
-2%U∞
-3
-5
-10
-15
-20
-25
-30
20

FIGURE E.4.1

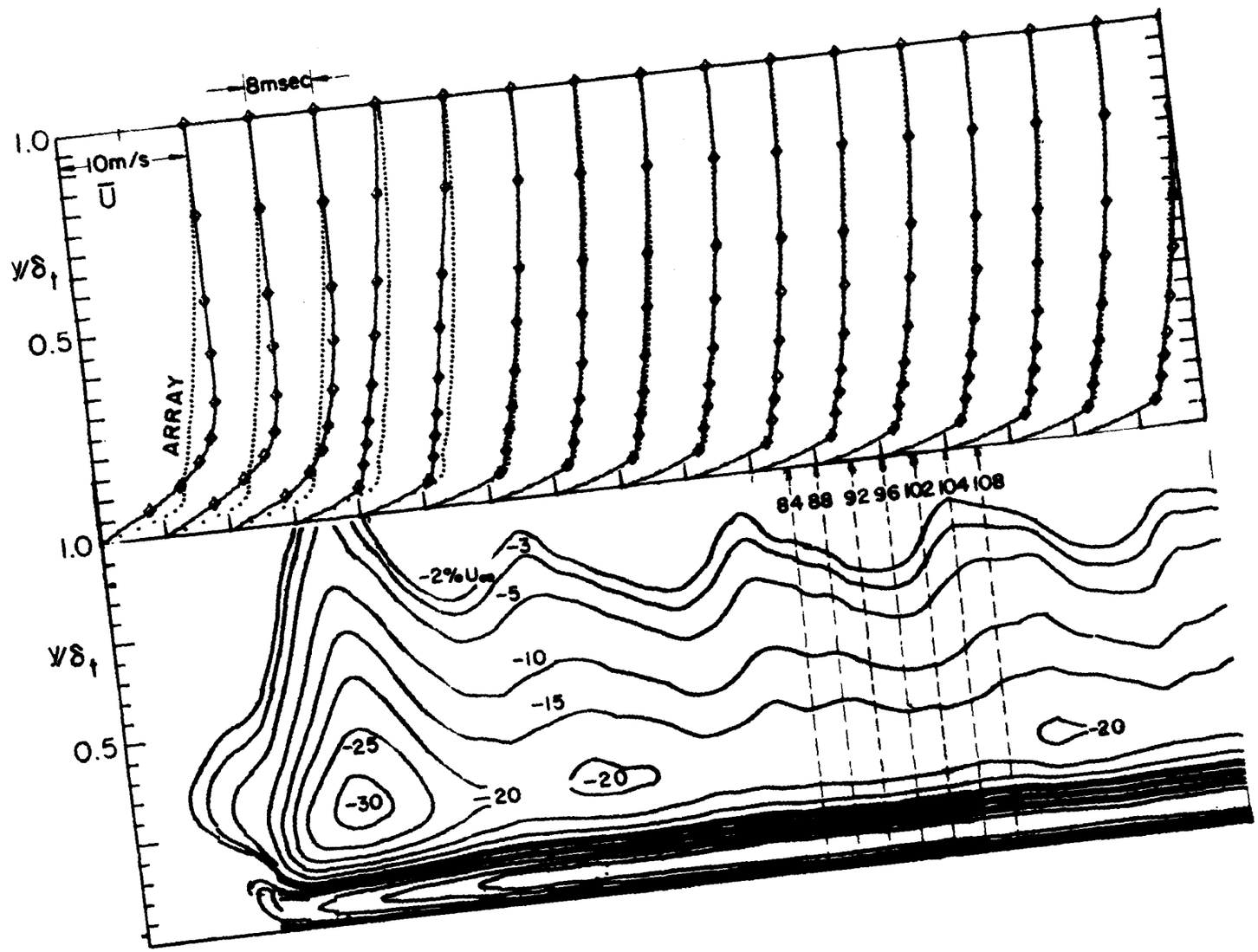
8msec
10m/s
$\bar{U}$
1.0
y/δ_t
0.5
ARRAY
84 88 92 96 102 104 108
-3
-2%U_∞
-5
-10
-15
-20
-25
-30
-20
-20

FIGURE E.4.2.

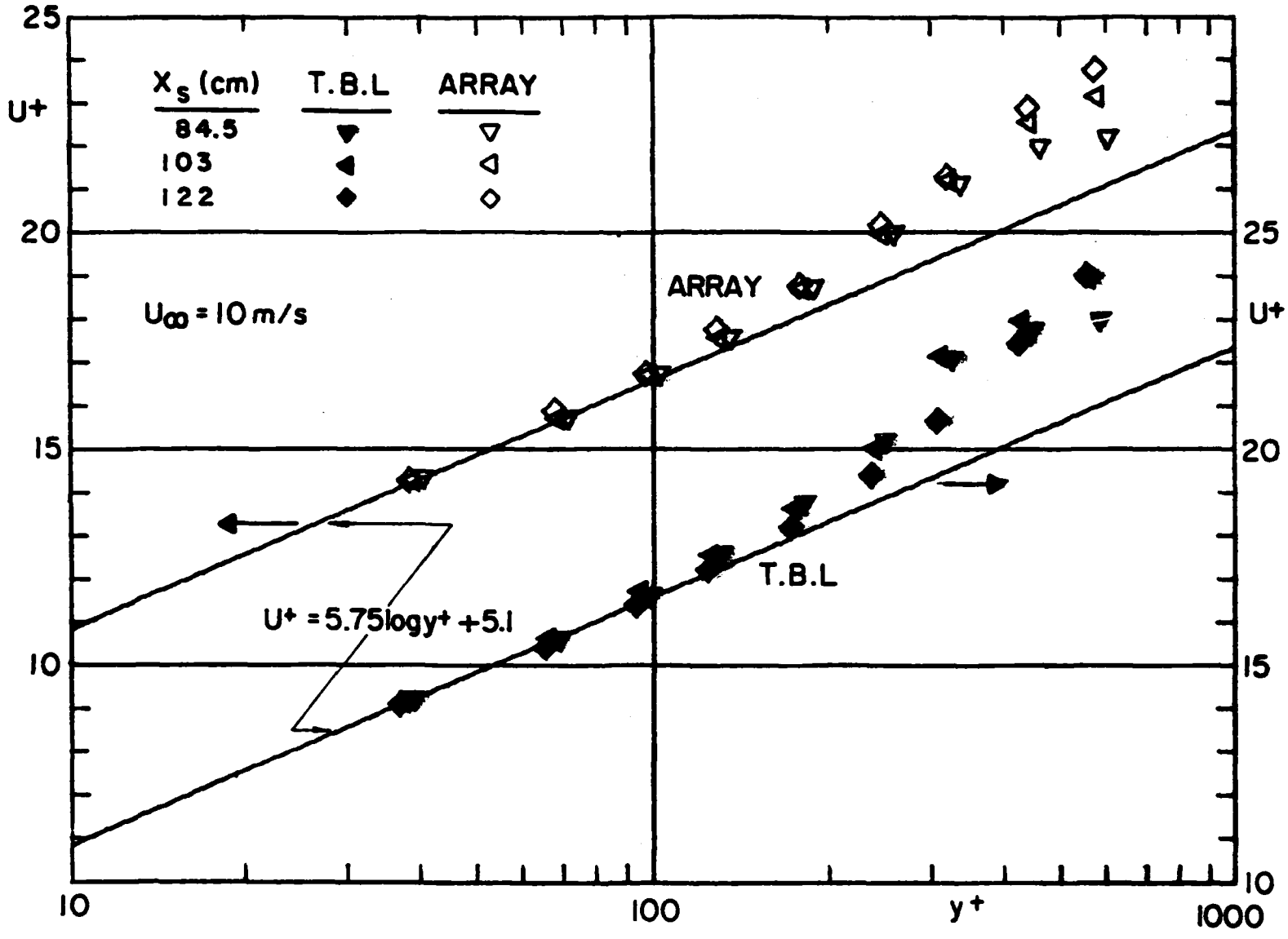
25
20
15
10
U+
X_s (cm)
T.B.L
ARRAY
84.5
103
122
U_∞ = 10 m/s
ARRAY
T.B.L
U+ = 5.75 log y+ + 5.1
10
100
1000
y+
25
20
15
10
U+

FIGURE E.4.3

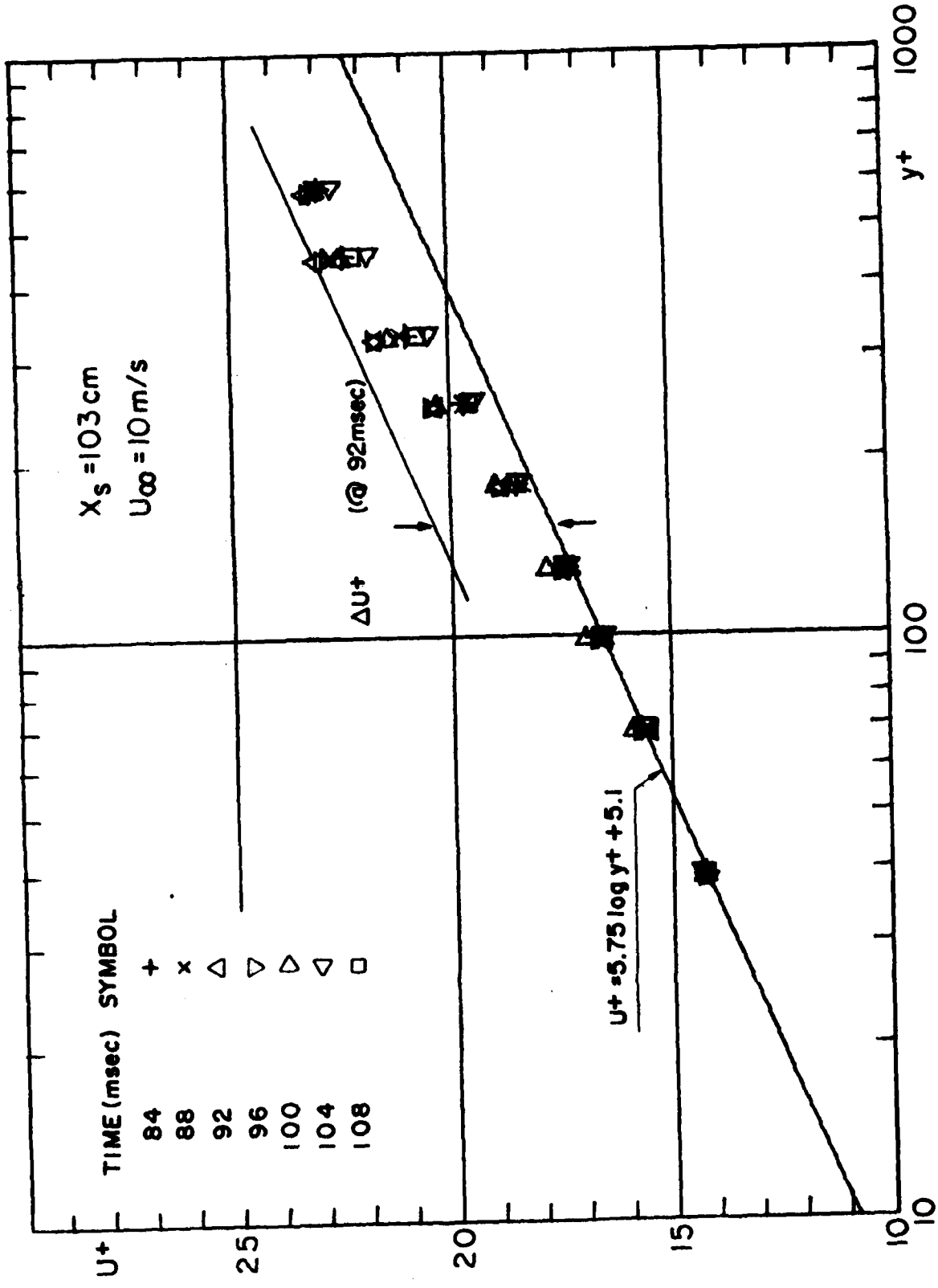
X_s = 103 cm
U_∞ = 10 m/s
ΔU+ (@ 92msec)
U+ = 5.75 log y+ + 5.1
TIME (msec) SYMBOL
84
88
92
96
100
104
108
U+
y+
25
20
15
10
10
100
1000

FIGURE E.4.4

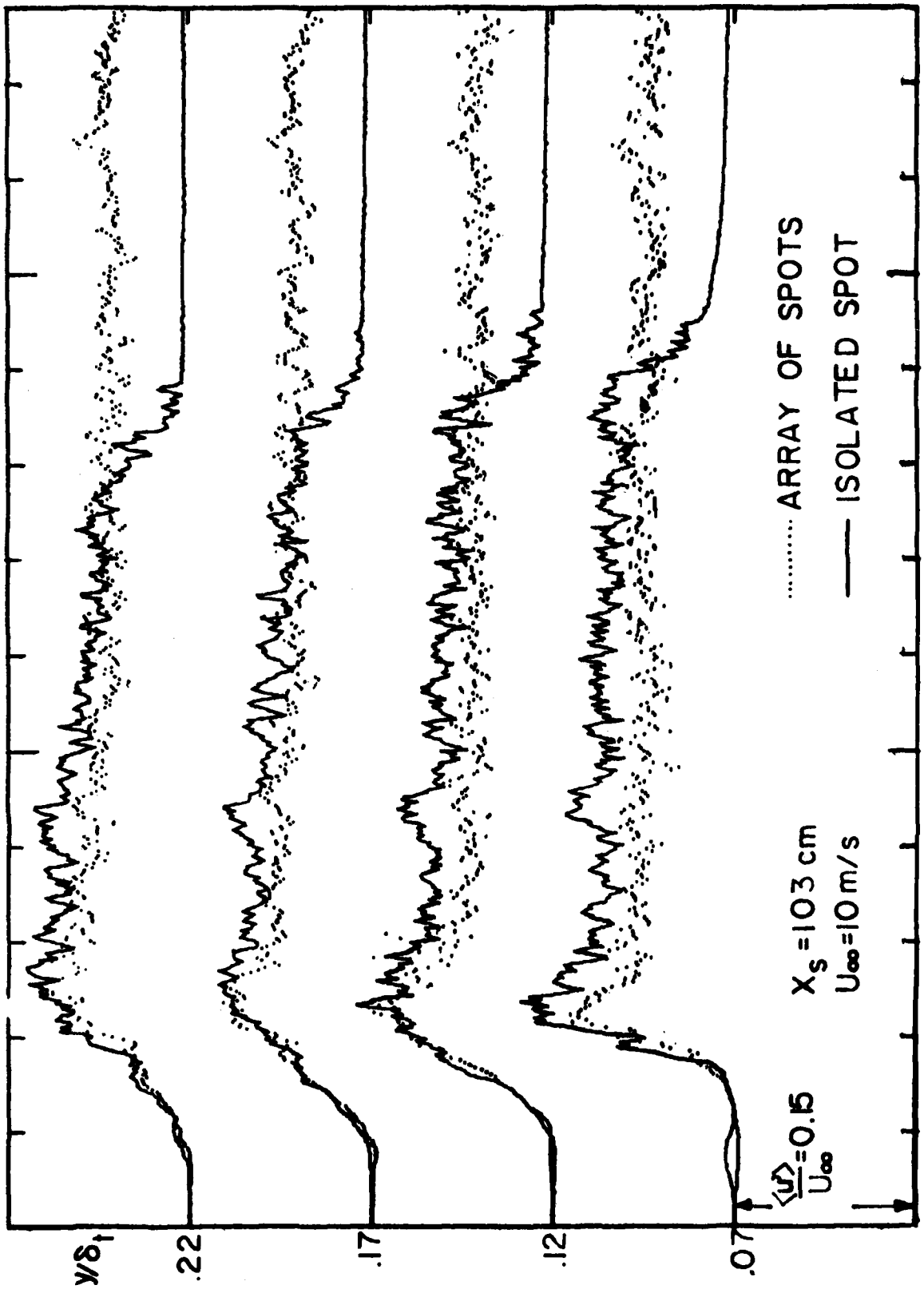
y/δ1
.22
.17
.12
.07
⟨u⟩/U∞=0.15
Xs=103 cm
U∞=10 m/s
..... ARRAY OF SPOTS
—— ISOLATED SPOT

FIGURE E.5.1

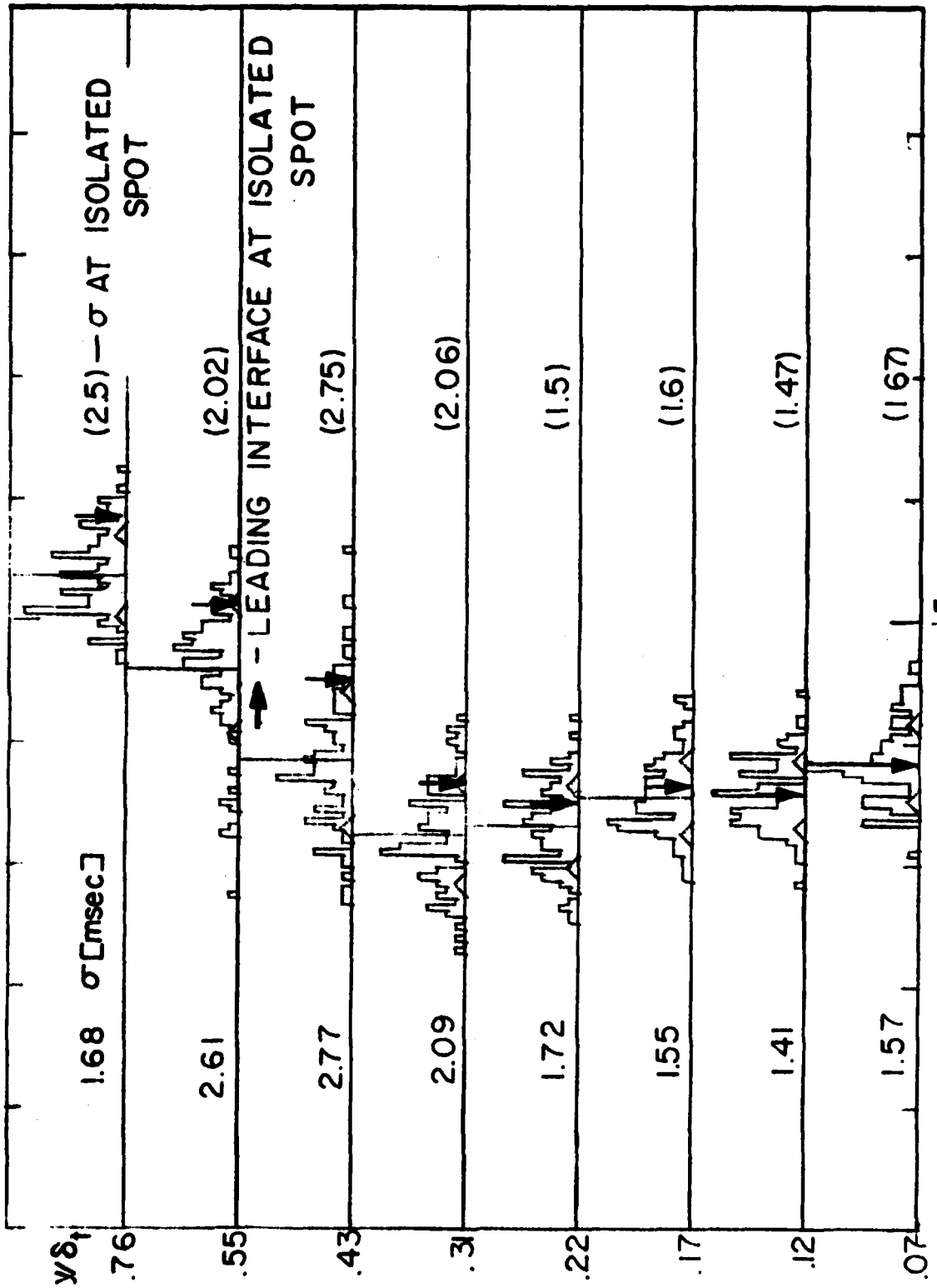
y/δ1
.76
.55
.43
.31
.22
.17
.12
.07
1.68 σ[msec]
2.61
2.77
2.09
1.72
1.55
1.41
1.57
(2.5) — σ AT ISOLATED SPOT
(2.02)
(2.75)
(2.06)
(1.5)
(1.6)
(1.47)
(1.67)
LEADING INTERFACE AT ISOLATED SPOT
5 msec

FIGURE E.5.2

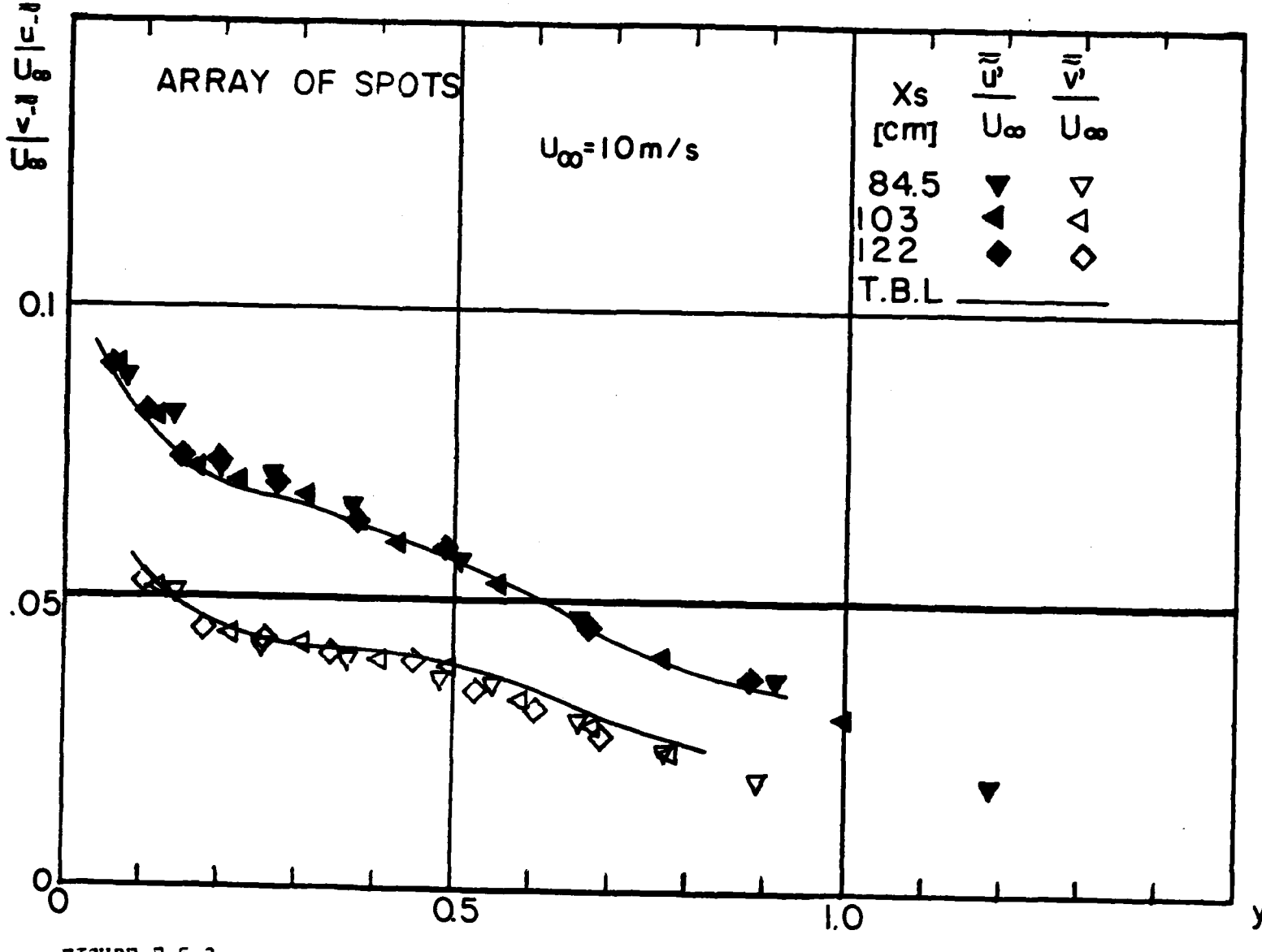
ARRAY OF SPOTS
U_∞=10m/s
Xs [cm]
$\frac{\sqrt{u'^2}}{U_\infty}$
$\frac{\sqrt{v'^2}}{U_\infty}$
84.5
103
122
T.B.L
0.1
.05
0
0
0.5
1.0
y/δ_t
$\frac{\sqrt{v'^2}}{U_\infty}$ $\frac{\sqrt{u'^2}}{U_\infty}$

FIGURE E.5.3

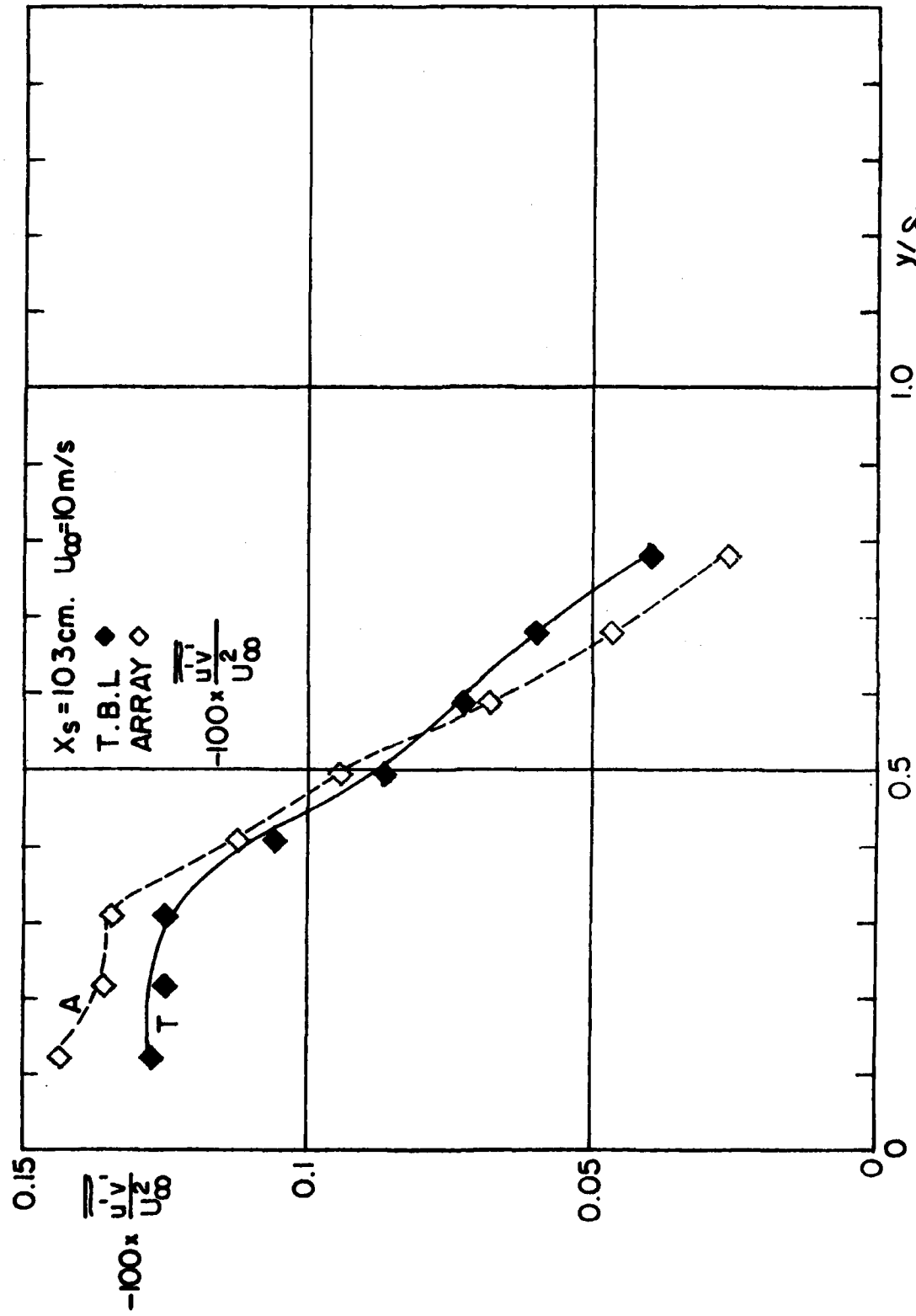
Xs = 103cm. U∞=10 m/s
T.B.L. ◆
ARRAY ◇
$-100\times\frac{\overline{u'v'}}{U_\infty^2}$
A
T
0.15
0.1
0.05
0
0.5
1.0
y/δ_1
$-100\times\frac{\overline{u'v'}}{U_\infty^2}$

FIGURE E.5.4

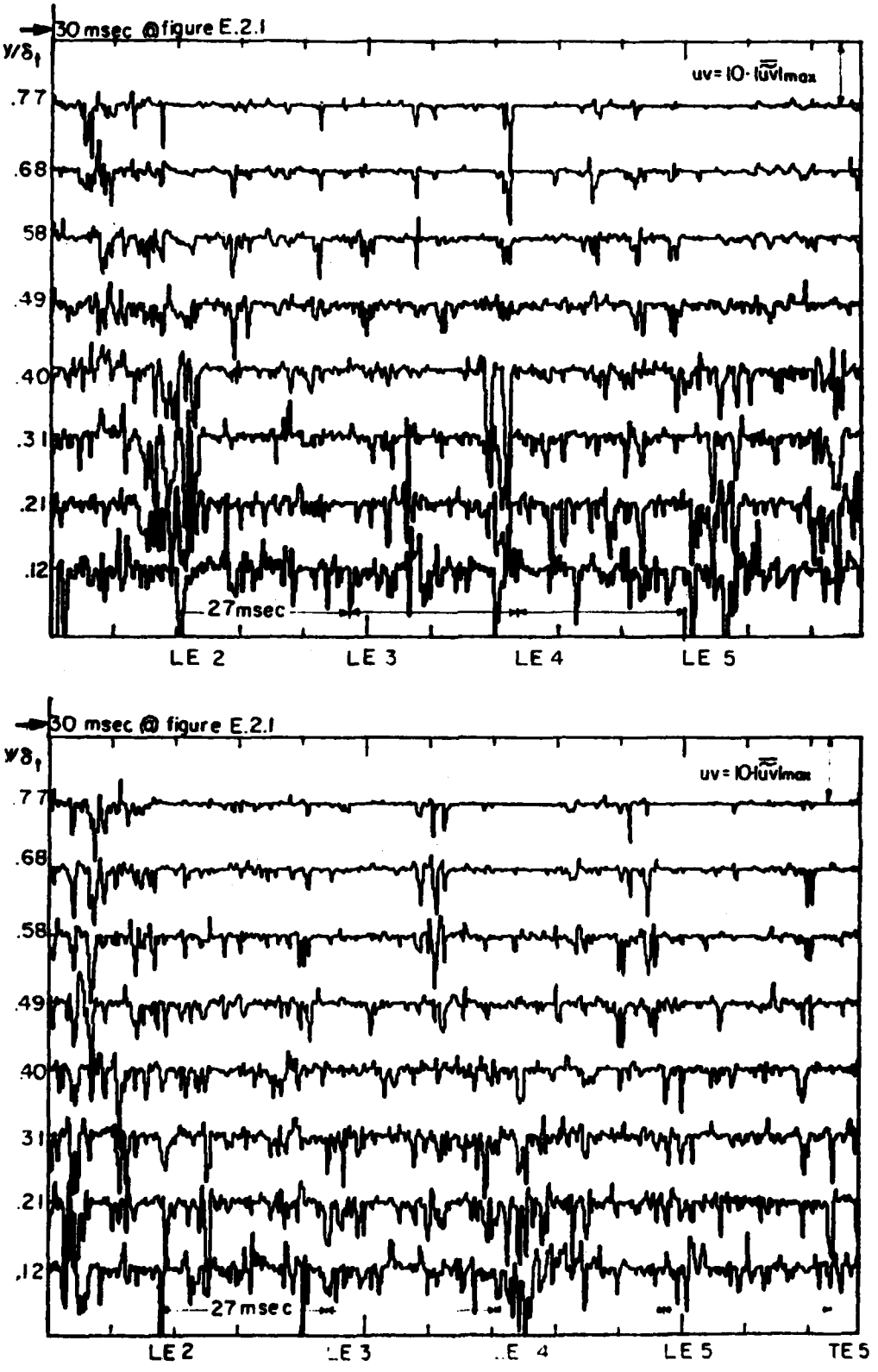

FIGURES E.5.5a,b

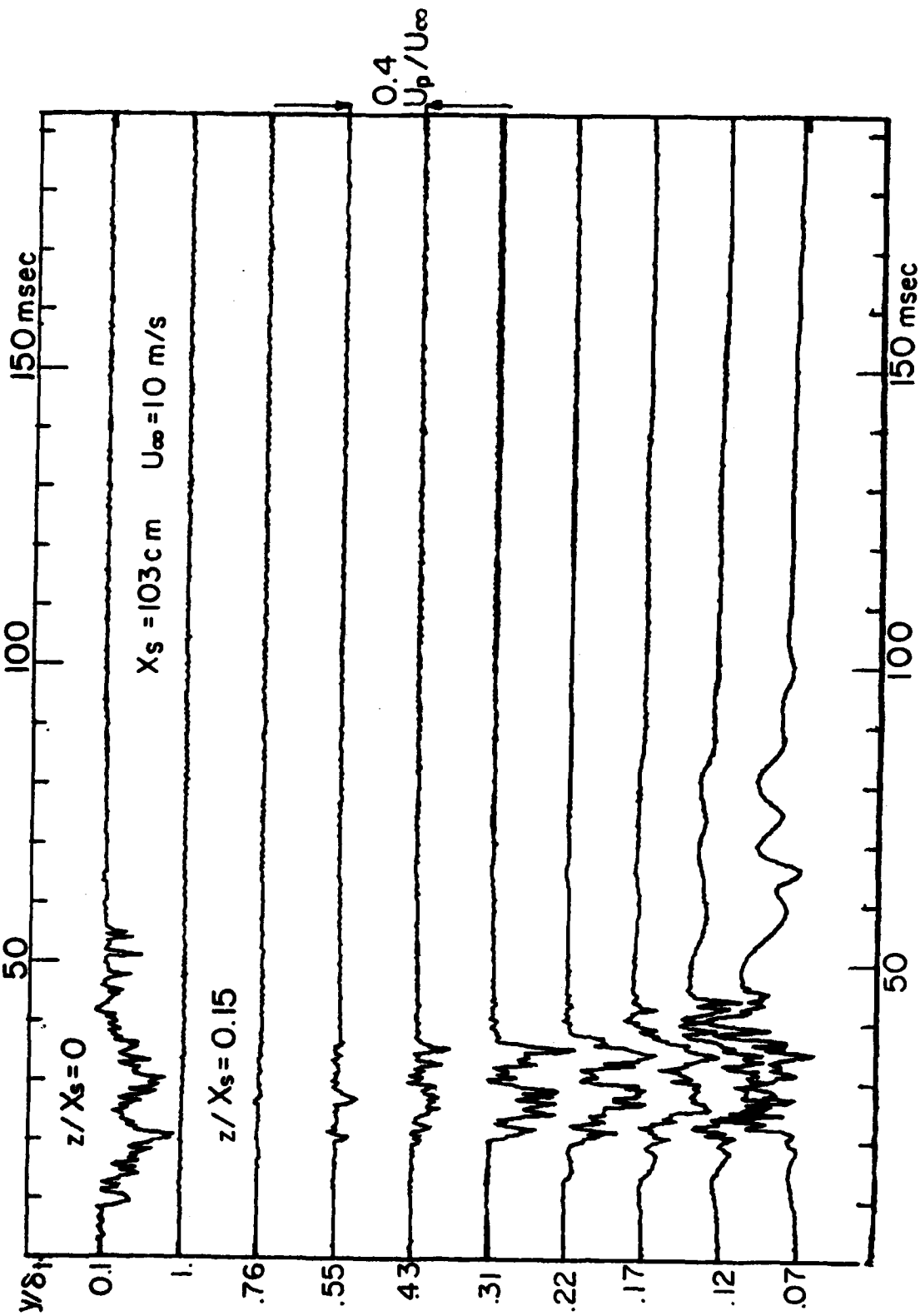
0.4
U_p/U_∞
150msec
100
50
X_s =103cm U_∞=10 m/s
z/X_s=0
z/X_s=0.15
y/δ_t
0.1
1.
.76
.55
.43
.31
.22
.17
.12
.07
150 msec
100
50

FIGURE E.6.1

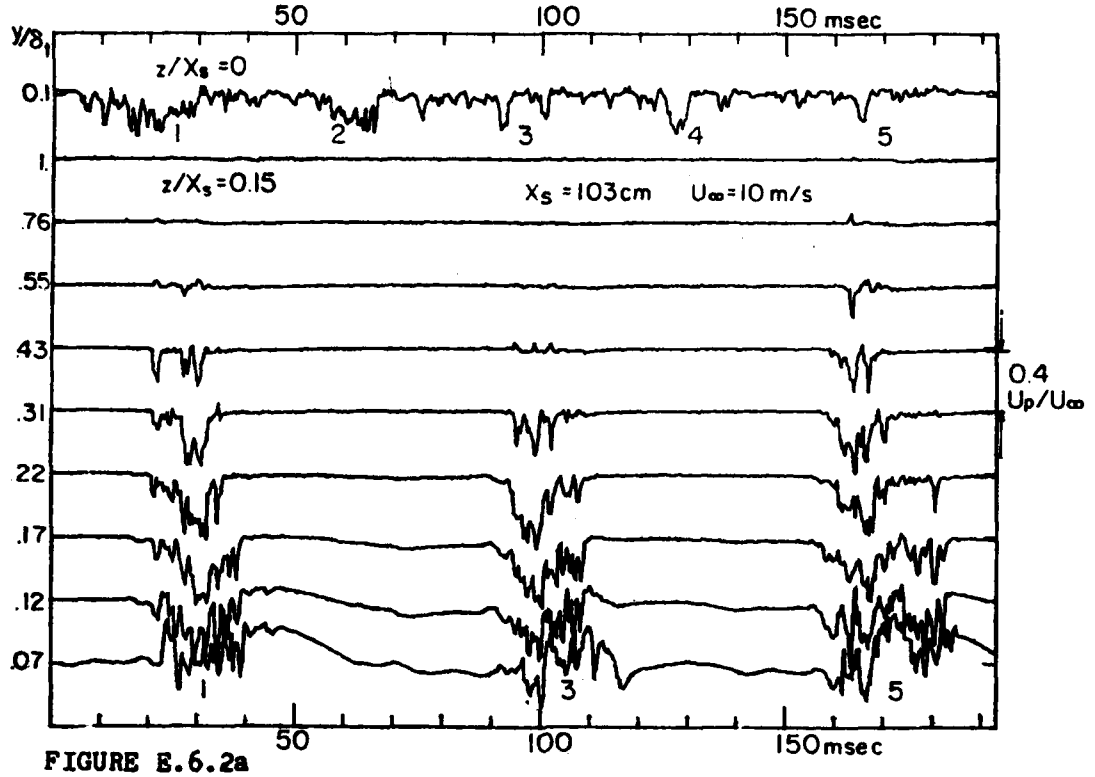

FIGURE E.6.2a

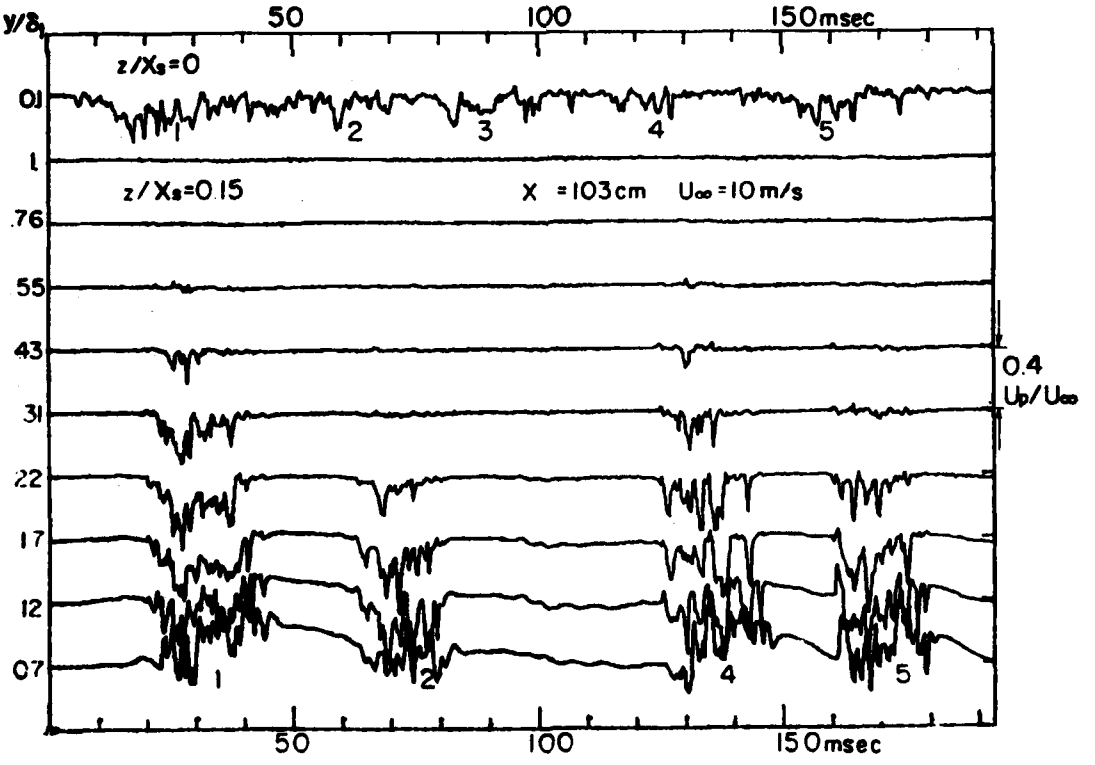

FIGURE E.6.2b

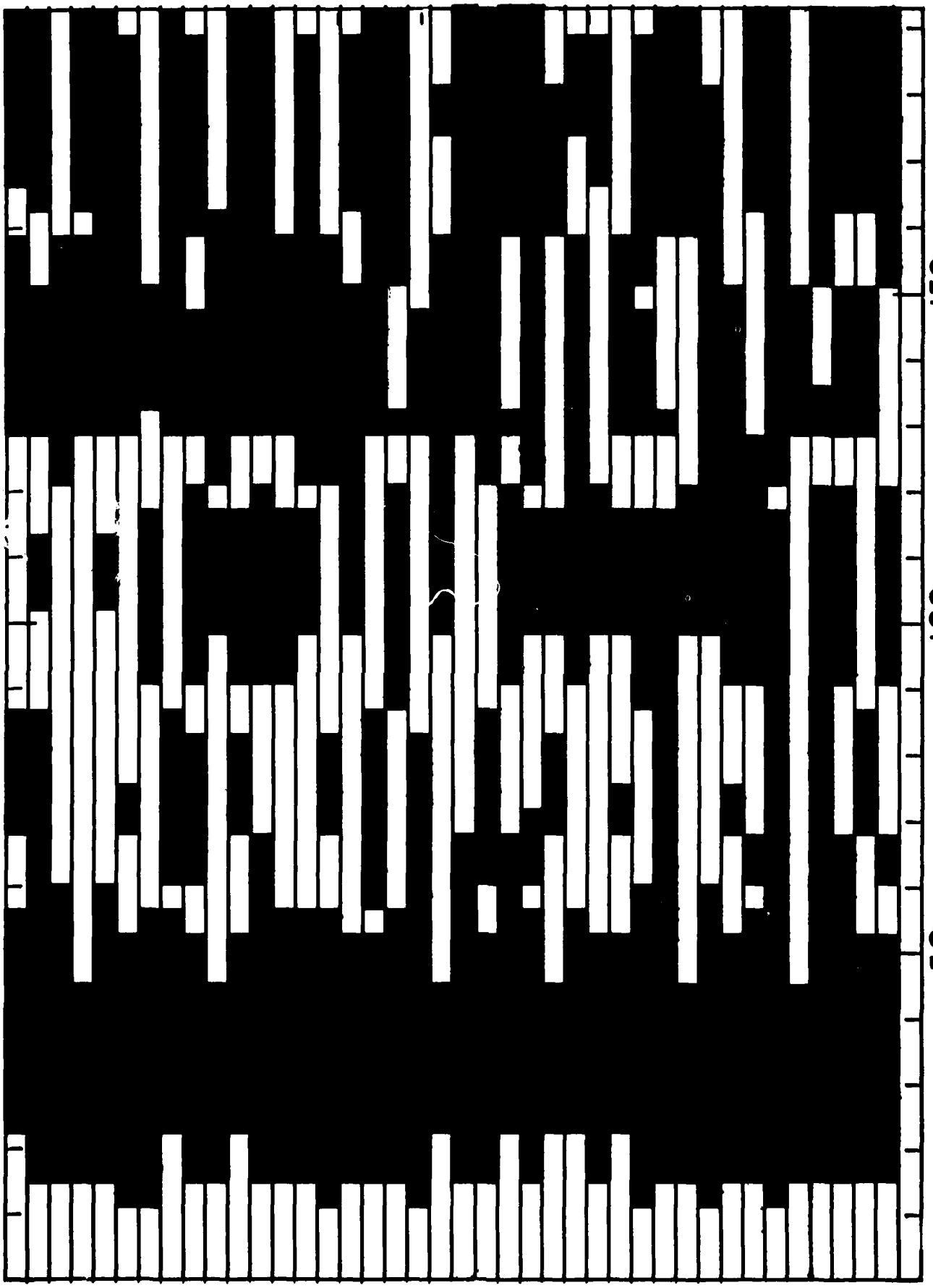

FIGURE E.6.3

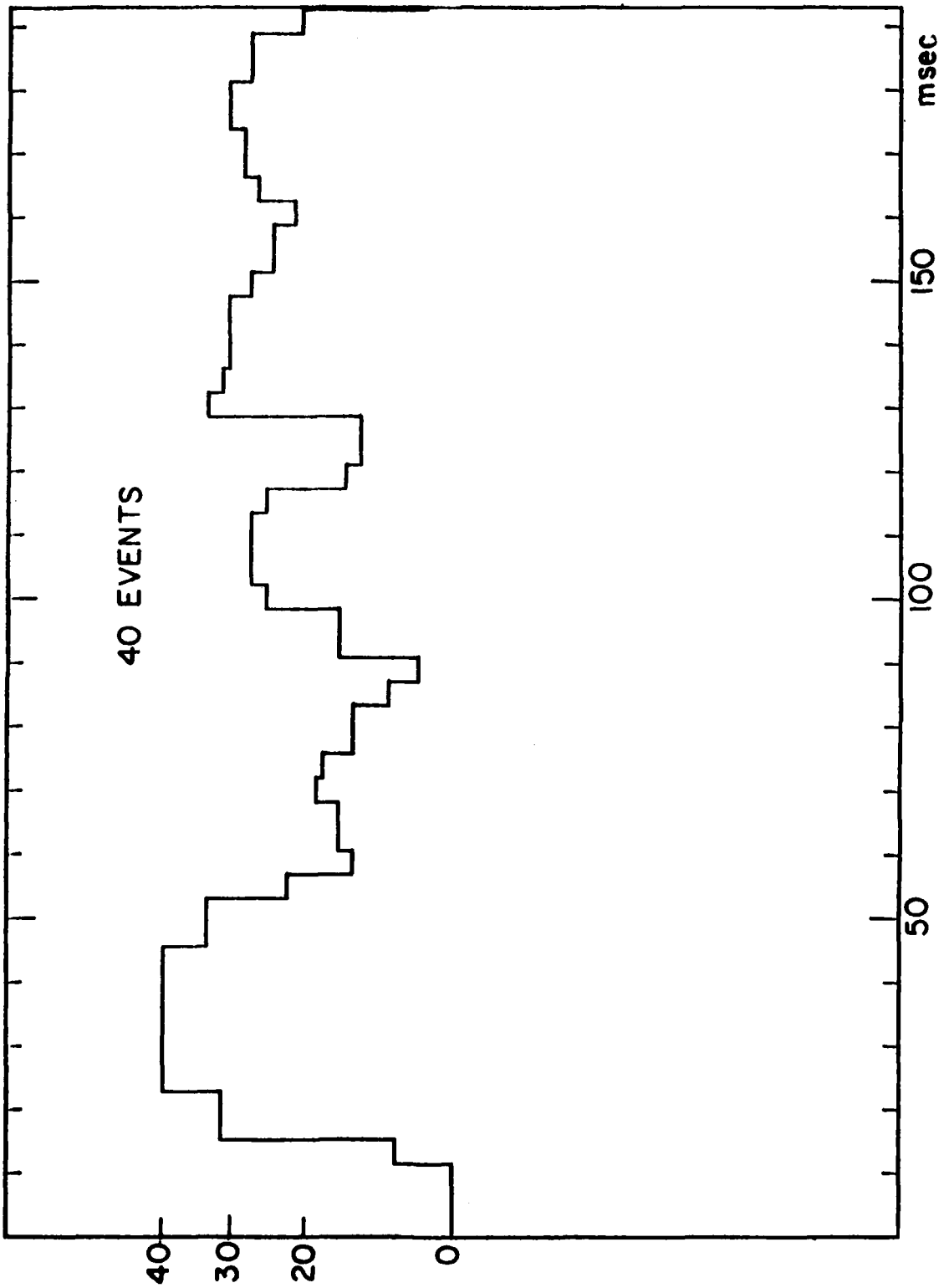

FIGURE E.6.4

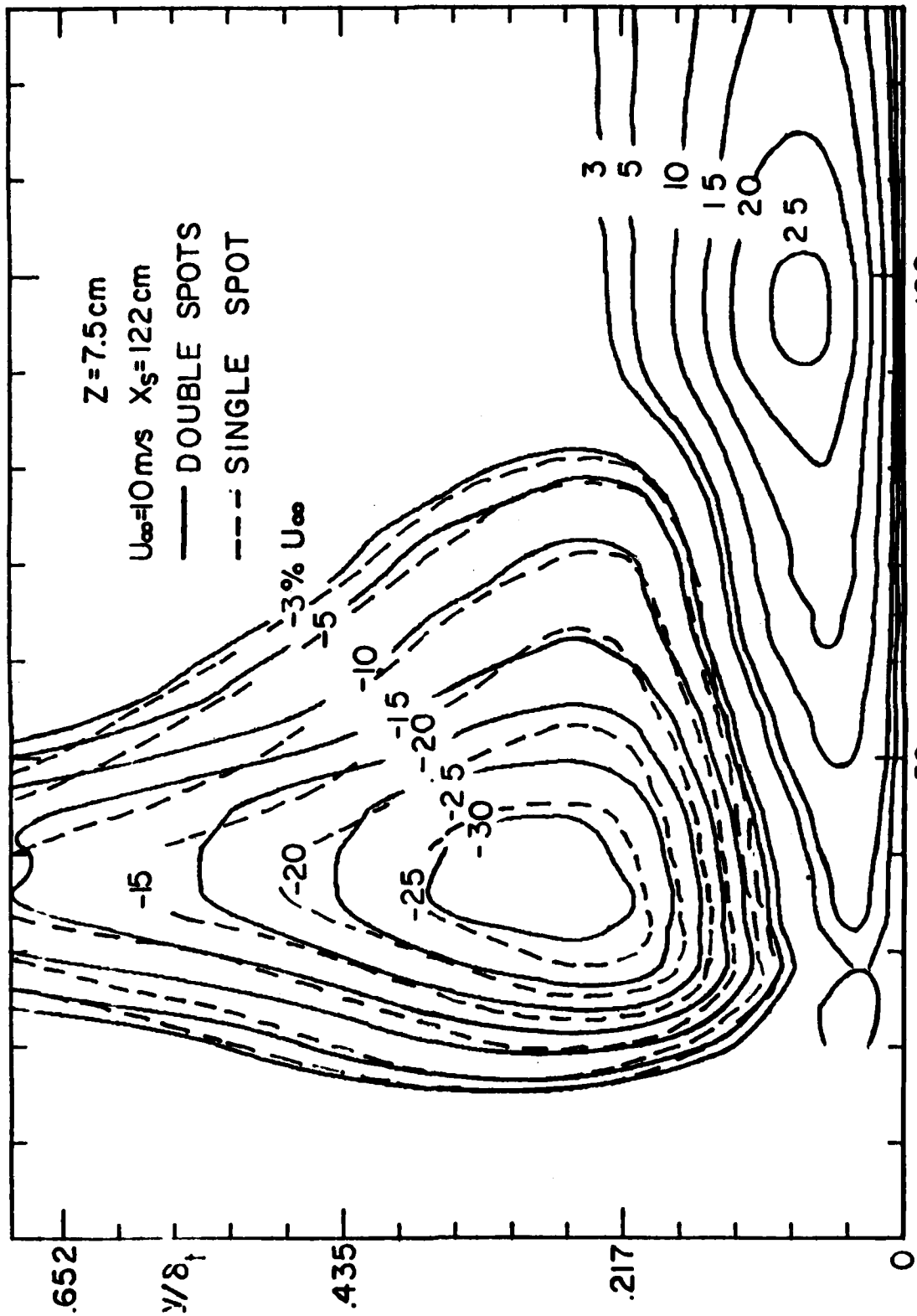
Z=7.5cm
U∞=10m/s Xs=122cm
DOUBLE SPOTS
SINGLE SPOT
-3% U∞
-5
-10
-15
-20
-25
-30
3
5
10
15
20
25
-15
-20
-25
.652
.435
.217
0
y/δt
50
100
msec

FIGURE F.1

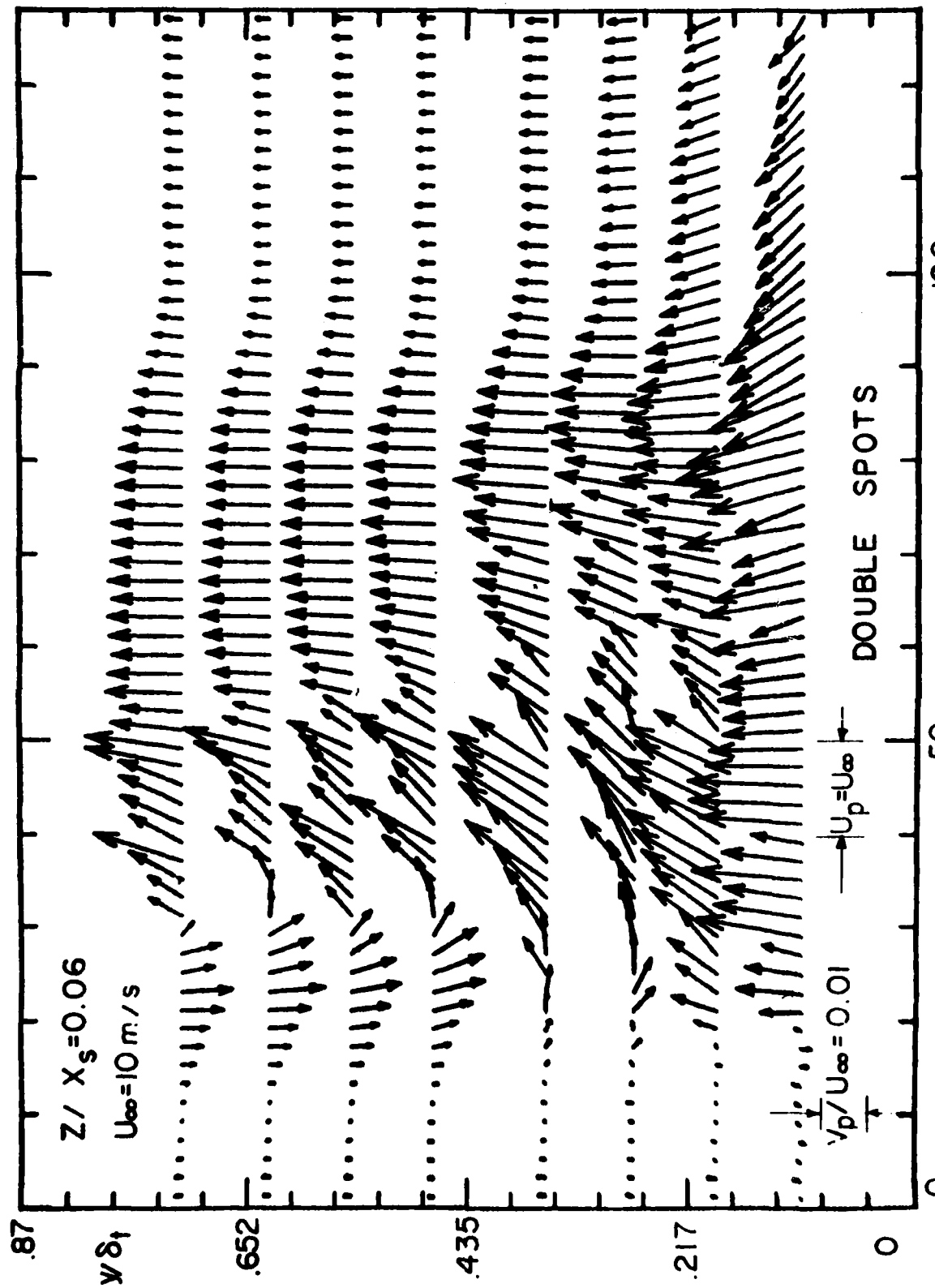
Z/ Xs=0.06
U∞=10 m/s
y/δ1
.87
.652
.435
.217
0
0
50
100 msec
DOUBLE SPOTS
Up=U∞
Vp/U∞=0.01

FIGURE F.2a

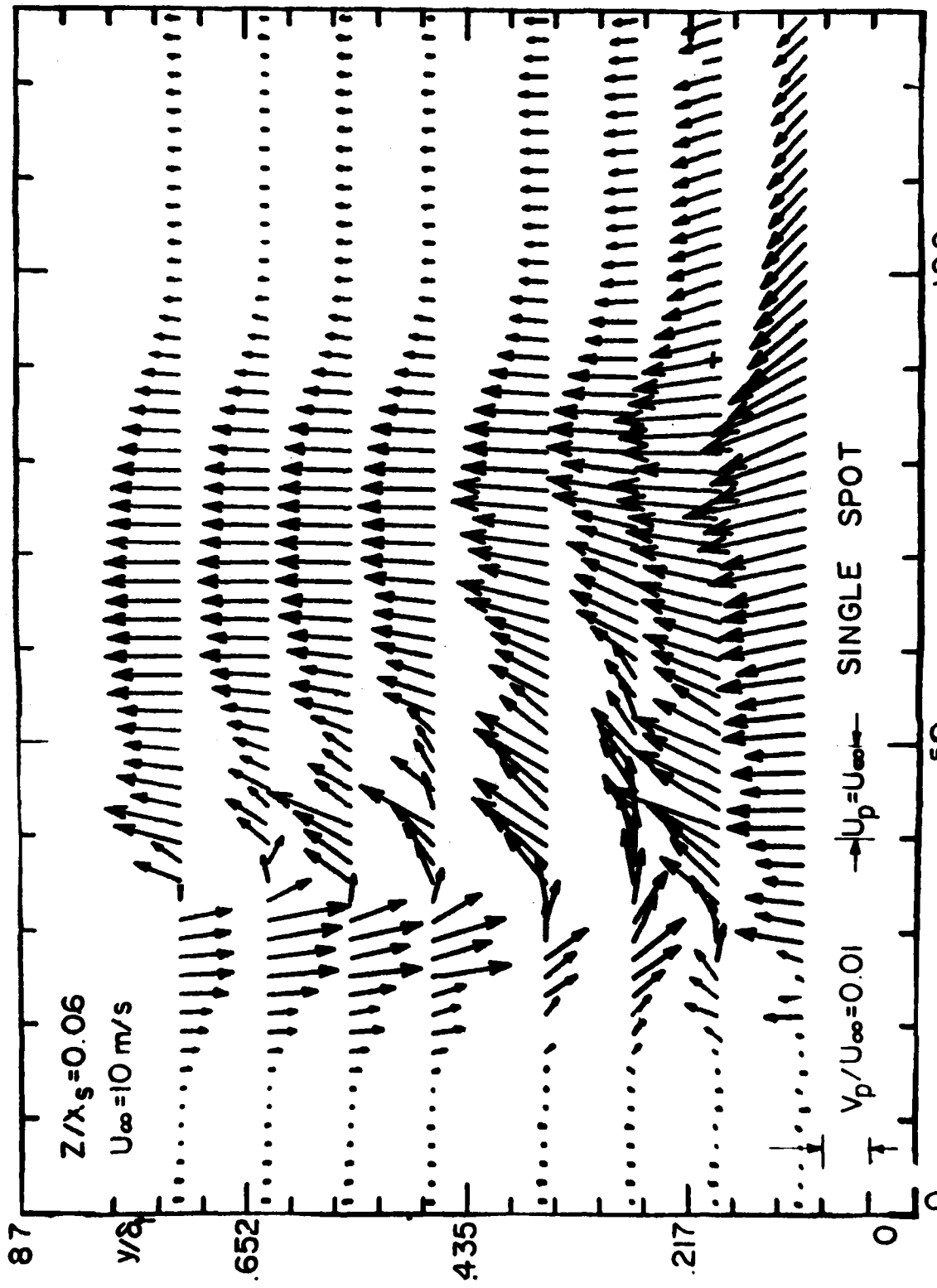
Z/λs=0.06
U∞=10 m/s
y/δ
.87
.652
.435
.217
0
Vp/U∞=0.01
Up=U∞
SINGLE SPOT
0
50
100 msec

FIGURE F 2r

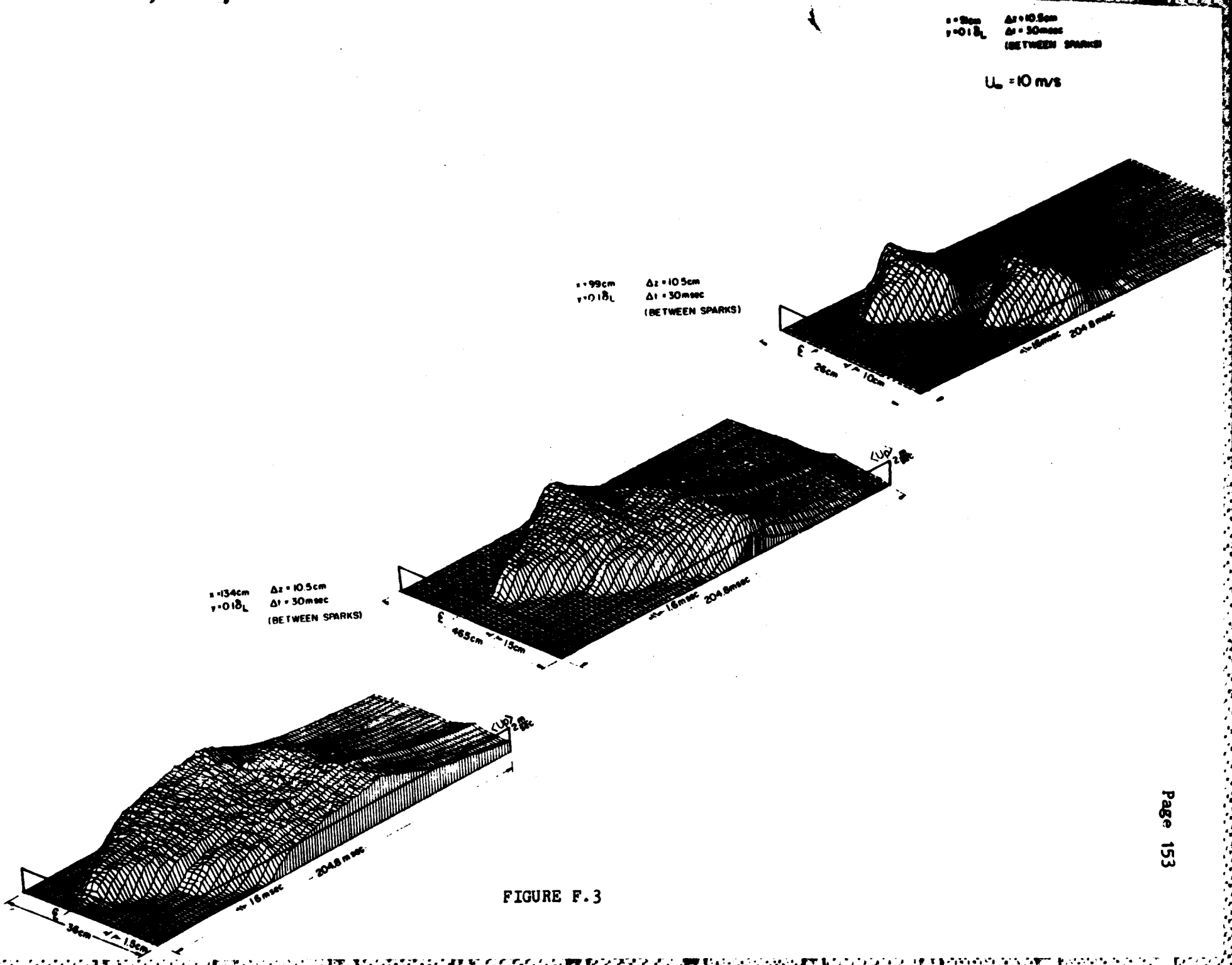
U_∞ = 10 m/s
x = 99cm
y = 0.18δ_L
Δz = 10.5cm
Δt = 30msec
(BETWEEN SPARKS)
x = 134cm
y = 0.18δ_L
Δz = 10.5cm
Δt = 30msec
(BETWEEN SPARKS)
26cm
10cm
16msec
204.8msec
46.5cm
15cm
16msec
204.8msec
36cm
15cm
16msec
204.8 msec

FIGURE F.3

END

FILMED

11-83

DTIC